A New Bayesian Inference Calibration Platform for Building Energy and Environment Predictions

Danlin Hou

A Thesis

In the Department

of

Building, Civil and Environmental Engineering

Presented in Partial Fulfillment of the Requirements

For the Degree of

Doctor of Philosophy (Building Engineering) at

Concordia University

Montreal, Quebec, Canada

January 2022

CONCORDIA UNIVERSITY

SCHOOL OF GRADUATE STUDIES

This is to certify that the thesis prepared

By: Danlin Hou

Entitled: A New Bayesian Inference Calibration Platform for Building Energy and Environment Predictions

and submitted in partial fulfillment of the requirements for the degree of

Doctor Of Philosophy (Building Engineering)

complies with the regulations of the University and meets the accepted standards with respect to originality and quality.

Signed by the final examining committee:

_____ Chair
Dr. John Xiupu Zhang

_____ External Examiner
Dr. Louis Gosselin

_____ External to Program
Dr. Abdel R. Sebak

_____ Thesis Co-Supervisor
Dr. Liangzhu Wang

_____ Examiner
Dr. Hua Ge

_____ Examiner
Dr. Mazdak Nik-Bakht

_____ Thesis Co-Supervisor
Dr. Ibrahim Galal Hassan

Approved by   _____
                   Dr. Mazdak Nik-Bakht, Graduate Program Director

1/27/2022   _____
                   Gina Cody School of Engineering and Computer Science

ABSTRACT

A New Bayesian Inference Calibration Platform for Building Energy and Environment Predictions

Danlin , Hou , Ph.D.

Concordia University, 20 22

Buildings account for nearly 40% of total global energy consumption. It is predicted that by 2050 the combined energy consumptions of the residential and commercial sectors will have increased to 22% of the world's total delivered energy. Moreover, requirements for indoor health, safety, thermal comfort, and air quality have become more demanding due to more intensive and frequent extreme climate events, such as heatwaves and cold waves. Such issues have become challenging for the building energy and environment field, especially during the COVID-19 pandemic.

Computer simulations play a crucial role in achieving a safe, healthy, comfortable, and sustainable indoor environment. As an integral step in the development of the building models, model calibration can significantly affect simulation results, model accuracy, and model-based decision-making. Conventional calibration methods, however, are often deterministic. As a result, the uncertainties that have been investigated for a building computer model, and those from the inputs have not been given adequate attention and are thus worth studying in more depth.

Bayesian Inference is one of the most effective approaches to calibrate computer models with uncertainties. Several studies have explored its application in building energy modeling, but a comprehensive application in the general field of building energy and environment has not been adequate. This thesis started with a comprehensive literature review of Bayesian Inference calibration focusing on building energy modeling. Then, a systematic Bayesian calibration workflow and a new platform were developed. As well as a general study of its application for the predictions of building energy performance, the thesis investigated how to use the platform to calibrate thermal models of buildings and indoor air quality models. To solve the issue of the computing cost of Bayesian Inference, another calibration and prediction method, Ensemble Kalman Filter (EnKF), was proposed and applied to the estimation of ventilation performance and

predictions of free cooling load. The conclusion includes a summary of the contributions of this thesis and suggestions for future work.

For the most important person of my life,

my baby Larry .

ACKNOWLEDGEMENTS

I would like to express my great gratitude to my supervisors, Dr. Liangzhu (Leon) Wang and Dr. Ibrahim Galal Hassan. Thanks Dr. Wang's patience and guidance, and his commitment and overall responsibility in being my daily supervisor. He sacrificed his free time to discuss my research and correct my writings. Thanks for Dr. Ibrahim Galal Hassan's guidance, patience and all the invested time with writing this thesis and other publications. I learned how to think from the big picture and manage time and efforts efficiently from him. I'm deeply affected by the enthusiasm and dedication of my two supervisors in science research and their daily work.

Big thanks to the rest of my thesis committee: Dr. Hua Ge, Dr. Abdel Razik Sebak, and Dr. Mazdak Nik-Bakht, for your acceptance to be a part of this committee and your valuable advice and comments on the thesis from the comprehensive exam to the final defense. Your comments are a treasure to me not only for this thesis but also for my future research.

Thanks to the Department of Building, Construction, and Environmental Engineering secretaries, Jenny Drapeau and Jiwu Rao. Thanks for all the provided administrative.

I was fortunate to meet and work with Dr. Dahai Qi, Dr. Cheng-Chun Lin, Dr. Mohammad Mortezazadeh, Dr. Ali Katal, Dr. Chang Shu, Senwen Yang, Cheng Zhang, Chen Ling, Lili Ji, Bingyan Jia, Dongxue Zhan, Majd Moujahed, Maher Albettar, Jiwei Zou, and Shujie Yan, and Kathryn Chung Cheong. It was a pleasure to learn from them. Thanks to my officemate, Tiantian and Vera, who are an essential part of my Ph. D. life, and also became my dear friend.

During my Ph. D. research, I had a chance to supervise the master student, Bingyan Jia. Thank her for her hard work and the given experience in supervision.

Special thanks to my friends, Tao and Xing. Thanks for the lovely time we spent together. Thanks for their understanding and encouragement.

At last, I would like to express my heartfelt thanks to my baby Larry. Thanks for always being there for me. I cannot imagine how blue my Ph. D. life would be without him.

TABLE OF CONTENTS

LIST OF FIGURES

LIST OF TABLES

NOMENCLATURE

ACH	Air Change per Hour
ASHRAE	American Society of Heating, Refrigerating and Air-Conditioning Engineers
ANN	Artificial Neural Network
BEM	Building energy model
BIR-BEM	Bayesian Inference on R for Building Energy Model
BMARS	Bagging Multivariate Adaptive Regression Splines
CBES	Commercial Building Energy Saver
CDEM	Community Domestic Energy Model
CRPS	Continuous Rank Probability Score
CVRMSE	Coefficient of Variance of Root Mean Squared Error
DOE	Department of Energy
ECM	Energy Conservation Measure
EIA	Energy Information Administration
EPC	Energy Performance Coefficient Calculator
EPD	Equipment Power Density
EPSCT	Energy Performance Standard Calculation Toolkit
ESCO	Energy Service Company
EST	Energy Savings Trust
EUI	Energy Use Intensity
GA	Genetic Algorithm
GDP	Gross Domestic Product
GP	Gaussian process
GSHPS	Ground Source Heat Pump System
HMC	Hamiltonian Monte Carlo
HPS	Heat Pump System
IAQ	Indoor Air Quality
IES-VE	Integrated Environmental Solutions Virtual Environment

INLA	Integrated Nested Laplace Approximation
IPMVP	International Performance Measurement and Verification Protocol
LHS	Latin Hypercube Sampling
LM	Linear Model
MAP	Maximum A Posteriori
MARS	Multivariate Adaptive Regression Splines
MBE	Mean Bias Error
MC	Monte Carlo
MCMC	Markov Chain Monte Carlo
MLR	Multiple Linear Regression
MOBO	Multi-Objective Building Optimization
M&V	Measurement and Verification
NMEB	Normalized Mean Bias Error
NN	Neural Network
NST	Nash-Sutcliffe Efficiency Coefficient
NUTS	No-U-Turn Sampler
OECD	Organization of Economic Cooperation and Development
PAM	Posterior Approximation Method
PAT	Parametric Analysis Tool
PDF	Probability Density Function
RF	Random Forest
RFVI	Random Forest Variable Importance
RMSE	Root Mean Square Error
SRC	Standardized Regression Coefficient
SUSDEM	Stochastic Urban-Scale Domestic Energy Model
SVI	Sensitivity value index
SVM	Support Vector Machine
TMY	Typical Meteorological Year

TRYOPT   TESS Optimization Library

UBEM   Urban Building Energy Modeling

VIC   Virtual In-Situ Sensor Calibration

Chanpter 1   Introduction

1.1   Problem Statement

Buildings consume nearly 40% of total global energy consumption [1]. It has been reported that global energy consumption is anticipated to rise by nearly 50% by 2050, and global energy-related CO_2 emissions are expected to grow at an annual average rate of 0.6% for the same period [2]. The combined energy consumptions of the residential and commercial sectors will increase from 20% of the world's total delivered energy in 2018 to 22% in 2050 [2]. Due to greenhouse gas emissions, climate change and global warming have become more conspicuous. Extreme events, such as heatwaves and cold waves, are more intensive and frequent. Peoples' health and comfort are under threat to an unprecedented degree, including in buildings. With the breakout of the COVID-19 pandemic at the end of 2019, in the field of heating, ventilation, and air conditioning, assessments of ventilation rate and indoor air quality have gained more attention.

Different stakeholders and organizations have undertaken various measures and actions to achieve safe, healthy, comfortable, and sustainable indoor environments. Policymakers have been actively engaged in establishing regulations and incentives to promote strategies for energy and greenhouse gas reduction. To assist such decision-making, accurate and dynamic prediction and analysis of building energy and environments are required. Conventional calibration approaches, however, are often deterministic. The inevitable uncertainties from model inputs and the model itself are ignored. The probabilistic auto-calibration platform is limited.

Building environment models, which concern thermal performance and indoor air quality, have received little attention. Most studies have focused on the calibration of building energy models. The validated modeling tools can predict and analyze the implications of new technologies, products, and policies on the current and future energy use and occupancy comfort of cities.

1.2   Research Objectives

The research consists of two main parts: developing a methodology and evaluating the methodology through variable field tests. Most of the existing calibration approaches can calibrate building energy and environment performance deterministically, but they ignore the inevitable uncertainties, whether from model inputs or the model itself. As the uncertainties are ignored, the predictions of the calibrated models are potentially risky.

Bayesian Inference has gained more attention, especially after 2010, when Kennedy and O'Hagan systematically illustrated the Bayesian calibration of computer models [23]. Compared with the conventional deterministic calibration methods, Bayesian Inference calibration has the following advantages:

1) When the calibration measurements are qualitatively/quantitatively insufficient, the estimated model parameters in traditional methods can be far from their original values; for Bayesian calibration, however, the calibration results are more stable and reasonable, since the uncertainties are taken into considered.

2) In traditional calibration methods, the results are often deterministic, whereas in the Bayesian Inference calibration method, the results are derived from quantitative stochastic analysis and include possibilities that can be regarded as a degree of belief. The Bayesian-based calibrated model is more comprehensive and reliable in its analysis.

Currently, studies using Bayesian Inference in the building engineering field have focused only on building energy modeling. The method has not been applied to the building environment. However, with intensive and frequent extreme weather events and the breakout of COVID-19, the building environment should be considered seriously. The calibration of building environment models, especially with uncertainties, deserves more study. Although Bayesian Inference is a promising approach, its complicated theoretical algorithm is a significant impediment to many modeler developers and engineers. No available calibration platform employs Bayesian Inference. Additionally, the computing cost of Bayesian Inference is high. How to decrease the computing time and requirement is another issue.

In this thesis, a systematic Bayesian Inference calibration workflow is proposed to address these challenges, starting from the preparation of measurements to future model analysis. A new auto-calibrated Bayesian Inference platform is developed based on the workflow. A deterministic engineering-based tool (e.g., EnergyPlus) can represent the target building with probabilistic inputs (e.g., envelop materials, indoor heat gains, human behaviors). Using probabilistic-based calibrated models, the target building's energy consumption and environmental performance can be estimated.

1.3 Thesis Organization
The thesis is ornanized as follows:

Chapter 1 presents an overview of and motivations for the calibration of building energy and environment models with degrees of uncertainty.

Chapter 2 provides a comprehensive literature review of building energy model calibration using Bayesian Inference. The calibration of building environment models is not discussed, since no study has used the proposed calibration method.

Chapter 3 introduces the proposed Bayesian Inference calibration platform and detailed step-by-step methodologies. Two case studies are provided, including a synthetic office building and a real residential building. The complicated relationship between the number of calibration parameters, meta-model accuracy, computing cost, and calibration performance is also discussed.

Chapter 4 describes how to calibrate and predict the thermal performance of buildings using the proposed Bayesian Inference platform. A real school building is used as a case study to demonstrate the procedure and the calibration performance. The predictions of indoor temperature with uncertainties are also presented.

Chapter 5 investigats the estimation of ventilation performance using the proposed platform and indoor and outdoor environment measurements. Based on the calibrated profile of the ventilation rate, transmission risk was estimated with probabilities, which is more reliable than traditional deterministic calculations.

Chapter 6 proposes another calibration and prediction method, Ensemble Kalman Filter (EnKF), a data assimilation method often used in weather prediction, for the assessment of ventilation performance and predictions of free cooling load. The impact of spurious correlations and ensemble numbers is also discussed.

Chapter 7 provides a conclusion including a summary of the contributions of this thesis and suggestions for future work.

Chanpter 2　　Literature Review

This chapter is presents a systematic literature review of the use of Bayesian Inference in the calibration of building energy and environment models, including building energy models, building thermal models, and indoor air quality models. There are currently few studies, however, of Bayesian Inference calibration in building engineering, and most of them concern building energy models. This review therefore focuses on the calibration of building energy models by Bayesian Inference[1].

A building energy model (BEM) is essential for understanding building energy consumption, evaluating energy-saving measures, and developing associated codes, standards, and policies. The calibration of BEM helps to ensure the accuracy of the model, whereas it remains a challenge. Conventional manual or automated methods are mostly deterministic and neglect the inherent uncertainties of BEM. In comparison, the recent development of the stochastic BEM calibration based on Bayesian inference has gained attention, whereas many are baffled by its underlying theory, strengths, limitations, and implementations. There are also various mathematical models and tools in the literature, making it hard for selection. This paper aims to unravel the myths about the Bayesian inference and critically review various implementation options with a series of model selections suggested so that a user would be able to employ the Bayesian inference calibration at the end of the paper. We also hope that the review contributes to facilitating a broader implementation of the method for BEM calibrations. First, an overview is summarized for the current status and development of Bayesian inference calibration in building energy modeling. Second, the theory and methodology of model calibration, Bayesian statistics, and Markov Chain Monte Carlo are illustrated. Third, the implementation of Bayesian inference is described, including several practical issues such as BEM determination, unknown calibration parameters number, their ranges and distributions, Meta-model selections, and programming languages based on the statistical package R. The review ends with conclusions and future work identified.

2.1　Introduction

In a recent report of the International Energy Outlook by the U.S. Energy Information Administration [2], the gross domestic product (GDP) between 2018 and 2050 is expected to grow 1.5%/year in the countries of the OECD and 3.8%/year in non-OECD countries. Meanwhile, the world energy consumption is anticipated to rise by nearly 50% by 2050, and worldwide energy-related CO_2 emissions grow at an annual average rate of 0.6% for the same period. Although the industrial sector is still the largest energy consumer, the building sector energy consumption has increased drastically over the past decades as a result of rapid population growth and urbanization process, higher requirements for indoor air quality and comfort, more indoor time, more diversified building functions, and global climate change. The combined energy consumptions from the residential and commercial sections worldwide will increase from around 20% in 2018 to 22% in 2050 of the world total delivered energy, corresponding to an increase from 91 quadrillions to 139 quadrillions British thermal units (Btu) for the same period with an average annual growth of 1.3%. For the world's largest economic entities, building energy consumption increases more significantly than the world average: for the U.S., the largest building energy consumer in the world, the end-use energy consumption by the residential sector and commercial sector was about 21 quadrillion Btu, equal to 28% of total U.S. end-use energy consumption in 2019 [3]; for the second-largest consumer, China, in 2016, around 20% of total energy use was consumed by commercial building sector [4]. In the European Union, buildings are accounted for about 41% of the final energy consumption in 2016 [5].

To slow down the increasing building energy consumptions, different stakeholders and organizations have undertaken various measures and actions. Governments adopted a variety of policies to promote more utilization of renewables such as wind, solar power, and biomass energy. Professional associations such as ASHRAE tailored their standards and codes for more energy-efficient designs and operations of high-performance buildings. Among research communities, most recent developments on smart buildings [6], smart cities [7,8], smart grids [9], Internet of Things (IoT) [10], and various advanced data-driven control strategies have started to contribute to optimizing building energy usages. During this process, computer simulations using BEMs play a crucial role: a successful BEM can provide many insights into the complicated building physics and evaluate different energy-saving measures. On the other hand, the performance of a building energy model is subject to many uncertainties from the model itself (e.g., model-form uncertainty) and the inputs (i.e., parameter uncertainty) [11]. The uncertainties are often inevitable due to the

complexities of a building and its system, and many model parameters. The model-form uncertainties originate from numerical approximations, quality of computer programming and coding, and underlying assumptions of building models. For example, it remains a challenge to model the dynamic correlations and interactions among multiple physics components, including building envelopes, facility responses, interior impacts (e.g., occupants and appliances), and exterior impacts (e.g., weather conditions and impacts from neighboring buildings such as microclimates and shading). For the parameter uncertainties, hundreds to thousands of inputs/parameters are often required to create a building model. It is estimated that for a typical building energy model developed in EnergyPlus [12], about 3000 input parameters need to be specified [13]. The parameter uncertainties can thus be introduced through the input data from 1). the outdoors, including the long-term and short-term macroclimate and microclimate information around the building, 2). the building itself, including building material discrepancies from the design to the built process, property transformations and function changes during operations, and 3). the indoor building parameters from the randomness of occupancy behaviors and equipment deteriorations during the service life.

To reduce the uncertainties and align simulation results with measured data, model calibration is an integral step for developing a reliable and accurate BEM, which can then be applied to building optimization, retrofit analysis, fault detections, and diagnoses, and advanced model-based controls. From a mathematical perspective, model calibration is a searching process for the highly-parameterized model in an undetermined search space with a large number of independent and interdependent parameters. Model calibration often includes manual and automated calibrations [14]. The former heavily relies on a user's expertise in building science and simulation and his/her knowledge about the target building. So a few key parameters are manually selected and tuned to obtain the simulation results close to the measured information from audited and monitored energy usage data. Manual calibration is, therefore, a very time-consuming, labor-intensive, and cost-expensive process, and the manually calibrated model is often questionable due to the limited expertise of the user and the complexity of the calibrated problem.

Automated calibration is a non-user driven and mathematically-based process in which an objective function or penalty function is defined for matching simulation results with measured data [15]. Although the input variables under search and the actual physical properties may not match each other well, they should have physical significance and meaning in reality. With the

mathematical/statistical methods coded in a computer program, the calibration activity can be iterated automatically for a large batch of simulations with many combinations of parameters. The automated search process is considered complete when the calibration error rate (the difference between simulation and measurement) is less than a threshold criterion, or the calibration activity runs long enough and should be stopped by a given time. In this case, the group of input parameters of the specific simulation with the lowest error rate is selected as the calibration result. When both criteria are often applied, there is a trade-off because automated calibration is often an iterative total permutation process with a heavy computing burden. With the recent development in computing power and advanced mathematical and statistical methods, the calibration process is speeded up. So automated calibration is always more efficient and faster than manual calibration. Nowadays, combined with online metering, continuously automated calibration becomes possible in buildings [16].

Conventional calibrations are often deterministic, leading to estimated parameters far off from their original values when the training data is qualitatively/quantitatively insufficient. Sometimes, the deterministic calibration approaches are inadequate and even risky. For example, for a building retrofit project, different ECMs can be evaluated by BEMs following the IPMVP [17]. However, because of the deterministic process, the ECMs are compared by their absolute performance without uncertainties quantified. As a result, there exist unknown risks of the underperformance of a suggested ECM, which may not be expected from the performance contract. In practice, to avoid the risk, ESCOs generally provide building owners with one fixed minimum guaranteed savings for each selected ECM based on the rules of the thumbs of the experts. It was reported that the experts' subjective judgment is estimated to be between 60% and 70% of the deterministic energy-saving prediction [18].

Besides, with more big data available from the advancement of sensor technologies, and more research on larger scale BEMs, e.g., urban-scale analysis, the calibrations of BEMs face unprecedented challenges: (a) how to extract high-quality information from big data and use them as much as possible for model calibrations while maintaining acceptable computing costs; (b) how to adequately consider the impact of measurement errors on calibrations; (c) how to reduce uncertainties in assumed data and model parameters for a large scale problem; (d) how to understand the causes of errors and improve the accuracy of BEMs. In some previous work, the average error of around 69% of UBEM has been considered the acceptable level [19].

As a scientific way to interpret and quantify these uncertainties and risks, Bayesian inference has gained interest recently. Bayesian inference is "the process of fitting a probability model to a set of data and summarizing the results by a probability distribution on the parameters of the model and unobserved quantities such as predictions for new observations" [20]. Based on the literature review, the history with the central mark stones of Bayesian statistics and inference is shown in Figure 2-1. It was first proposed by Reverend Thomas Bayes from England in his 1763 doctoral dissertation [21], then developed by Pierre Simon Laplace to form the Bayes theorem in France and then spread to other parts of Europe in the nineteenth century. But because of limited computing resources, its development did not gain momentum until the twentieth century thanks to the development of MCMC [22] and modern computers. In 2001, Kennedy and O'Hagan systematically illustrated the Bayesian calibration of computer models [23], signifying the boom of Bayesian calibration and inference. Since then, it has been utilized in a variety of topics, including environment [24–27], hydrology [28–30], transportation [31], and medicine research [32], etc. By propagating parameters using probabilistic analysis, Bayesian inference incorporates uncertainties into the approximations of real systems by computer models. Combining multiple sources of information at different scales and with different reliabilities, the inadequacy of a model, which is revealed by the discrepancy between the predictions and observed data, can be corrected [14].
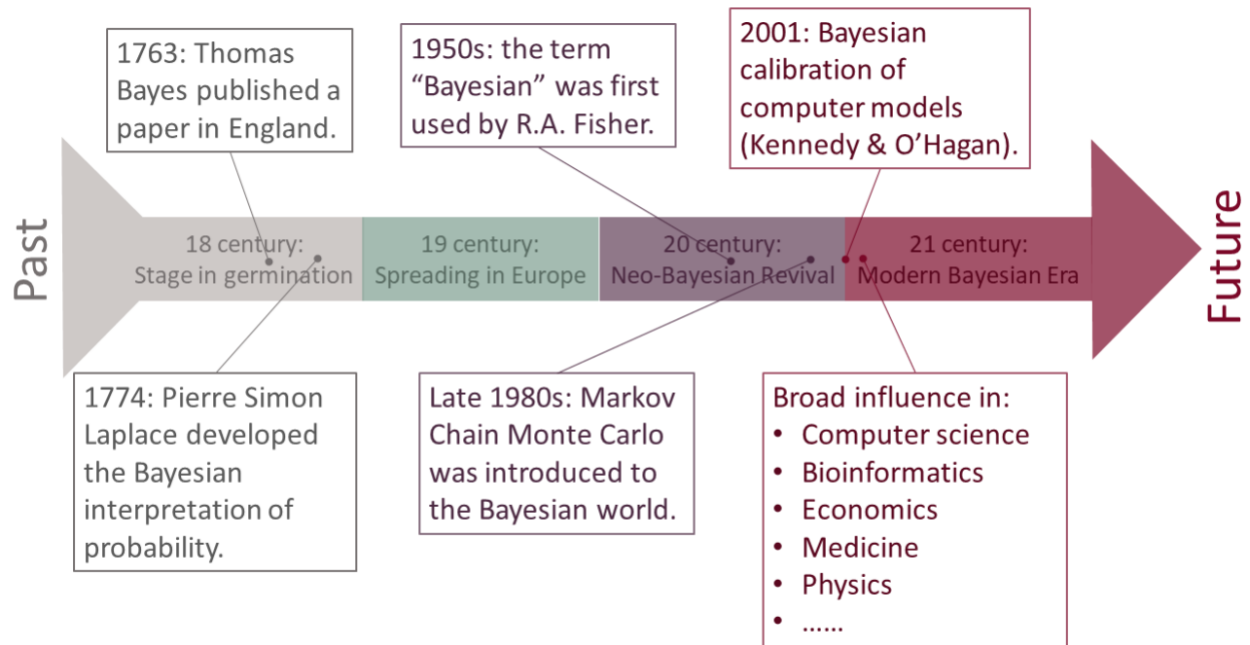
Figure 2-1 Bayesian statistics development.

For building energy modeling, one of the first applications of Bayesian inference may be presented by Heo [33]. A Bayesian inference begins with modelers' prior knowledge and expertise beyond the impact of observations in the forms of the prior distributions of model parameters. Then these prior distributions are incorporated into the building simulation and mapped into a probability distribution of model outputs. The prior distributions may then be updated and improved based on field observations and output distributions via the Bayes' rule. In the end, the posterior distribution of selected parameters can be obtained and employed to forecast building energy demand and consumption or retrofit benefits more accurately and reliably.

Since the posterior distribution is intractable analytically, approximation methods are needed. Variational Inference is an optimization-based method from machine learning. It fits a variational distribution to the posterior under an objective function to improve computational efficiency and more suitable for the high-dimensional problem. Researchers already started to employ it on occupancy behavior, building energy/thermal performance, forecast of wind speed, and solar irradiation. Sadeghi et al. [34] trained a visual preference model using Variational Inference with 565 observations of 75 participants. Different models based on different combinations of variables were developed. It is found that the best model's prediction accuracy is 0.69, which is satisfactory compared to the acceptable value of 0.33. Lee et al. [35] used Automatic Differentiation

Variational Inference to train a high-dimensional thermal preference model with 5454 latent variables. Then the trained model was used as a prior for personalized thermal preference models to learn new occupants. Results show that the proposed method can better predict performance, even with limited data. Garstens et al. [36] demonstrated the Variational Inference's potential to building energy measurements and savings. The method was applied to the example from IPMVP to estimate the mean value of 12 monthly measurements. Simulations show that, with 100,000 draws, the case can be done, and the result is stable and converges on the posterior distribution in 10.76s on a middle-range laptop computer. Besides, Liu et al. [37] employed Variational Inference to approximate the posterior parameter distribution of a spatial-temporal neural network to forecast wind speed with probability. It is concluded that the proposed method is better than other point forecast models by performing 14.1% lower in terms of RMSE value. The authors also leveraged Variational Inference on solar irradiation prediction [38]. An ensemble spatio-temporal deep learning model was proposed for solving the problem with the collaboration of Variation Inference to quantify the uncertainty. The results demonstrate that the proposed model outperforms the other four models in terms of RMSE, MAE, and NSE in all months. These machine learning-based models show great potentials for inference studies. On the other hand, they are relatively new, and the publications are still limited compared to other methods, especially for building energy model calibration.

Another method is MCMC that has been the dominant paradigm to approximate posterior distributions for decades. It's a sampling-based approach and often unbiased, guaranteed to converge to the true posteriors [39], which has been widely studied, extended, and applied [40]. In the field of building energy, MCMC is more commonly used. Details about its application is presented in Section 2.

When compared to conventional calibration approaches, the benefits of Bayesian inference-based calibrations have been previously revealed. Kim et al. [41] compared the deterministic calibration based on a constrained optimization method and the stochastic Bayesian calibration. It is shown that the Bayesian calibration performed better and reduced the variance of unknown inputs. By considering the sensor error of -3%, the MBE can reduce from 4.53% to 0.25% using the Bayesian calibration instead of the deterministic method. Pavlak et al. [42] compared the traditional least-square approaches and the Bayesian inference for a gray box model. For the cases with uniform priors and noises neglected, the two methods had similar performances, whereas, for the noisy

situations, especially when the noise level is over 25%, the Bayesian inference had prior knowledge of the system and outperformed the traditional method. For the load calibration, the values of MBE performed by the conventional method and Bayesian method are 347 and -24, respectively. And for the cumulative error, the Bayesian method can reduce it from 0.869% to -0.059%. Similar conclusions were also reached by Kim and Park [43]. For the calibration of heat extraction of an AHU, the MBE calculated based on the deterministic and Bayesian method are -22.46 and 9.44, respectively. In Zhang et al.'s study [44], the calibration performance of the Bayesian inference method and GA are compared. It is found that the GA method performs worse accuracy. This may be because for the GA method, it only minimizes the explicitly defined objective functions. If a specific error metric is not included in the objective function, its calibration ability will be limited and can lead to the error metrics' poor performance. And how to define a suitable objective function is difficult. In contrast, Bayesian inference calibration calculating the conditional distribution of calibration parameters given the observations instead of an explicit optimization objective function makes a more stable performance no matter what error metrics are employed. Rouchier et al. [45] compared the forecast performance of a BEM calibrated using Bayesian inference and Kalman Filter. Results show that the Bayesian-based stochastic model is more robust and offers more reliable forecasting since parameter uncertainties are considered. These studies all highlighted the unique feature of the Bayesian inference of the inclusion of uncertainties and associated possibilities into calibrations, making it a highly promising calibration method for building energy analyses.

There existed some previous but brief introduction of Bayesian calibrations applied to the building sectors [46,47]. It was also mentioned in a review on the uncertainty analysis in building energy assessment as an inverse uncertainty quantification method [11]. In Lim and Zhai's review of stochastic modeling for building stock energy predictions, the basic theory of Bayesian inference and its application in UBEM were presented [48]. However, owing to fewer implementations at that time, the authors did not thoroughly introduce Bayesian inference applications in individual BEMs. The review may be complete but a bit general, and they did not provide details on the methods, tools, and settings of key Bayesian parameters for a regular user, so he/she still may not know how to proceed with implementation and realization. Coakley et al. [14] summarized the characteristics of the Bayesian calibration: natural incorporation of uncertainties in the calibration process, correction of model inadequacy, and the combination of multiple sources of information.

On the other hand, currently, no comprehensive and informative review study focuses on the Bayesian application specifically to building energy modeling with current development status, detailed Bayesian principles unraveled, and actual implementations through practical software tools illustrated. Adopting the Bayesian-inference-based BEM calibration is mostly hindered by the theoretical myths and the various but non-systematical options of implementation tools.

As a result, this literature review is developed under the enlightenment and belief that Bayesian inference, as an innovative calibration approach, will carry forward in the following decades in building energy simulations and other similar topics. In this review, the framework and calibration process of Bayesian calibration in building energy modeling are presented. Current research status, limitations, challenges, and future work are also discussed. Besides, for those who are interested in Bayesian statistics but without a strong mathematical/statistical background, this paper clarifies the theory and application for them. The paper is organized as follows: following the introduction, the previous studies on Bayesian calibrations of building energy fields are summarized in Section 2; then theoretical fundamentals are demonstrated schematically in Section 3; the implementation of Bayesian inference including its programming, especially by using the R language, is presented in Section 4; conclusions and identified future research work are at the end of the paper. As a critical review, many figures and tables are original contributions by default after synthesizing the information collected.

2.2   Applications

Bayesian inference is developed quickly after Kennedy and O'Hagan's publication in 2001, which illustrated a Bayesian calibration procedure of computer models [23]. One of the first applications of Bayesian inference to building modeling was presented by Heo [33]. Since then, it has gained researchers' interest in the building energy field and has been applied from building energy models to the related research field, such as occupancy behavior calibration, thermal property estimations, and sensor calibrations. This section summarized the previous studies focused on building energy calibration to the end of Sep. 2020.

During the past decade, more than 50 papers, including doctoral dissertations, journal/conference papers on building energy modeling, were found to be closely related to Bayesian inference, as summarized in Figure 2-2 and Table 2-1. The Bayesian inference was first applied to retrofit analysis and prediction of building stock energy consumption for the application domains. Later,

more research focuses on increasing the calibration accuracy using individual buildings as an example, including the improvement of the MCMC algorithm and the impact of the prior distribution, Meta-model, and informative data. Dr. Choudhary and her colleagues, Dr. Heo and Dr. Tian, from the University of Cambridge, might be the most active researchers in this field. Their studies based on Bayesian inference began in 2011 and continue until now. During this period, several other researchers employed Bayesian inference through cooperation with Dr. Choudhary. Meanwhile, research teams within the University of Colorado Boulder have been focusing on this topic as well. From Figure 2-2, it is shown that EnergyPlus and R language are the most often used BEM and program environments for Bayesian inference calibration.
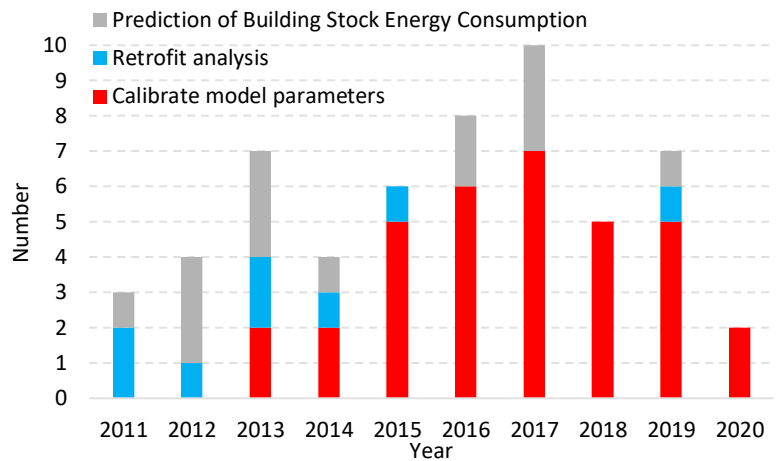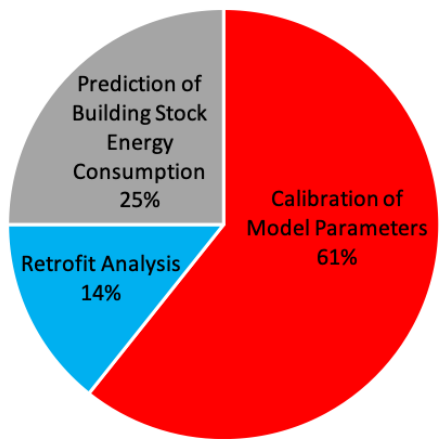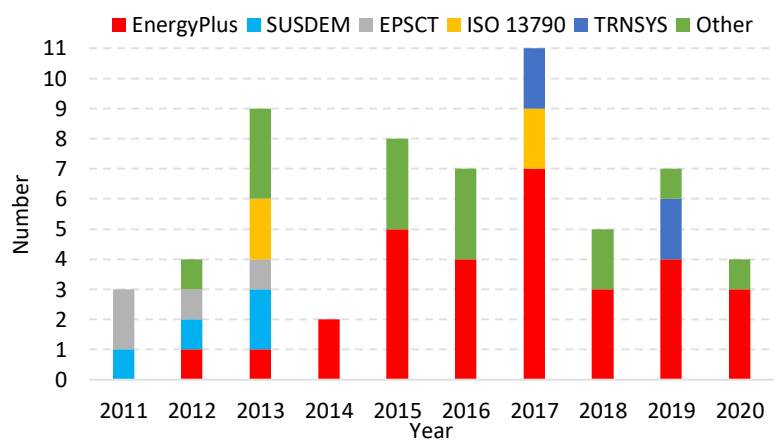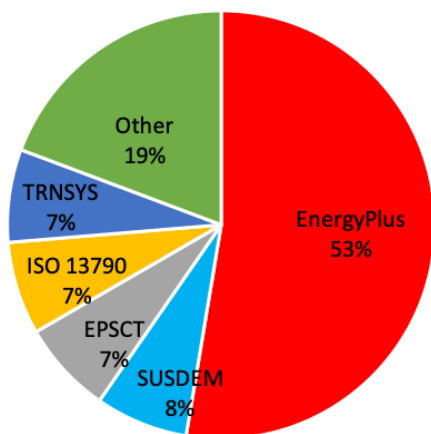
(a)

(b)
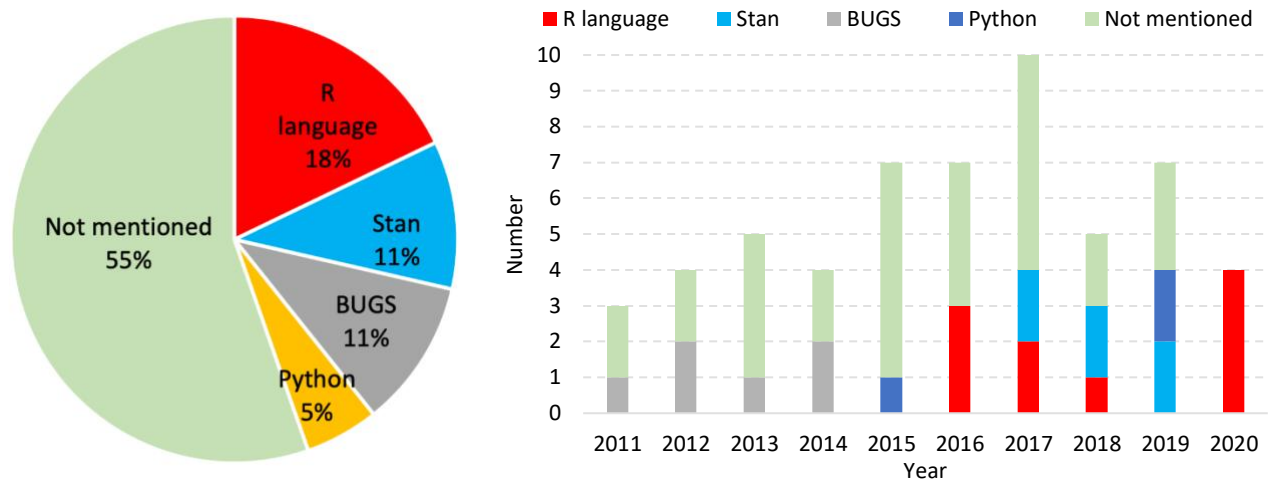
(c)

Figure 2-2 Summary of annual publications focus on Bayesian inference calibration of BEM based on different perspectives (a) application domain; (b) building simulation tool; (c) Bayesian program environment.

The most widespread application of Bayesian inference in BEM is the calibration of unknown model parameters, either continuous or discrete. Due to the concerns over computing resources and time, a sensitivity analysis is often necessary to identify the key parameters with the most significant impacts before the calibration is deployed. The key parameters will be ranked and then fed into the calibration process. Although for each calibrated parameter, the Bayesian-based calibration result is a PDF in which each value's possibility can be regarded as a degree of certainty, the mean value or mode value of the PDF is potentially improperly considered as calibrated results by some researchers and used to calculate the calibration tolerance criteria such as CVRMSE and conduct further study. This utilization approach ignored the unique feature of Bayesian inference as a probabilistic method. From a statistic perspective, the Bayesian parameter estimation is precisely the entire posterior distribution, not a single number. Instead, it maps each unique parameter value onto a plausibility value [49].

For the application of Bayesian-based stochastic building energy models, there are two main fields: predictions of building stock energy consumption and retrofit analysis. There are two primary

approaches to applying Bayesian inference to the prediction of building stock energy consumption. For the first method [50], individual reference building models are selected, calibrated using Bayesian inference, and then aggregated for the energy prediction of the building stock. Two aggregation methods are available: in the 1st method, every posterior distribution of the representative building from the iterated Bayesian inference is combined to represent one building stock type; in the 2nd method, each distribution is used to describe a different building type. For multiple building classifications, the result for every building type is combined to represent the whole building stock. Booth et al. [51] applied this method to 35 flats in the UK by using the average daily values of measured energy consumptions as observations but not each energy consumption of the 35 units. The results showed that there were minimal discrepancies between the Bayesian calibrated model outputs and the observation data.

For the second method, combining regression analysis and Bayesian inference, the measured macro-level data (e.g., at the district, urban, national level) are used to calculate the micro-level models (e.g., at an individual building level). Booth et al. [52] leveraged the proposed method to the area of Salford in Greater Manchester, UK, containing approximately 86,400 households. Tian and Choudhary [53] applied this method to the school buildings in London, UK. In the study by Yamaguchi et al. [54] to calculate the supermarkets' energy consumption at the urban scale, it was revealed that the building insulation performance might impact significantly on the seasonal and weekly energy consumption. In contrast, its effect on annual energy use might be modest.

As the other application of stochastic models, retrofit analysis has been done in several studies. One of Heo's early studies in his Ph.D. dissertation in 2011 [33] focused on building retrofit analysis. Later, similar studies were conducted to include retrofit modeling and risk analysis for individual buildings and building stock. The energy-saving performances of different ECMs are presented with the degree of belief, based on which the risk analysis can be further conducted. This method protects the interests of ESCOs, which cannot be obtained when they are provided with a fixed minimum guaranteed saving. Booth and Choudhary [55] applied a Bayesian-calibrated stochastic model to predict the energy savings of retrofit measures of approximately 15,000 houses in the UK, considering not only the installation costs and future energy prices but also the lifetime carbon savings and increased thermal comfort. The posterior distribution was distorted when using the Meta-models instead of the original BEMs in Bayesian inference to save computing time. For

the case of MLR, the errors were within 0.71%. It was confirmed from the conclusion of Lim's study [50] that the distorted posterior distribution can be used to evaluate the effects of ECMs.

Table 2-1 Summary of publications about BEM calibration based on Bayesian inference

Author	Year	Study scope	Building Scale	Building Simulation Tool	Bayesian Program Environment	Emulator/ Surrogate	Sensitivity Analysis	Posterior Distribution Estimation	Data Resolution	Data Type	Ref.
Booth and Choudhary	2011	Calibrating a bottom-up engineering-based housing stock model	Stock	SUSDEM	BUGS: WinBUGS	MLR	N/A	Gibbs	Annual	Electricity and gas consumption	[56]
Booth et al.	2012	Prediction of stock energy consumption	Stock	SUSDEM	--	N/A	Morris	--	Daily	Electricity Consumption	[51]
Booth and Choudhary	2013	Retrofit analysis	Stock	SUSDEM	--	N/A	Morris	--	Annual	Total energy consumption	[55]
Booth et al.	2013	Prediction of stock energy consumption	Stock	CDEM; EST; SUSDEM	BUGS: WinBUGS	N/A	N/A	Gibbs	Annual	Total energy consumption	[52]
Heo	2011	Retrofit analysis	Individual	EPSCT	--	GP	Morris	Metropolis-Hastings	Monthly	Gas consumption	[33]
Heo et al.	2011	Retrofit analysis	Individual	EPSCT	--	GP	Morris	Metropolis-Hastings	Monthly	Gas consumption	[57]
Heo et al.	2012	Retrofit analysis	Individual	EPSCT	--	GP	Morris	Metropolis–Hastings	Monthly	Gas consumption	[58]
Heo et al.	2013	Retrofit analysis	Individual	EPSCT	--	GP	Morris	Metropolis–Hastings	Monthly	Gas consumption	[59]

Author	Year	Topic	Scale	Model	Software	Emulator	Sensitivity	MCMC	Temporal	Output	Ref
Heo et al.	2015	Calibration efficacy under different uncertainty level	Individual	EnergyPlus	--	GP	Morris	Metropolis–Hastings	Monthly	Electricity consumption	[60]
Heo et al.	2015	Retrofit analysis	Individual	Normative model	--	GP	Morris	Metropolis–Hastings	Monthly	Total energy consumption	[61]
Tian and Choudhary	2012	Building stock energy modeling; Retrofit analysis	Stock	EnergyPlus	BUGS: OpenBUGS	N/A	SRC; MARS	Gibbs	Annual	Gas consumption	[53]
Tian et al.	2016	Identification of informative energy data	Individual	EnergyPlus	R: BRugs	MLR	SRC; RFVI	Gibbs	Monthly	Electricity consumption; Gas consumption	[62]
Choudhary	2012	Prediction of stock energy consumption	Stock	Statistic model	BUGS: WinBUGS	N/A	N/A	Gibbs	Annual	Total energy consumption	[63]
Choudhary and Tian	2014	Influence of district feature on energy consumption	Stock	Statistic model	BUGS	N/A	N/A	Gibbs	Annual	Total energy consumption	[64]
Kim et al.	2013	Performance comparison of different energy models	Individual	ISO 13790; EnergyPlus	--	GP	Morris	Metropolis-Hastings	Monthly	Electricity consumption	[65]
Kim et al.	2014	Comparison to conventional calibration method	Individual	EnergyPlus	--	GP	Morris	MAP	Daily	Gas consumption	[41]
Kim et al.	2014	Decision making of HVAC system	Individual	EnergyPlus	BUGS: WinBUGS	MLR	Morris	Gibbs	Daily	initial construction cost and total energy consumption	[66]
Kim	2015	Calibrating unknown parameters	Individual	EnergyPlus	--	GP	N/A	Hybrid Monte Carlo	Monthly	Total energy consumption	[67]

	Year	Purpose		Model	Tool	Meta-model	SA	MCMC	Resolution	Output	Ref
Kim and Park	2016	Comparison to conventional calibration method	Individual	EnergyPlus	--	GP	Morris	Metropolis–Hastings	Monthly	Heat extraction; Gas consumption	[43]
Manfren et al.	2013	Calibrating unknown parameters	Individual			GP	N/A			Electricity and gas demand	[68]
Yamaguchi et al.	2013	Prediction of stock energy consumption	Stock	Statistic model	--	N/A	N/A	--	Weekly; Annual	Energy consumption	[54]
Pavlak et al.	2014	Comparison to conventional calibration method	Individual	RC model	--	N/A	N/A	Metropolis	Hourly	Sensible zone loads and corresponding temperatures	[42]
Li et al.	2015	Calibrating unknown parameters	Individual	EnergyPlus; EPC	--	MLR	Lasso	Metropolis	Daily; Monthly	Chilled water consumption (daily), peak demand of chilled water (monthly)	[69]
Li et al.	2015	Calibrating unknown parameters	Individual	EnergyPlus	--	MLR	Lasso	Metropolis	Daily; Monthly	Chilled water consumption (daily), peak demand of chilled water (monthly)	[70]
Li et al.	2016	Comparison of different meta-models	Individual	EnergyPlus	--	MLR; GP	Lasso	Metropolis	Daily; Monthly	Chilled water consumption (daily), peak demand of chilled water (monthly)	[71]
Chong and Lam	2015	Calibrating unknown parameters	Individual	EnergyPlus	Python: PyMC	GP	None	Metropolis-Hastings	Hourly	Electricity consumption; Gas consumption	[72]
Chong and Lam	2017	Comparison of different MCMC methods	Individual	EnergyPlus	--	GP	Morris	Metropolis; Gibbs;	Hourly	Cooling energy consumption	[73]

								NUTS			
Chong et al.	2017	Selection of representative subset of the entire dataset and its performance	Individual	TRNSYS; EnergyPlus	R: RStan	GP	Morris	NUTS	Hourly	Electricity consumption	[40]
Chong and Menberg	2018	Introduction of Bayesian inference	Individual	EnergyPlus	Stan	GP	Morris	NUTS	Monthly	Electricity consumption	[74]
Chong et al.	2019	Continuous-time model calibration	Individual	EnergyPlus	Stan	GP	Morris	HMC	Monthly	Electricity consumption	[75]
Henze et al.	2015	Distinguish normal and abnormal energy usage profile	Individual	Reduced-order BEM	--	N/A	None	Metropolis	Hourly	Energy end-use	[76]
Braulio-Gonzalo et al.	2016	Prediction of stock energy consumption	Stock	EnergyPlus	R	INLA	None	MCMC	Annual	Heating and cooling demand; discomfort heating and cooling hours	[77]
Kang and Krarti	2016	Calibrating unknown parameters	Individual	eQUEST	--	GP	Local sensitivity analysis	Metropolis Hastings	Monthly	Total energy consumption	[78]
Muehleisen	2016	Introduction of Bayesian inference	Individual	OpenStudio	--	--	Morris	--	Monthly	Total energy consumption	[46]
Zhao et al.	2016	Efficient energy model development at a city scale	Stock	Normative model	R	MLR	Absolute t statistic values	MCMC (coordinate directions algorithm (CDA))	Annual	Total energy consumption	[79]

Author	Year	Topic	Scale	Tool	Lang	Meta-model	Sensitivity	Method	Temporal	Output	Ref
Sokol et al.	2017	Prediction of stock energy consumption	Stock	EnergyPlus	--	N/A	N/A	Defined by authors	Monthly; Annual	Electricity consumption; Gas consumption	[80]
Kristensen et al.	2017	Performance comparison of measurements under different temporal resolution	Individual	ISO 13790:2008	--	GP	Sobol	Metropolis-Hastings	Six-hourly; daily; weekly; Monthly	District heating energy	[81]
Kristensen et al.	2017	Building clusters and building stock energy modeling	Stock	ISO 13790:2008	--	GP	Sobol	Metropolis-Hastings	Annual	District heating energy	[82]
Lim	2017	Prediction of urban-scale energy consumption; ECM analysis	Stock	EnergyPlus	R	MLR	SVI	Metropolis-Hastings	Annual	Total energy consumption	[83]
Lim and Zhai	2017	Performance comparison of different meta-models	Individual	EnergyPlus	R	MLR; NN; SVM; MARS; GP	SVI	Metropolis-Hastings	Monthly	Electricity consumption; Gas consumption	[84]
Lim and Zhai	2018	Identification of informative energy data	Individual	EnergyPlus	R	MLR	SVI	Metropolis-Hastings	Monthly	Electricity consumption; Gas consumption	[85]
Menberg et al.	2017	Calibrating unknown parameters	Individual (GSHPS)	TRNSYS	Stan	GP	Morris	NUTS	15 min	Inlet and outlet temperature of the heat pump of load side	[86]

Menberg et al.	2019	Influence of error terms in Bayesian calibration	Individual (HPS)	TRNSYS	Stan	GP	Morris	NUTS	15 min	Inlet and outlet temperatures on both load and source sides	[87]
Yuan et al.	2017	Performance of proposed posterior distribution estimation method	Individual	EnergyPlus	--	GP	Pre-defined	Gibbs; PAM	Monthly	Electricity consumption	[88]
Yuan et al.	2017	A simultaneous calibration and parameter ranking method	Individual	EnergyPlus	--	GP	GP based method	Gibbs	Monthly	Electricity consumption	[89]
Yuan et al.	2019	Retrofit analysis	Individual	EnergyPlus	--	GP	N/A	Gibbs	Annual	Total energy consumption	[90]
Raillon and Ghiaus	2018	Calibrating unknown parameters	Individual	RC model	--	GP	Predefined	Metropolis-Hastings	10 mins	Indoor temperature	[91]
Rouchier et al.	2018	Comparison to deterministic calibration method	Individual	RC model	--	N/A	Predefined	Metropolis-Hastings	Hourly	Indoor temperature and heating power	[45]
Zhang et al.	2018	Calibrating unknown parameters	Individual	EnergyPlus	R: RStan	MLR	Morris	NUTS	5 mins	Calculated heating energy consumption based on the measured radiant system inlet/outlet water temperature and water mass flow rate.	[92]
Zhang et al.	2019	HVAC control optimizing	Individual	EnergyPlus	--	GP	Morris	NUTS	Hourly	Average indoor air temperature and heating demand	[44]

Chen et al.	2019	Prediction of stock energy consumption	Stock	IES-VE	--	GP	None	--	Monthly	Heat demand	[93]
Rysanek et al.	2019	Calibrating unknown parameters	Individual	TRNSYS	Python: PyMC	N/A	--	Metropolis-Hastings	Hourly	Electricity consumption	[94]
Yi et al.	2019	Calibrating unknown parameters	Individual	EnergyPlus	Python: PyMC	ANN	None	Adaptive metropolis algorithm	Annual	Gas and electricity consumption	[95]
Ahmadi et al.	2020	Calibrating unknown parameters	Stock	Statistic model	R	N/A	N/A	--	Annual	Energy demand	[96]
Zhu et al.	2020	Calibrating unknown parameters	Individual	EnergyPlus	R	LM, SVM, MARS, BMARS, RF	Sobol	Approximate Bayesian computation	Monthly	Heating and electricity consumption	[97, 98]

Notes: "--" means the information was not mentioned.

2.3   Methodology

2.3.1   Model calibration

From a statistical perspective, a model calibration process can be expressed as [23]:

$$y(x) = \eta(x,t) + \delta(x) + \varepsilon_m \qquad (2\text{-}1)$$

where y and η are the field observation and simulation output, respectively. x represents the model input, and t represents the model parameter. $\delta(x)$ is the model error due to the model input x while ε_m is the random observation error, which is often assumed to follow a Gaussian distribution, i.e. $\varepsilon_m \sim N(0, \sigma_m{}^2)$. With the same model input x, the model parameter t can significantly affect the simulation output accuracy. The process of model calibration is about adjusting the model parameters and forcing within the margins of the uncertainties. Its objective is to obtain a model that can represent the process of interest within acceptable criteria. Note here for simplicity, we use the singular form of the parameter. In the case of many parameters, the singular form can represent the vector form of multiple parameters.

2.3.2   Bayesian Inference

As the footstone of all Bayesian statistics, Bayes' theorem was first proposed by Reverend Thomas Bayes in his doctoral dissertation [21] and can be described as:

$$Posterior = \frac{Probability\ of\ the\ data\ \times Prior}{Average\ probability\ of\ the\ data} \qquad (2\text{-}2)$$

The probability of an event is inferred based on the prior knowledge of conditions that might be related to the event. Bayesian inference is one application of Bayes' theorem and can be written as:

$$p(\theta|y) = \frac{p(y|\theta) \cdot p(\theta)}{p(y)} \propto p(y|\theta) \cdot p(\theta) \qquad (2\text{-}3)$$

where $p(\theta|y)$ is the posterior distribution of the unknown parameter θ based on known observation y. $p(y|\theta)$ is the likelihood function of observation conditional on the unknown parameter. $p(\theta)$ is the prior distribution of the unknown parameter which is the marginal probability that means it is irrespective of the outcome of another variable, and $p(y)$ is the

probability of the observation that is marginal as well to normalize $p(y|\theta)$. Therefore, the posterior probability is proportional to the product of the prior probability and the likelihood.

2.3.3 MCMC algorithm

In reality, not all problems can be solved analytically using Bayesian inference since the integrals of the likelihood can be computationally costly or are sometimes impossible to be calculated. Compared to Variational Inference, which is an optimization-based approximation method, MCMC is a sampling-based approach widely applied to building energy field to solve the parameter estimation problem with two components. One is the well-known Monte Carlo method. It is a computational algorithm to solve statistically challenging problems relying on repeated random samplings and approximate the target value (e.g., mean value) using the independent samples' results. The other is the Markov Chain method for solving a sequence of possible events in which the probability of each event depends only on the state attained in the previous event. By integrating MCMC and Bayesian inference, posterior distribution can be estimated efficiently.

Here, we developed Figure 2-3 to illustrate the Bayesian inference calibration using MCMC, which is the most important step of the Bayesian inference BEM calibration (in the next section). In the first step, a value within the proposal distribution is set arbitrarily to represent the unknown model parameter θ^1. Then combining with predefined prior distribution and Bayesian inference, the posterior probability of the unknown parameter θ^1 conditional on observations y is obtained. Then it proposes a second value θ^* random sample from the proposal distribution based on the characteristic parameter of θ^1 and repeats the procedure in the next time step. Hereto, θ^1 and θ^*, and their based $p(\theta^1|y)$ and $p(\theta^*|y)$ are obtained. An acceptance-rejection criterion is applied to determine which one moves in the right direction to approach the posterior distribution. The satisfactory sample will be regarded as θ^2, which is used in the next time step meanwhile regarded as a member of the potential posterior sampling trunk. Iterations are conducted, and the chain's convergence is checked. Finally, only randomly generated values after the convergence point apply to the statistics of the posterior distribution.
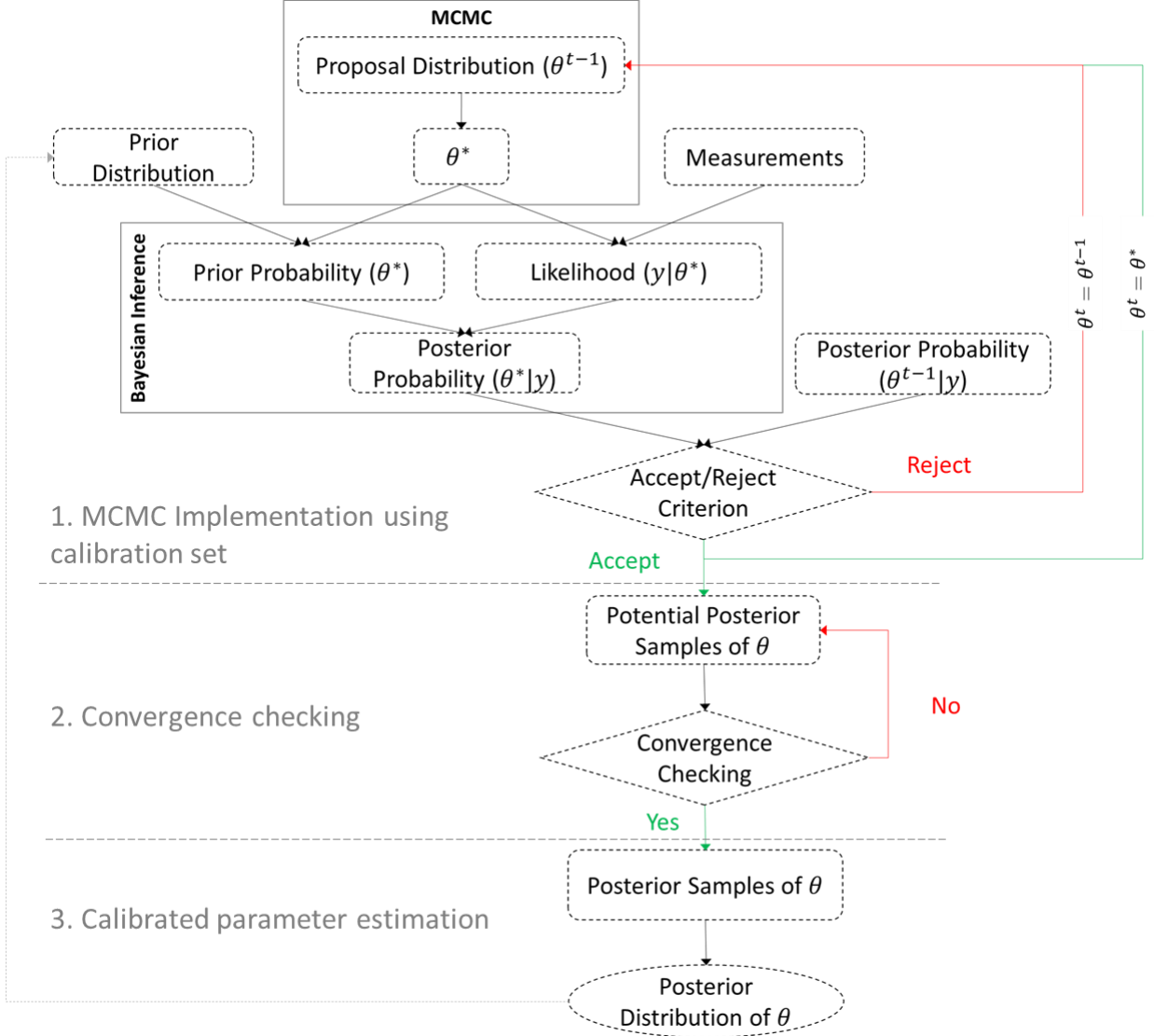
Figure 2-3 Schematic of Bayesian inference calibration using MCMC.

For the acceptance-rejection criterion, different MCMC algorithms adopt different criteria. Generally, it is classified into either a "random walking" group or a gradient-based group. Metropolis algorithm is the origin of several different algorithms for unknown posterior distributions [99]. This algorithm assumes that the sampling proposal distribution should be symmetric. Acceptance probability is defined as:

$$r = min\left\{\frac{p(\theta^*|y)}{p(\theta^{t-1}|y)}, 1\right\} \tag{2-4}$$

where θ^* is the proposal unknown model parameter.

The generated value at the t time step is determined as:

$$\theta^t = \begin{cases} \theta^*, p(\theta^*|y) > p(\theta^{t-1}|y) \\ \theta^{t-1}, others \end{cases} \tag{2-5}$$

To avoid automatically rejecting θ^*, which could be because the acceptance probability is less than one, and to allow asymmetric proposals, an advanced version of Metropolis, which is called Metropolis-Hastings [100], was developed. After the calculation of Eq. 2-4, a random value u is drawn from a Uniform distribution (0, 1) and compared to the acceptance probability r. Then Eq. 2-5 is revised as:

$$\theta^t = \begin{cases} \theta^*, u < r \\ \theta^{t-1}, others \end{cases} \tag{2-6}$$

When θ^t represents a vector, $\theta^t = [\theta_1^t, \theta_2^t, ..., \theta_n^t]$, and the sample of θ_j^t is updated according to the distribution specified by $p(\theta_j^t|\theta_1^t, ..., \theta_{j-1}^t, \theta_{j+1}^{t-1}, ..., \theta_n^{t-1})$, it features the Gibbs [100] algorithm to better estimate posterior with fewer samples.

For the gradient-based algorithm, HMC is a typical representation. It avoids the random walk behavior inherent by using the first-order gradient information to determine how it moves through the target distribution [101]. The properties of HMC allow it to converge to the target distribution more quickly for a complicated high-dimensional problem. However, HMC requires users to provide values of two hyperparameters: a step size ϵ and the number of steps L, making it difficult and time consuming to tune. To mitigate the challenges of tuning, the NUTS was developed [101]. NUTS uses a recursive algorithm to automatically tune the HMC algorithm without requiring user intervention or the time-consuming tuning runs. Studies about Bayesian inference in building energy modeling have shown that NUTS is one of the most practical and efficient sampling methods [73].

To diagnose the convergence to the posterior distribution, trace plot, trace rank plot, and Gelman-Rubin statistics are always applied, which will be illustrated in the next section.

2.4   Realization

The framework of Bayesian inference applied to the BEM calibration is detailed and shown in Figure 2-4. Note that Figure 2-4 was based on Tian et al. [62] with more details and steps: e.g., the measurement preparation was added as the first step, and the tool for each

step by the R language was included for the implementation and realization of Bayesian inference. The first step is to analyze and understand the measurement data. Then the second step is to develop the energy model for the target building. To reduce the number of calibrated model parameters and the computing cost, the third step is the parameter screening to select the most important inputs and model parameters. Prior distributions of the unknown model parameters are defined to represent parameter uncertainty. During this step, parametric simulation is conducted to create an input-output dataset used for sensitivity analysis. The fourth step of the informative data selection is optional to reduce the computing cost for better Bayesian performance. Based on the input-output dataset, a Meta-model is developed in the fifth step to replace the original BEM to save the computing time for the next step. The sixth step is the Bayesian inference of the posterior distribution based on MCMC. In the end, the seventh step is the validation and analysis of the calibrated model and parameters. The computational burden by the Bayesian inference calibration framework is heavily intensive for parameter screening, Meta-model generation, posterior estimation, and further simulation for energy prediction. Although it can be conducted in various ways, how the whole process is implemented will profoundly affect the estimation accuracy and efficiency. In the remainder of this section, each step will be illustrated in detail for the corresponding implementation based on a combination of base functions and packages of the R language [102,103]. The R language is one of the widely used statistical tools. This review shares the experiences and knowledge of using the R language as one single programming environment to fulfill the whole Bayesian calibration procedure.

Procedure	Details	Tools
1 Measurements Preparation	• Be familiar with the data and its measured situation; • Adjust the singular point; • Classify the data into calibration and validation set.	R: plot()
2 Building Energy Modeling	• Collect information about the target building; • Create the building's energy model.	EnergyPlus
3 Sensitivity Analysis	• Specify unknown model parameters and their range and distribution; • Monte Carlo simulation; • Importance rank.	R: lhs; eplus
4 Informative Data Identification	• Correlation analysis of the measurements; • Filter out the most informative measured dataset.	R: correlogram; plot.hclust()
5 Meta-Model Development	• Determine the calibrated parameters; • Build the Meta-model.	R: lm()
6 Bayesian Inference Calibration	• MCMC Implementation using calibration set; • Convergence checking; • Calibrated parameter estimation.	R: greta/coda
7 Validation & Analysis	• Validate the model using validation set; • Apply the stochastic model for further analysis.	R: eplusr

Notes: for the "Tool" column, words with brackets means the R base functions while others represent the R packages.

Figure 2-4 Procedure of Bayesian inference calibration for building energy models.

2.4.1 Step 1 - Measurements preparation

Measurement data are the target of calibration. The quality and quantity of measurements will strongly affect calibration accuracy. To be familiar with the measured data, such as the type, resolution, primary trend, and measuring conditions, should be the first step for a Bayesian modeler. Due to sensor/metering errors, unexpected events, and conditions, there often exist outlier data. Low-quality data will undoubtedly reduce the calibration performance and accuracy. Using the R base function "plot()" to visualize the measurements, these singular points can be identified and removed or adjusted accordingly.

2.4.2 Step 2 - Building energy modeling

The second step is to build the energy model based on reasonable assumptions of unknown parameters and collected building information from audits, site-visits, surveys, and design documents. A range of simulation tools include but are not limited to DOE-2 [104], EnergyPlus [12], TRNSYS [105], ESP-r [106], or user-developed models. Under the same conditions, different BEMs should attain consistent calibration results. However, the selection of a BEM should consider the model development feasibility, the calibration problem, and its further application. It is also important to select a tool suitable for parametric studies because many simulations will be conducted during the sensitivity analysis and Bayesian inference steps later. Figure 2-2 indicates that EnergyPlus is one of the most commonly used tools since its input data file can be modified as a text file for easier editing and integration with other programming environments. In addition, within the R language, there is a package "eplusr" which was designed for EnergyPlus. Therefore, EnergyPlus is introduced here.

To evaluate the impact of different energy models on the performance of Bayesian calibration for a target office building, Kim et al. [65] developed two models by using a simplified calculation method (ISO 13790) and dynamic simulation tool (EnergyPlus). It is concluded that the simplified approach can perform comparably to the dynamic model. Li et al. [69] conducted a similar study using a dynamic model (EnergyPlus) and a reduced-order model (EPC). It is demonstrated that the calculation results for EPC are better than EnergyPlus. But this may be caused by fewer calibration parameters in EPC than in EnergyPlus.

2.4.3   Step 3 - Sensitivity analysis

Ideally, with sufficient measurements and computer resources, all the uncertain parameters should be included in the calibration parameter set. The posterior distributions may still be uncertain when the data is insufficient in quantity/quality. It indicates the information provided by data is limited rather than a failure of calibration activity. Many parameters and inputs could also manifest different levels of uncertainties and significances on simulation outputs. The identification of dominant parameters cannot merely rely on arbitrary parameter selections from modelers' knowledge but should be based on a scientific process, i.e., a sensitivity analysis. Tian [107] summarized various sensitivity

analysis methods in the Bayesian inference framework and their corresponding R packages. But, how to do the parametric simulation to generate the input-output dataset used for sensitivity analysis, especially based on R, was not mentioned.

For the parametric simulation, prior distributions and ranges of selected unknown parameters should be determined first. Then MC simulation is employed to propagate simulations whose model parameters' values are randomly selected from the predefined ranges using a specific sampling method to perform simulation runs iteratively. Here, the Latin Hypercube Sampling (LHS) method [71] is recommended, which can be realized using the R "lhs" package since it provides good convergence of parameter space with relatively fewer samples. To perform the MC simulation and collect input-output dataset automatically, an R package named "eplusr" developed by Jia [108] is suggested to use EnergyPlus directly in R. "eplusr" enables programmatic navigation, modification of EnergyPlus, parametric simulations, and retrievals of outputs. The obtained input-output dataset is then employed to identify the dominant model parameters that strongly affect the outputs.

The importance ranking results may vary with different combinations of sensitivity methods and outputs depending on the variety of fundamental algorithms and conditions of each sensitivity analysis method [109]. To avoid the potential inconsistency, Lim and Zhai proposed a new sensitivity analysis method, SVI, to account for the differences in sensitivity analysis methods and target outputs [84]. Eq. 2-7 shows how SVI is applied to recognizing and comparing the importance rankings from different sensitivity analysis methods through the normalization and aggregation process.

$$\sum_{l=1}^{m} \frac{\frac{\sum_{j=1}^{k}\left(\frac{V_{i,j}}{\sum_{i=1}^{n}|V_{i,j}|}\right)}{k}}{m \cdot k} \times 100 = Sensitivity\ Value\ Index\ (SVI)\ (\%) \tag{2-7}$$

where V is the value of a sensitivity analysis method, i is a parameter, n is the total number of the parameters, j is a sensitivity method, k is the total number of sensitivity methods, l is the target output, and m is the total number of target outputs.

The most important parameter is ranked as 1, and only parameters with smaller rankings will be selected for the subsequent Bayesian inference. How many parameters and what parameters to be selected is "balancing art." It would become computationally costly to select many parameters, whereas a calibration with few parameters may not be adequate to identify the uncertainties and disclose the hidden information. It was suggested that a maximum of ten parameters be selected based on the importance ranking for acceptable performance of Bayesian inference [110].

Chong and Menberg [74] investigated the influence of the number of calibration parameters on the posterior distribution by increasing the parameter number from 2 to 6 with one resolution. They found that over-parameterization occurs, indicated by the increase of posterior uncertainty. Especially when the observations are insufficient, this phenomenon becomes obvious in Kang and Krarti's study [78], which concluded that both the CPU time and the posterior errors increased gradually as the calibrated parameter number increased.

The informative levels of prior distributions also affect the calibrated posterior results. Chong and Menberg [74] studied Bayesian inference with three levels of prior distributions (non-informative: a uniform prior; weakly informative: a normal prior with a large standard deviation; specifically informative: a normal prior with a small standard deviation). From the calibration results, it was observed that for the non-informative prior, the posterior distribution is also relatively uninformative and primarily driven by the measured data. In contrast, the result from a specific prior distribution is highly constrained, suggesting that the posterior is driven primarily by the prior, and the influence of measured data is limited. Nevertheless, the weakly informative prior shows the best performance by balancing the flat and highly informative priors.

Lim and Zhai [84] investigated the impacts of a range of prior distributions on the posterior distributions and predictions. The study was conducted using a 30% extension of the original range of uniform distributions. The results showed that the prior distribution with a narrower range performed better. By extending the range, the prior distribution becomes less informative, and its capability to generate an accurate posterior distribution is weakened.

2.4.4   Step 4 - Informative data identification

Many observation data, e.g., monthly/annual building energy usage data and hourly/weekly indoor thermal conditions, can be collected through site visits and sub-metering. It may be beneficial for more accurate calibration results to include many measurements, which may result in high computing costs in the meantime [81,85]. Therefore, it is essential to analyze and understand the collected information deeper through correlation analysis and hierarchical clustering methods by using the R "correlogram" package and "plot.hclust()" base function. It is shown that by the classification of the collected information, the informative data from different groups led to reliable results at low computing cost [62,85].

2.4.5   Step 5 - Meta -model development

In building energy modeling, many models are developed, including white-box, black-box, and gray-box models. Many of these models are quite complicated and could make computing expensive when applied to Bayesian calibrations [84]. For example, it was estimated that if a DOE reference medium office building developed using EnergyPlus used in the MCMC process that 100,000 iteration number was used, the computing time might exceed 70 days [84]. One solution is to use a Meta-model, or a surrogate model, which is a simplified representation or approximation of the computer model but with lower computing costs and acceptable accuracy. The Meta-model is often developed as the correlation based on the input-output dataset. Six Meta-models are often used in building energy and system analysis: MLR [68,70,79,80], NN [111–113], SVM [114], MARS [115], GP [47,68,79,115,116], and PR [80]. Their implementation in R is summarized in [84]. Table 2-1 shows that the GP emulator and MLR model are the two commonly used Meta-models. The GP model is with superior accuracy, while the computing cost could increase much with the augmentation of sample size and calibration parameters [71]. The MLR emulator is a relatively simpler and faster model with a lower overfitting risk when many parameter variations are involved [110].

The following statistical criteria can be used to define the performance of a Meta-model:

Coefficient of determination (R2):

$$R^2 = 1 - \frac{\sum_{i=1}^{n}(\hat{y}_i - \bar{y})^2}{\sum_{i=1}^{n}(y_i - \bar{y})^2} \tag{2-8}$$

where $\hat{y}_i$ is a predicted variable value for period i, y_i is an observed value for period i, $\bar{y}$ is the mean of the observed value, and n is the sample size.

RMSE:

$$RMSE = \sqrt{\frac{\sum_{i=1}^{n}(y_i - \hat{y}_i)^2}{n}} \tag{2-9}$$

CVRMSE:

$$CVRMSE = \frac{RMSE}{\bar{y}} \tag{2-10}$$

In Kang and Krarti's study [78], by utilizing a Meta-model instead of the actual building energy model to estimate two unknown input parameter values, the CPU time reduced from 40 hours to just 5 minutes at a marginal loss of accuracy.

To analyze the Meta-model's influence on Bayesian calibration, Lim and Zhai [84] researched a total of five types of Meta-model: MLR, NN, SVM, MARS, GPE using 100 training samples. For the first four Meta-models, their developing time ranges from 0.05 seconds to 4.03 seconds, among which the MLR model is the fastest one. While generating a GP emulator, it took almost 20 mins. The accuracy rankings of five meta-models differ for each monthly energy model. Using averages of absolute errors for 100 testing data as the index shows that the GP is the most accurate while the MLR is the least accurate. The non-linear model performs better than the linear model (MLR) due to its inherent limitation to represent the non-linear complex building energy model. For the MCMC with 100,000 chains, MLR was the fastest one (2.2 mins), while GP took about 48.2 hrs. For the posterior distribution accuracy, the GP is the best one, while MLR is the worst one, but it still is accepted.

Li et al. [71] developed three MLR models as the emulator to optimize prediction performance. For a linear-main (LM) emulator, only the significant main effects are included. For a linear-interaction (LI) emulator, both significant main effects and interaction effects are considered. Based on the LI emulator, quadratic effects are

considered in the linear-quadratic (LQ) emulator as well. Results show that the performance of LQ is quite close to GP, which could provide the most informative posterior distribution, while the posterior distribution based on LM is less informative. But for the normal MBE estimation, the LM performance is as good as a GP, and LI is the best selection based on the CVRMSE.

2.4.6   Step 6 - Bayesian calibration

This step is to apply the actual Bayesian inference to calibrate the unknown key parameters based on the Meta-model developed in the previous step. This is implemented through MCMC [117] for saving computing time, and several common MCMC algorithms and the fundamental theory were introduced in an earlier section. To study the effectiveness of three different MCMC algorithms: Metropolis, Gibbs sampling, and NUTS, Chong and Lam [73] diagnosed their convergence performance. It was found that NUTS can achieve adequate convergence to the posterior distribution the fastest, with a significantly reduced number of iterations. An improved Metropolis-Hastings algorithm was proposed in Ref. [91] by using gradient and second-order Metropolis-Hastings to improve the algorithm's tuning. In two calibration cases of 18 and 19 unknown parameters, the proposed algorithm was more robust than the conventional Metropolis-Hastings.

To diagnose the convergence to the posterior distribution, trace plot, trace rank plot, and Gelman-Rubin statistics are always applied. A trace plot merely plots the samples in sequential order, joined by a line. The trace plot of each parameter is often the first task for an analyst to diagnose common problems. A healthy chain typically has three features: stationarity, good mixing, and convergence. For stationarity, it is defined when the mean value of the chain is quite stable from beginning to end. Good mixing means that the chain rapidly zig-zags around to explore the full region. Convergence means that when more than one chains are used, multiple independent chains stick around the same region of high probability. An example of an effective trace plot is shown in Figure 2-5a.

When many chains are employed in Bayesian inference, it is hard to read trace plots since chain traces are overlapped, so some pathologies in some chains are hidden. In this situation, the trace rank plot or trank plot is a better way to visualize the chains by plotting the ranked samples' distribution. The lowest sample gets rank "1". It is stacked histograms

of ranked samples. In a "healthy" chain, these histograms should be reasonably uniform, without significant chain spiking above or below the others, like Figure 2-5b.

<table>
<tr><td>(a)</td><td>(b)</td></tr>
</table>
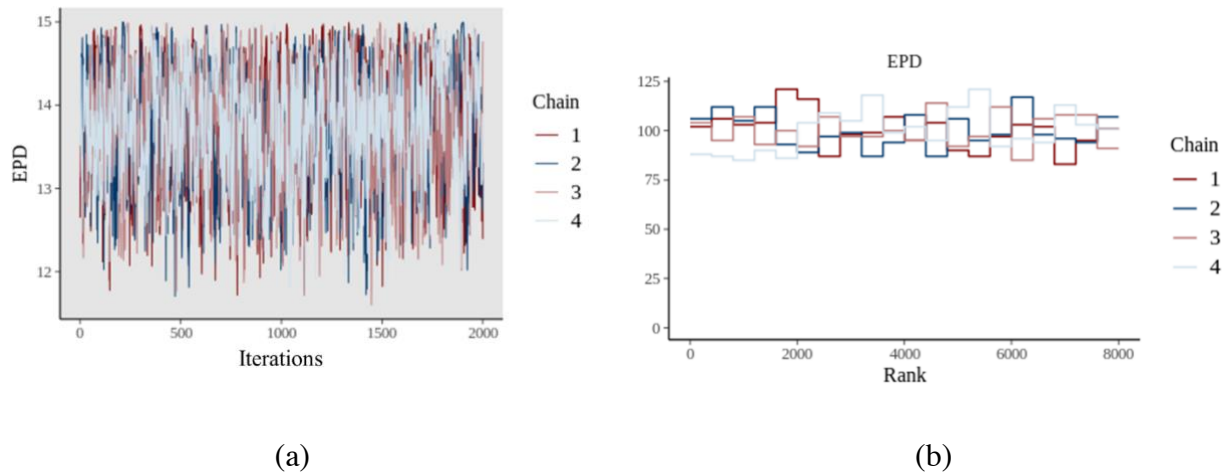
Figure 2-5 Examples of (a) trace plot; (b) trace rank plot.

Moreover, Gelman-Rubin statistics ($\hat{R}$) is often applied in diagnosing the convergence of the Markov Chain. $\hat{R}$ is the ratio of between-chain variance to within-chain variance, which is based on the concept that, if multiple chains have converged, there should be little variability between and within the chains. For convergence, $\hat{R}$ should be approximately 1 ± 0.1 [73].

Several software MCMC packages have been developed since 1997, including the initial release of WinBUGS [118], one version of BUGS, a software package for performing Bayesian Inference Using Gibbs Sampling, before which new users had to create everything from scratch. WinBUGS is stable and still available but will not be further developed. OpenBUGS [119] is another version of BUGS, which will be developed further. Another early and preferred programming environment is Stan [120], featured by probability models, inference algorithms for model fitting and predictions, and posterior analysis. However, these three packages do not use general programming languages such as Python, so users must first learn their specialized programming language. In R, an abundance of packages was developed for the MCMC estimation. Some of them are the interfaces to specific software tools like RStan [121] and BRugs [122], while others are independent R packages without the need to understand any other language like Stan and BUGS. But some packages are designed with limited capability, e.g., only applicable for

GP. Two elegant R packages are recommended here. The first one is "greta" [123], which uses Google TensorFlow directly in R. Simple examples and explanations are shown on its website to provide a straightforward way for beginners to build their own MCMC models. A plot function is provided by "greta" to visualize and check the relationship between the unknown parameters in forming an MCMC model to guarantee its corrections. The package is fast, even for the massive dataset, and runs on CPU clusters and GPUs. The other suggested package is "coda" [124]. It provides functions for summarizing and plotting the output from MCMC simulations, as well as diagnostic tests of convergence to the equilibrium distribution of the Markov Chain, which is more comprehensive and suitable for intermediate users.

2.4.7 Step 7 - Validation and additional analysis

The final step of the framework of Bayesian inference in BEM is to estimate and validate the calibrated model and conduct further analysis based on the calibrated model. For the validation, there are two types of criteria: point estimation and probabilistic estimation. For point estimation, it is the same as the conventional calibration and validation method. As usual, the mean value or a mode value of the posterior distribution is selected as the representative point to do the estimation. Criteria like NMBE and CVRMSE are frequently applied, and their tolerance is shown in Table 2-2.

Table 2-2 Acceptable calibration tolerances.

Standard/Guideline	Acceptable Value [a]			
	Monthly		Hourly	
	NMBE	CVRMSE	NMBE	CVRMSE
ASHRAE Guideline 14 [125]	±5%	15%	±10%	30%
IPMVP [126]	20%	-	5%	20%
FEMP [127]	±5%	15%	±10%	30%

[a] Lower values indicate better calibration.

MBE is defined by the average of the differences of the simulated energy consumptions and the measured data for all the intervals over a given period.

$$MBE(\%) = \frac{\sum_{i=1}^{n}(y_i - \hat{y}_i)}{n} \times 100 \qquad (2\text{-}11)$$

where M is the measured kilowatt-hours or fuel consumption during the time interval, S is the simulated kilowatt-hours or fuel consumption during the same time interval.

NMBE is a normalization of the MBE index. It quantifies the MBE by dividing it by the mean of measured values ($\bar{y}$).

$$NMBE(\%) = \frac{1}{\bar{y}} \frac{\sum_{i=1}^{n}(y_i - \hat{y}_i)}{n} \times 100 \qquad (2\text{-}12)$$

For probabilistic estimation, CRPS is an index to evaluate the performance of the whole distribution. It estimates how close the predictive distributions and corresponding observations are, and has been widely used in forecast verification [128], and have also been applied to building performance predictions [129]. When the predictive distribution is obtained from the MC simulation, the score can be calculated as:

$$CRPS = E_F|Y - y| - \frac{1}{2}E_F|Y - Y'| \qquad (2\text{-}13)$$

where F is the predictive distribution of random variable Y represented by the sample set, y is a single observation, E_F is the expectation over F, Y' is an independent random variable with identical distribution as Y. This identical distribution can be obtained by random permutations of the sample set F. A larger CRPS value indicates more discrepancy between the predictive and observed distributions. More details can be found in Ref. [128].

2.5 Conclusions and Future Work

This paper has reviewed the status and development of applying Bayesian inference in calibrating BEMs. Compared with the conventional deterministic calibration methods, the advantages of Bayesian inference calibration are:

1) When the calibration measurements are qualitatively/quantitatively insufficient, for traditional methods, the estimated model parameters can be far off from their original values; however, for Bayesian calibration, since the uncertainties are considered, the calibration results are more stable and reasonable;

2) For the traditional calibration method, the results are often deterministic. While for the Bayesian inference calibration method, the results are derived from quantitative stochastic analysis and with possibilities that can be regarded as a degree of belief. The Bayesian-based calibrated model is more comprehensive and reliable in its analysis.

Since Bayesian inference is a new calibration technique, which is fundamentally different from conventional approaches, and both Bayesian inference and MCMC algorithms involve many statistics and various options during the implementation, it can be quite challenging for new users to understand its underlying theory, methodology, and implementation. The learning curve is perhaps the most critical factor limiting the adoption of Bayesian calibration. This paper helps to enlighten beginners with explanations and details to ease their learning curves and facilitate the migration from the deterministic calibration to the stochastic one. A generic procedure of Bayesian inference calibration of BEMs is summarized. The corresponding implementation for each step of the process based on the R language is detailed as well. Here is a list of the conclusions, contributions, and future work in summary:

a. Depending on different levels of reliabilities, singular measurement points exist. This kind of measurement should be removed or adjusted to ensure the proper informativity of the measurement data.

b. Under the same conditions, different BEMs should attain consistent calibration results. However, the BEM selection should consider the model development feasibility, the calibration problem, and its further application. Since many simulations are needed for sensitivity analysis and Meta-model development, the feasibility of automatic parametric simulations and the attainment of input-output datasets should be considered.

c. Prior distributions of calibrated parameters can impact the calibration results, especially when the measurement data are insufficient. Informative distributions are suggested since they can provide more information. Based on the Bayesian inference property, a pilot study is suggested in the case with uniform prior distributions. A pilot study is suggested for a Bayesian experimental design or

Bayesian model update to reduce the data collection effort and the computational load.

d. Sensitivity analysis is a crucial step for Bayesian inference calibration since the determined calibrated model parameters will be selected based on the importance of ranking. The selection of the calibration parameter number is a balancing art. Although it is suggested that the number should be less than 10, more studies should be explored owing to its insufficient application cases.

e. When the measurements are redundant, an informative data identification process can be conducted to filter out the most informative combination of different data to reduce the computing time while maintaining the calibration performance.

f. Meta-model development can be critical, and a Meta-model could reduce the computing time dramatically. It shows that the GP model is relatively more accurate but needs longer computing time. In comparison, the MLR model is simpler and more computing-efficient, and its accuracy depends on the specific calibration scenario, so how to improve MLR accuracy still needs more future work.

g. For the MCMC algorithm, currently, NUTS seems one of the preferred methods. More efficient algorithms should be explored to increase sampling efficiency further and to ensure the chains' convergence in shorter steps. Convergence checking of the chains should be done to make sure the samplers come from the posterior distribution. In addition, the parameters of the MCMC model should be appropriately set up to aid the convergence.

h. It is still an issue whether the calibrated building parameter distributions can accurately represent the real distribution. Zhao et al. [79] argued that the calibrated building parameter distributions should be regarded as the "best guess" of the real world, which is agreed by McElreath [49]. Future research should be conducted on the relationship between numerically estimated distributions and actual real-world ones. Although it may be possible to develop more accurate building energy models to reflect reality with the advancements of science and computer technology, there is a trade-off between the effort to develop the model and the added value from the increased accuracy. A balance should be maintained depending on applications and

real needs. Again, this also shows the necessity of more high-quality measurement data and more Bayesian calibrated BEMs applications in the near future.

Currently, the application of Bayesian inference to BEM calibration is still limited. There are no sufficient studies to support specific conclusions from previous studies, such as the relationship between the calibrated parameter number and the phenomenon of "over-fitting"/"over-parameterization," which means fewer/more model parameters than necessary. In addition, how to apply Bayesian inference to a BEM for a particular application can be a challenge. So more applications and demonstrations are needed to provide more examples for new users to master this technique. Also, it seems that no studies have yet compared the calibration performance using different types of BEMs (e.g., white model, gray model, and black model), especially at the urban scale. More studies are necessary not only on the improvement of Bayesian inference and MCMC algorithms from a statistical perspective but also on the strengths and weaknesses of Bayesian inference that should be explored more in the field of building energy modeling and other building-related topics.

Chanpter 3   Bayesian Inference Calibration for B uilding Energy Predictions

Building energy modeling is an effective approach to developing energy-saving solutions, and its calibration and sensitivity analysis is essential to managing uncertainties. Existing calibrations are often deterministic without uncertainties quantified. The selection of parameters for calibration may often depend on users' experiences, so a more rigorous selection process is needed. This study developed a new automated calibration platform, BIR-BEM (Bayesian Inference on R for Building Energy Model), based on the R programming language. The calibration parameters are determined by the sensitivity analysis module and the uncertainties by the Bayesian inference module. The meta-model module is developed to replace a building energy model for the Markov Chain Monte Carlo process to save computing time. The proposed platform was demonstrated by a synthetic high-rise office building and a real high-rise residential building in a hot and arid climate. The number of calibration parameters, calibration performance, and meta-model's accuracy were discussed.[2]

3.1   Introduction

In a recent report of the International Energy Outlook by the U.S. Energy Information Administration (EIA) [2], the world energy consumption is anticipated to rise by nearly 50% by 2050, and the worldwide energy-related CO_2 emissions grow at an annual average rate of 0.6% for the same period. Coupling with rapid population growth and urbanization process, and more diversified building functions, building energy consumption has increased drastically over the past decades. Many efforts have been invested in building energy savings and developing energy-efficient solutions, for which computer simulations by building energy models (BEMs) play a crucial role. The accuracy of the results of a BEM could directly determine the quality of different energy-saving measures. Generally, the BEM's accuracy can be improved from three aspects. The first one is to provide more accurate model inputs, which are limited by data availability and quality. The second is to

---

[2] This chapter has been submitted for publication in a peer-reviewed journal: Danlin Hou, Ibrahim Galal Hassan and Liangzhu (Leon) Wang (2021). "A New Bayesian Inference R Platform for Building Energy Model Calibration."

improve the simulation algorithm, which may perform better than the first one, but it may need much more effort and expertise from a modeler. The last, whereas probably the best solution, is the model calibration. Based on optimization/estimation methods available, the optimum combination of model parameters with specific model inputs can be found to align the simulation results to observations.

Model calibration can be conducted manually or automatedly [14]. A manual calibration approach relies on a user's expertise in building science and simulation and his/her knowledge about the target building. So a few key parameters are manually selected and tuned to obtain the simulation results close to the measured information from audited and monitored energy usage data. Manual calibration is, therefore, a very time-consuming, labor-intensive, and cost-expensive process. The manually calibrated model may often be questionable due to the limited expertise of the user and the complexity of the calibrated problem.

Automated calibration is commonly preferred [46,130]. It is a non-user-driven and mathematically-based process to match simulation results with measured data [15]. With the mathematical/statistical methods coded in a computer program, the calibration activity can be iterated automatically for a large batch of simulations with various combinations of parameters. The automated search process is considered complete when the calibration error rate (the difference ratio between simulation and measurement) is less than a threshold criterion or the calibration activity runs long enough to be stopped by a given time. In this case, the group of input parameters of the specific simulation with the lowest error rate is selected as the calibration results.

Currently, several calibration platforms have been developed and released. Some are embedded within a building energy simulation software, such as the DesignBuilder Optimization module [131], Parametric Analysis Tool for OpenStudio [132], and TESS Optimization Library of TRNSYS [133]. In comparison, some were designed as software to work with certain types of building energy models [134–136]. For example, the US Lawrence Berkeley National Laboratory developed a web-based platform for small-to-medium office and retail buildings in California [137]. They also extended the platform for building energy model calibration from single building to district/city scale [138,139]. For

the platform of Autotune, supercomputer-assisted generation of machine learning agents was employed to calibrate building energy models [13]. The Hydro-Québec Research Institute in Canada created ExCalibBEM as a combination of GenOpt, an optimization engine, and building performance simulation engines to process the calibration [140]. Multi-objective building optimization tool (MOBO) [141] focuses on IDA-ICE and TRNSYS models' calibration based on optimization method. Unfortunately, the calibration results of most of these platforms are often deterministic, and no uncertainty is considered. The calibration parameters can be far off from their original value when the quality/quantity of the calibration data is limited. Considering the variety of uncertainties, in reality, a BEM with probability outputs seems more intuitively reasonable. In addition, to employ the platform for calibration, users need to select calibration parameters often without a guide on selecting. So it is often that the selection has to reply on the rule of thumb and subjective decisions, which may affect the final calibration results.

As one way to interpret and quantify these uncertainties, Bayesian inference has gained broad interest recently. We have reviewed the applications of Bayesian inference to BEM calibrations and proposed a systematic Bayesian calibration procedure [142]. In fact, it remains challenging for new users to understand the underlying theory, methodology, and implementation of Bayesian inference. Some researchers shared their Bayesian calibration code to facilitate the application for new users while modifying the code developed in R [143] and Stan [144] may still be challenging for readers who are not have in-depth expertise in these programming languages [74]. In addition, the sensitivity analysis is not implemented yet, whereas it is an essential step for choosing the key parameters for calibration. In this study, a new calibration platform, BIR-BEM, was proposed for BEM calibration. A complete package including parametric simulation, sensitivity analysis, meta-model development, and Markov Chain Monte Carlo (MCMC) was developed on the R language programming platform. The comparison between the currently available calibration platforms and the proposed from this study is summarized in Table 3-1. Several platforms are still commercial, especially those for BEMs developed in TRNSYS, such as Multiopt2 and TRYOPT. Lack of parallel computing of some platforms will lead to more extended calibration computing time. Whether it can deal with discrete and continuous variables simultaneously is also one of the considerations for users. Some platforms focus

44

on one or two particular building types. BEopt [134] was developed for residential buildings. Commercial Building Energy Saver (CBES) [137]works for small/medium office and retail buildings. Opt-E-Plus [136] is limited to commercial ones. It is noted that few of them are equipped with sensitivity analysis, whose results can be used for the selection of calibration parameters. And none of the currently available platforms can develop meta-models that are used in the calibration process instead of the original BEM to reduce computing time. While for the proposed platform in this study, BIR-BEM can perform the whole calibration process starting from measurement data visualization, and be applied to all types of BEMs developed by the EnergyPlus, a free simulation software. The including sensitivity analysis module is able to determine the parameters to be calibrated. The capabilities of parallel computing and Meta-model development make major contributions to reducing the calibration computing time. By employing Bayesian inference, uncertainties are considered to avoid calibration results significantly deviating from the true values and make them more reliable.

This paper is organized as follows: the procedure of Bayesian inference calibration for BEM with the implementation is presented in Section 2. To demonstrate how to use the platform and its calibration performance, two case studies of an office building and a residential building in a hot and arid climate are illustrated in Section 3 and Section 4, respectively. To provide an insight into the relationship among calibration parameter numbers, Meta-model accuracy, calibration performance, and computational cost, we discussed these aspects in Section 5. The paper then concluded with the contributions and future work identified.

Table 3-1 Summary of building energy model calibration platform

NO.	Tool	Freeware	Parallel Computing	Variables (Discrete & Continuous)	Sensitivity Analysis	Meta-Model Development	Uncertainty Prediction	All Buildings	Free BES	Calibration Method
1	Autotune	√	--	√	x	x	x	√	√	Machine Learning
2	BEopt	√	x	x	x	x	x	x	√	Optimization
3	City Building Energy Saver (CityBES)	√	--	--	x	x	x	√	√	Pattern recognition
4	Commercial Building Energy Saver (CBES)	√	--	--	x	x	x	x	√	Hierarchy calibration
5	DesignBuilder Optimization module	x	--	√	√	x	√	√	x	Optimization
6	ExCalibBEM	√	--	√	x	x	x	√	√	Optimization (GenOpt)
7	jEPlus+EA	x	x	x	x	x	x	√	√/ x*	Optimization (Enhanced NSGA2-based algorithm)
8	Multi-objective building optimization tool (MOBO)	√	√	√	x	x	x	√	x	Optimization
9	Multiopt2	x	√	√	x	x	x	√	x	Optimization
10	Opt-E-Plus	√	x	x	x	x	x	x	√	Optimization
11	Parametric Analysis Tool (PAT)	√	--	√	x	x	x	√	√	Optimization
12	TESS Optimization Library (TRNOPT)	x	√	√	x	x	x	√	x	Optimization (GenOpt)
13	BIR-BEM	√	√	√	√	√	√	√	√	Bayesian Inference

BES: Building Energy Software.

√ means that the answer is "yes"; x means the answer is "no"; -- means that the information was not mentioned in the paper; √/ x* means that the answer is "yes" for some BESs and "no" for other BESs.

3.2   Methodology

The procedure of the proposed BIR-BEM is illustrated in Figure 3-1. The first step is measurement preparation. Modelers should be familiar with basic information of the energy data, like data type and measurement time resolution. Using the R base function "plot()" to visualize the measurements, singular points can be identified and removed or adjusted accordingly to avoid negative impacts on Bayesian inference. Then a BEM should be created for the target building based on collected/audited building information. In the third and fourth steps, unknown model parameters with ranges and distributions in practice are defined, and parametric simulations are performed to generate the input-output dataset used for sensitivity analysis in the fifth step and Meta-model development in the sixth step. Sequentially, the measurements combined with the prior distribution of the determined calibration parameters and Meta-model are fed into the Bayesian inference process using MCMC to estimate the optimal posterior distributions of the determined calibration parameters. Convergence criteria should be satisfied to ensure the MCMC results are steady and meaningful. Finally, the Bayesian inference-based stochastic BEM can be validated and further analyzed. The whole process is created using a single programming environment, R language [102,103], one of the widely used statistical tools. The implementation of each step is highlighted with blue color in Figure 3-1 Bayesian calibration procedure of the BIR-BEM platform..
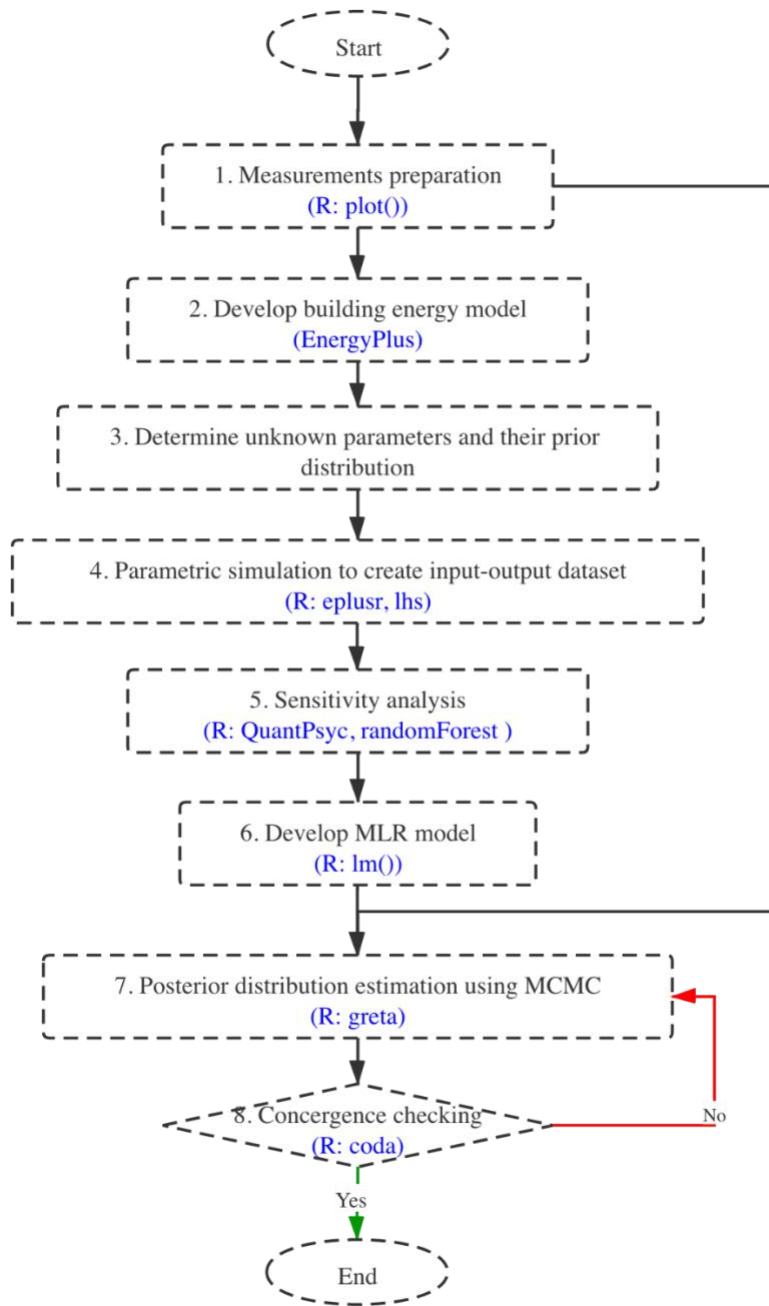
Notes: A software package that starts with R is base function from the R platform.

Figure 3-1 Bayesian calibration procedure of the BIR-BEM platform.

3.2.1 Building energy model and unknown parameters

To create the energy model for a target building, a few simulation tools are available but not limited to DOE-2 [104], EnergyPlus [12], TRNSYS [105], ESP-r [106], or user-developed models can be employed. According to previous studies, different BEMs will not significantly impact the

Bayesian inference calibration performance [65,69]. However, the feasibility of automatic conduction of the parametric simulation and extraction of the input-output dataset should be considered. EnergyPlus is one of the most popular BEMs due to its flexibility and accuracy in modeling the building and its system, so we selected it for this study. Another reason is that an R package "eplusr" is available for EnergyPlus, capable of programmatic navigation, parameter modification, parametric simulations, and retrievals of outputs [145].

Then preliminary unknown important model parameters should be selected based on users' experience or from the literature. Their distributions and ranges should be set according to building design codes/standards to ensure sensitivity analysis results in the following step are meaningful and practical. Finally, the unknown parameters and their distributions and ranges will be employed in the parametric simulation step.

3.2.2 Parametric simulation

A parametric simulation should be conducted to prepare for the input-output dataset used for sensitivity analysis and Meta-model development. A specific sampling method, the Latin Hypercube sampling (LHS) method [71], can be applied to obtaining different combinations of the selected parameters as the inputs of the BEM. This can be achieved by using the R package "lhs." The parametric simulation can be referred to as the "uncertainty propagation" and performed automatically using the R "eplusr" package, which can fulfill the input-output dataset extraction as well.

3.2.3 Sensitivity analysis

Based on the input-output dataset, dominant model parameters that strongly affect the outputs can be identified using sensitivity analysis. Tian summarized various sensitivity analysis methods [107]: Morris, Lasso, standard regression coefficient (SRC), random forest variable importance (RFVI), which have been used in the Bayesian inference framework. However, the results of the importance rank may vary with different combinations of sensitivity methods and outputs depending on the variety of fundamental algorithms and conditions for each sensitivity analysis method [109]. To avoid the potential inconsistency, Lim and Zhai proposed a new sensitivity analysis index, Sensitivity Value Index (SVI), to account for the differences in sensitivity analysis methods and target outputs [84]. Eq. 3-1 shows how SVI is applied to recognizing and comparing the importance rankings from different sensitivity analysis methods through the normalization and

aggregation process. In this study, three sensitivity analyses (SRC, RFVI, and T-value) are applied, which can be conducted using the R package "QuantPsyc" and "randomForest.

$$\sum_{l=1}^{m} \frac{\sum_{j=1}^{k}\left(\frac{v_{i,j}}{\sum_{i=1}^{n}|v_{i,j}|}\right)}{m \cdot k^2} \times 100 = Sensitivity\ Value\ Index\ (SVI)\ (\%) \tag{3-1}$$

where v is the value from a certain sensitivity analysis method, i is a model parameter, n is the total number of the parameters, j is a sensitivity method, k is the total number of sensitivity methods (k=3 in this study), l is a certain target output, and m is the total number of target outputs.

3.2.4 Meta-Model

A software tool, such as EnergyPlus, is a simulator that replicates actual phenomena. A Meta-model (also called surrogate model) is a simplified representation or approximation (i.e., an emulator) of the simulator for saving computing time. Generally, the following models can be used as Meta-model in Bayesian inference to replace original BEMs: MLR model, neural network (NN), support vector machine (SVM), multivariate adaptive regression splines (MARS), and Gaussian process emulator (GPE). Lim and Zhai [84] estimated that, when MLR was employed to represent the original EnergyPlus simulation for a case study of DOE reference medium office building, the computing time can be decreased from 70 days to 2.2 minutes for an MCMC process with 100,000 iterations using a computer with Intel Core CPU (i7-4790 3.6 GHz) and 12GB RAM. The calibration performance was still acceptable. Therefore, in this study, MLR is selected as Meta-model.

R^2 and Residual Standard Error (RSE) are used to define the performance of the Meta-model:

$$R^2 = 1 - \frac{\sum_{i=1}^{n}(\hat{y}_i - \bar{y})^2}{\sum_{i=1}^{n}(y_i - \bar{y})^2} \tag{3-2}$$

$$RSE = \sqrt{\frac{\sum_{i=1}^{n}(y_i - \hat{y}_i)^2}{n - 2}} \tag{3-3}$$

where $\hat{y}_i$ is a predicted variable value for period i, y_i is an observed value for period i, $\bar{y}$ is the mean of the observed value, n is the sample size.

3.2.5 Bayesian Inference calibration

As the footstone of all Bayesian statistics, Bayes' theorem was first proposed by Reverend Thomas Bayes in his doctoral dissertation [21] and can be described as:

$$Posterior = \frac{Probability\ of\ the\ data\ \times Prior}{Average\ probability\ of\ the\ data} \tag{3-4}$$

The probability of an event is inferred based on the prior knowledge of conditions that might be related to the event. Bayesian inference is one application of Bayes' theorem and can be written as:

$$p(\theta|y) = \frac{p(y|\theta) \cdot p(\theta)}{p(y)} \propto p(y|\theta) \cdot p(\theta) \tag{3-5}$$

where $p(\theta|y)$ is the posterior distribution of the calibration parameters θ based on the known observations y. $p(y|\theta)$ is the likelihood function of observations conditional on the unknown calibration parameters. $p(\theta)$ is the prior distribution of the unknown parameters, and $p(y)$ is the probability of the observations to normalize $p(y|\theta)$. Therefore, the posterior probability is proportional to the product of the prior probability and the likelihood.

In reality, not all problems can be solved analytically using Bayesian inference since the integrals of the likelihood can be computationally costly or sometimes impossible to calculate. MCMC is a versatile approach to solve the parameter estimation problem with two components. One is the well-known Monte Carlo method to solve statistically challenging problems by random samplings. The other is the Markov Chain method for solving a sequence of possible events, in which the probability of each event depends only on the state attained in the previous event. By integrating MCMC and Bayesian inference, posterior distribution can be estimated efficiently. Hamiltonian Monte Carlo (HMC) is an efficient MCMC algorithm. It utilizes first-order gradient information to determine how samplers should move to the target distribution [101]. This moving approach can guarantee it converge to the target distribution more quickly, especially for a complicated high-dimensional problem.

The calibration and validation performance can be assessed using two criteria: error rate (the difference ratio between calibration parameter's estimated value and its actual value) and the coefficient of variation with a root-mean-square error (CVRMSE) (Eq. 3-6).

$$CVRMSE = \frac{\sqrt{\frac{\sum_{i=1}^{n}(y_i - \hat{y}_i)^2}{n}}}{\bar{y}} \qquad \text{(3-6)}$$

3.3 Case 1: A synthetic office building

In this section, we provide the step-by-step methodology for using the BIR-BEM calibration platform. A building model was created, and primary model unknown parameters were selected to conduct the sensitivity analysis. Based on the sensitivity analysis results, the first five important unknown parameters were injected into the MLR model and then calibrated to evaluate the Bayesian calibration performance in recovering the original model.

3.3.1 Building energy model

In this study, a general office building model was developed based on the online information collected from more than 70 office buildings in Doha, Qatar, including their floor number and total floor area [146]. The model is for a 3504 m², rectangular, 31-story plus one basement office building, whose each floor was divided into five conditioned zones (four perimeters, one core) as shown in Figure 3-2. Windows are on all four facades for a window-to-wall ratio of 40%. A fan-powered variable-air-volume system provides air conditioning in the five zones. According to literature, a stand-alone cooling system applied to the BEM is typical in Qatar, with shares over 80% account of cooling demand from now until 2030, although a centralized cooling system (district cooling) is advocated [147]. A summary of the building characteristics is provided in Table 3-2. A general building energy model is selected instead of an actual building because it is impractical to obtain "true" values of model parameters for an actual building. Since this study aims to estimate the Bayesian inference calibration performance, a baseline (true values of model parameters) should be available for comparison.
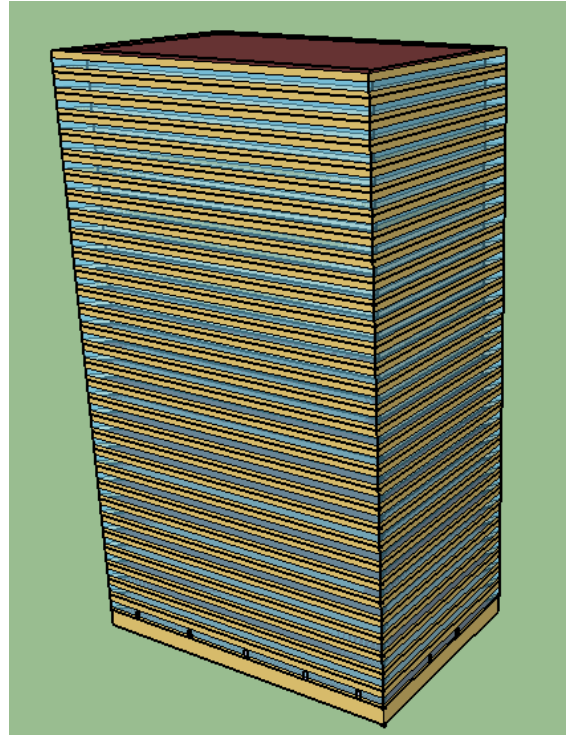
Figure 3-2 EnergyPlus model of the synthetic office building.

Table 3-2 Main features of the office building.

Component	Item	Parameters	Unit
Envelop	Floor area	3504 (73 × 48)	m^2
	Number of floors	31 (plus basement)	-
	Window-to-wall ratio	40% of above-grade gross walls	-
	Thermal zoning	Four perimeter zones and one core zone of each floor	-
Internal heat gains	Lighting power density	See Table 3-3	W/ m^2
	Equipment power density	See Table 3-3	W/ m^2
	Occupancy density	See Table 3-3	m^2/person
	Hourly schedules for heating and cooling	Default setting of DOE reference office building	-

	setpoint, occupants, lights, and equipment	
HVAC system	System type	VAV
	Heating type	Gas boiler
	Cooling type	Electric chiller

3.3.2 Calibration parameters

The Bayesian calibration platform requires a list of calibration parameters, which are altered to calibrate the model according to the measured data provided. A primary potential calibration parameter list should be defined by the user based on their knowledge and local building standards/codes. The primary unknown parameters are defined in a *.csv file, which allows a user to define: a class, object, and field to uniquely identify any parameter in an EnergyPlus input file; distributions of uncertainty (e.g., uniform, normal, and triangular) with their key factors can also be specified in the csv file. The parametric simulation will conduct, and the sensitivity analysis results are output in another csv file.

According to ASHRAE Standard 169 [148], hot/arid areas are defined as climate zone 0B. For Doha, a coastal city in Qatar, its summer is long, hot, and humid from May to September, while winter (December, January, and February) is mild and spring (March and April) and autumn (October and November) are warm. Due to the long-period high temperatures, building thermal insulations are required more strictly in such a hot/arid area. For this experiment, a total of 14 unknown model parameters, as shown in Table 3-3, selected from previous studies are conducted for the sensitivity analysis. Their ranges mainly were collected from Qatari building design codes and their dependent international standards, such as ASHRAE standards [149–152]. To respond to the sustainable development requirements in Qatar, some parameters are adjusted to make the building more energy-saving, such as a higher cooling setpoint (typically, the value is usually between 18 ~ 20 ℃ [153]), especially during the unoccupied period. Note that the uncertainty from occupant behavior only affects the cooling/heating setpoint, and other behavior impacts are not investigated in detail due to its complexity. Initially, each parameter is set with a uniform distribution for its range.

In this study, a total of 700 parametric simulations were conducted for the sensitivity analysis according to Matala's suggestion for the LHS sampling size [154]. Based on the sensitivity

analysis results, the first several significant parameters (default value is five, users can determine the calibration parameter number based on their experience or calibration accuracy requirement) are selected to develop the MLR model and calibrated during the MCMC process.

Table 3-3 Input parameters and ranges.

Parameters	Short names	Range	Unit
Roof Insulation U-Value	RINU	0.01-0.25	$W/m^2 \cdot K$
Wall U-Value	WALU	0.01-0.3	$W/m^2 \cdot K$
Floor U-Value	FLOU	0.5-1.8	$W/m^2 \cdot K$
Window U-Value	WINU	0.01-1.8	$W/m^2 \cdot K$
Window SHGC	SHGC	0-0.2	-
Equipment power density	EPD	11-15	W/m^2
Lighting power density	LPD	5-9	W/m^2
Occupancy	OCC	15-25	m^2/person
Infiltration	INF	0-2.0e-3	$m^3/s \cdot m^2$
Ventilation	VEN	0.00047-0.00247	$m^3/s \cdot m^2$
Cooling setpoint	CSP	Occupied: 22.5-25.5; Unoccupied: 25.5-28.5	℃
Heating setpoint	HSP	Occupied: 18-22.5; Unoccupied: 15-18	℃
Chiller COP	COP	3.3-6	-
Boiler efficiency	EFF	0.8-0.98	-

3.3.3 Calibration data

Calibration data can be provided in a *.csv file with two columns. The first column serves as the Date/Time, whereas the other column contains measured data from that timestep. The header of the second column must correspond to an EnergyPlus output. For demonstration purposes, in this

study, a selected dataset from the testing trunk (i.e., the first test sampler) is used as the target building. The sampler's input parameters and output energy consumption are regarded as actual values of model parameters and measurements. The monthly electricity consumption was considered as the "measured" data. Sun and Redyy showed the ambiguities in using monthly data for calibration [155]. Meanwhile, many recent studies have used monthly data, especially for Bayesian inference calibration [142]. Furthermore, high-resolution data may often be preferred when they are available.

3.3.4   Running calibration

To perform the calibration, firstly, an MLR Meta-model will be developed using the calibration parameters from the sensitivity analysis results as independent variables. The MLR model will be employed during the MCMC process. MLR is selected to represent the relationship between monthly energy use intensity (EUI) and determined calibration model parameters because of its robustness and low risk of overfitting with many variations [110]. Besides, Hamiltonian Monte Carlo (HMC) sampling method [156] was used for the MCMC. Two thousand steps of the HMC algorithms on each of 4 separate chains were explored in this study to make a total of 8000 samplers. One thousand samples were used during the "warming-up" stage to move chains toward the highest density area and tune sampler hyperparameters.

3.3.5   Results

3.3.5.1   Energy consumption

Instead of employing a typical meteorological year (TMY) file for EnergyPlus simulation, measured hourly outdoor air dry-bulb temperatures in 2018 and 2019 were applied to the calibration and validation, respectively (Figure 3-3). In this way, the calibrated model can be more robust by considering the weather impacts from different sources. Parametric simulations using 2018 weather data are conducted to generate an input-output dataset for sensitivity analysis and MLR development. Hourly percentage of outdoor air dry-bulb temperature ranges is presented in Figure 3-4. It is shown that the highest temperature is 47.2 ℃ in 2018 and 47.7 ℃ in 2019. During the whole year, almost 8% hourly percentage of temperatures are higher than 40 ℃ while the hourly percentage of temperatures less than 25 ℃ is about 30% ~ 35%.
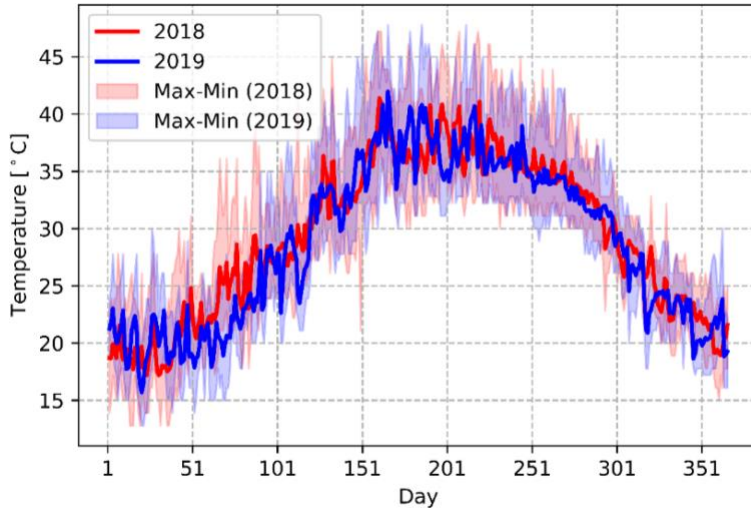
Figure 3-3 Hourly outdoor air dry-bulb temperature of Doha, Qatar.

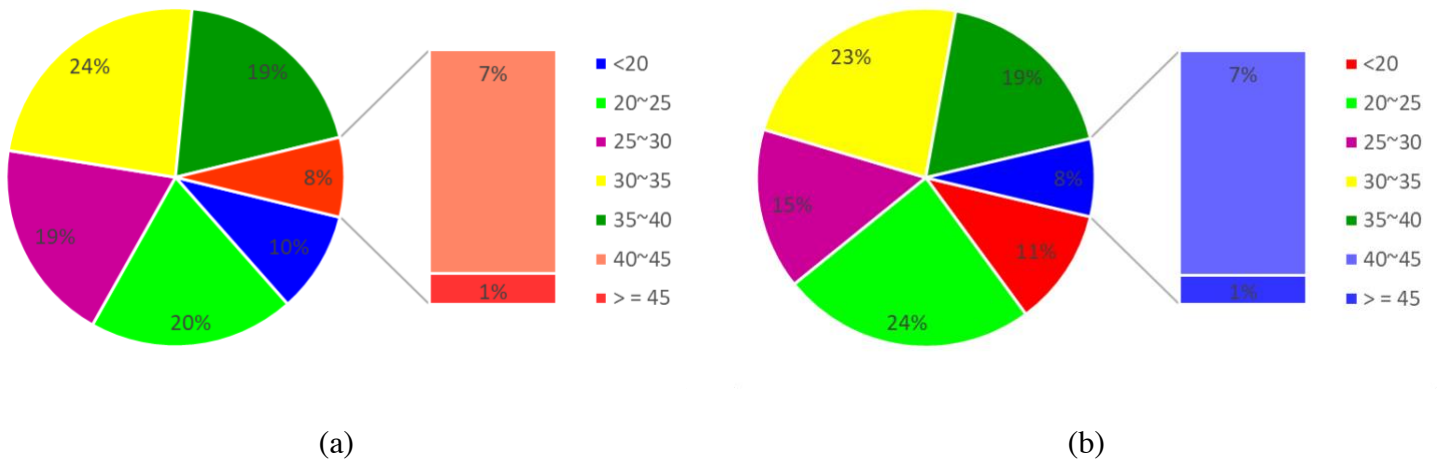(a)   (b)

Figure 3-4 Percentage of hours of outdoor air dry-bulb temperature of Doha, Qatar in (a) Year: 2018; and (b) Year: 2019).

Figure 3-5 shows the monthly EUI for the total 700 samplers and their average values. The EUI (MJ/m²) for electricity and gas were used as energy performance indicators. The electricity usage is dominant for the office building due to the enormous electric office supplies and long-term cooling model operation with electric chillers. The gas fluctuation caused by the uncertainty propagation of heating setpoint and boiler efficiency is unnoticeable since most of the gas consumption is used for domestic hot water service, and the heating hours are rare in hot/arid areas.
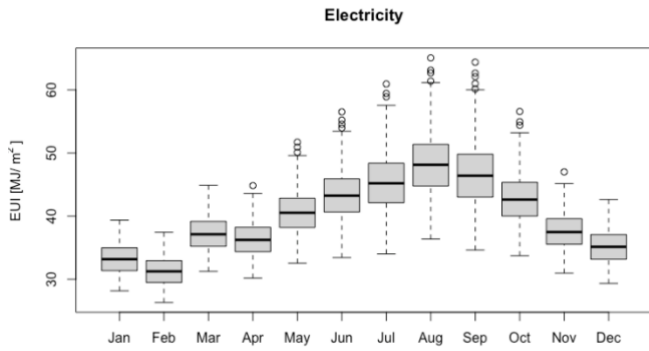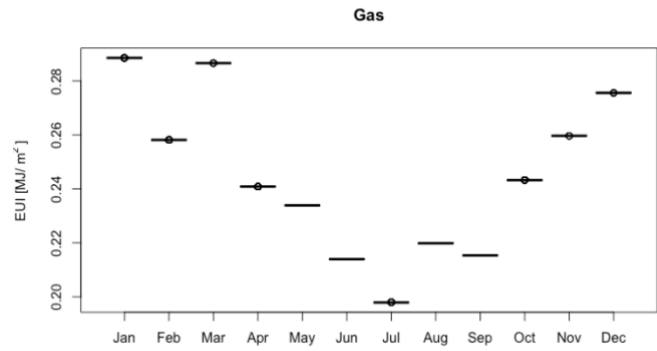
| (a) | (b) |

Figure 3-5 Monthly energy consumption (2018).

3.3.5.2   Sensitivity analysis results

Table 3-4 shows the sensitivity analysis results with the importance ranks based on the annual total energy consumptions. As described in Section 2, the SVI considers different results from three sensitivity analysis methods (SRC, Random forest variable importance, and T-value). The most important parameter for the annual total energy consumption is ranked as 1. It is found that, for the office building in hot/arid areas, the most dominant parameters are EPD, COP, INF, CSP, and SHGC. Equipment consumes significant electricity in an office building, and COP and cooling setpoint are two key parameters of an air conditioning system operating for long periods during the year. Fresh air infiltration and solar heat gain account for a large portion of the cooling load as well. According to ASHRAE Standards 90.1-2019 [150], the requirements for the envelopes of buildings in climate zone 0B are pretty high, as shown by low U-Values, e.g., the wall U-Values are almost half of those in warmer climate zone 3. As a result, the envelop parameters are not crucial due to their insignificant contribution to the total cooling energy demand. Since the heating period in Doha is very short, the heating setpoint and boiler efficiency are the least important parameters for hot/arid areas.

Table 3-4 SVI calculation and importance ranking based on annual total energy.

Parameter	Short Name	Sensitivity Analysis Method			SVI	Ranking
		SRC	Random Forest	T-value		
Equipment power density	EPD	0.7	145.6	155.0	33.6	1
Chiller COP	COP	-0.6	119.6	-129.1	27.8	2
Infiltration	INF	0.3	59.5	70.0	14.6	3
Cooling setpoint	CSP	-0.2	21.1	-40.6	7.3	4
Window SHGC	SHGC	0.1	16.1	33.8	6.0	5
Occupancy	OCC	-0.1	14.1	-31.5	5.5	6
Ventilation	VEN	0.1	5.0	17.5	2.8	7
Lighting power density	LPD	0.2E-1	-1.7	5.3	0.9	8
Wall U-Value	WALU	0.1E-1	0.3	2.9	0.4	9
Roof Insulation U-Value	RINU	0.6E-2	1.6	1.4	0.3	10
Floor U-Value	FLOU	0.2E-2	-2.1	-0.5	0.3	11
Boiler efficiency	EFF	6.5E-3	0.5	1.5	0.2	12
Window U-Value	WINU	5.8E-4	-1.6	0.1	0.2	13
Heating setpoint	HSP	5.7E-4	0.6	0.1	0.1	14

To further explore the importance rank results based on monthly total energy consumption and whether it is consistent with the results based on annual total energy consumption, the sensitivity analysis process was repeated for each month, and the results of importance rank are summarized in Figure 3-6. Owing to the weather characteristic of Doha, Qatar, where summer is scorching and lasts almost six months, the other three seasons are warm and mild, the importance rank results of most parameters are relatively stable. For most of the parameters, the result trends are similar to the annual total consumption. It is noted that, for the INF parameter, the importance rank varied significantly in different months. From May to October, the importance rank is lower, which shows it has a high impact on building energy consumption, while for other months, the impact becomes weaker. This can be explained by the variation of monthly outdoor air temperature. During summer, the outdoor air temperature could become unbearable; the outdoor air through infiltration can cause high cooling loads. During other seasons, especially in winter, the outdoor air temperature is mild, and the cooling energy consumption for the infiltration load reduces.
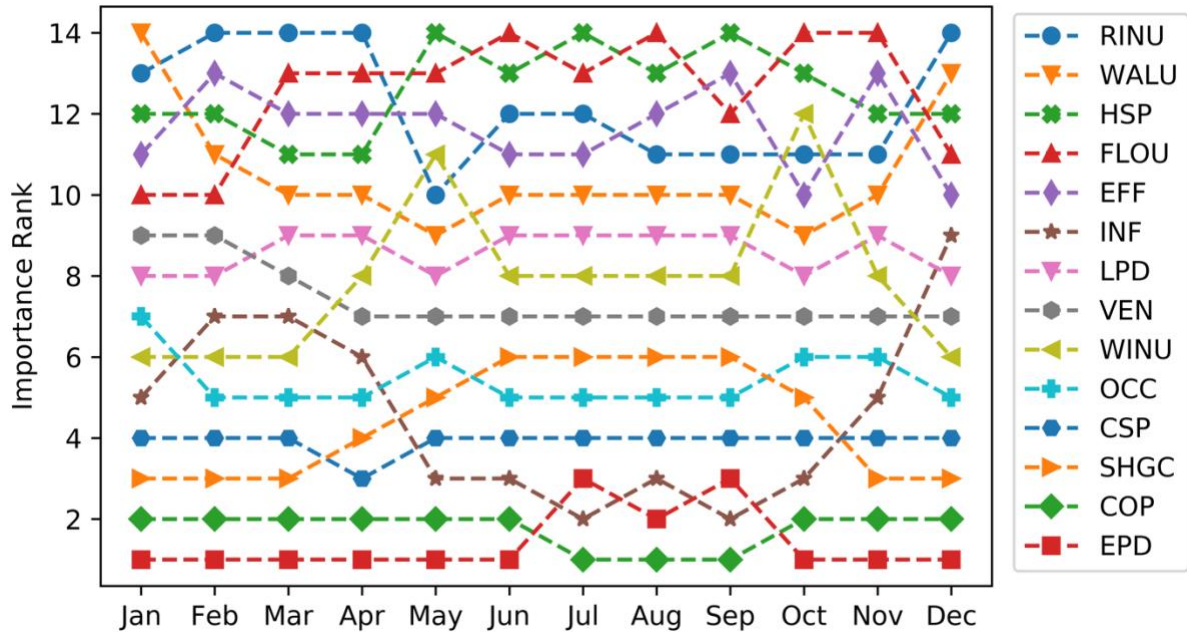
Figure 3-6 Importance rank results based on monthly total energy consumption.

3.3.5.3 Regression analysis

The results of the five calibration parameters are selected since the optimal calibration parameter number is five. The reason will be discussed in Section 5. The MLR model was selected as the Meta-model to replace the original EnergyPlus model. Generally, BEMs have complex and nonlinear characteristics, so using a linear model can yield significant errors. However, undeniably, building energy consumption is highly correlated to weather data. When MLR is applied for regression of monthly energy consumption and dominant model parameters, the training and testing accuracy is acceptable, as shown in Figure 3-7. The average monthly R^2 values of the training set and testing set are 0.94 and 0.94, respectively. Similar conclusions have been confirmed by Lim and Zhai [85]. Residual standard errors are 0.39 for training and test datasets.
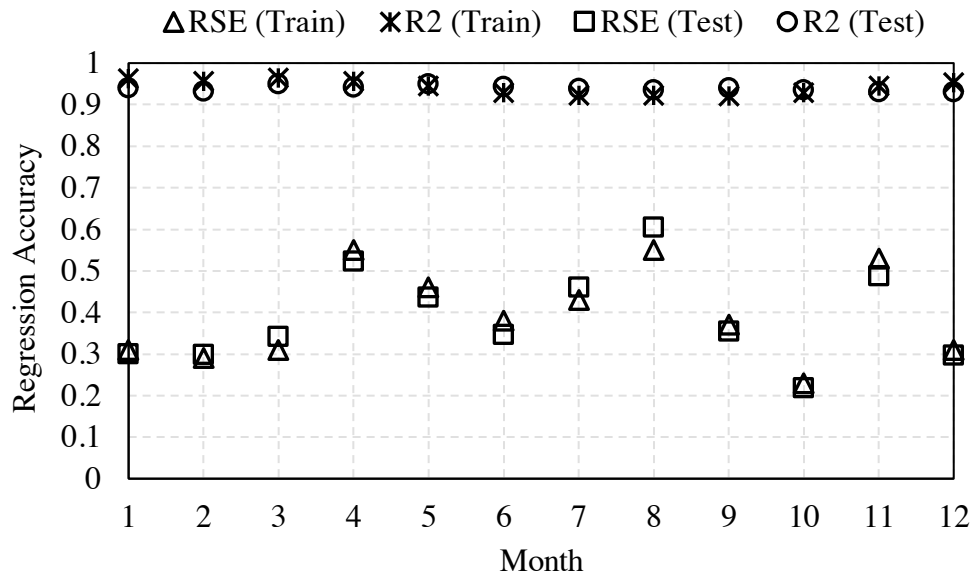
Figure 3-7 Results of regression analysis (Case 1).

3.3.5.4 Bayesian inference calibration

3.3.5.4.1 Convergence

To diagnose the convergence achievement for the posterior distribution, trace plots and Gelman-Rubin statistics were applied. A trace plot plots the samplers in sequential order, joined by a line, and it is the first and the best way to diagnose common problems for an analyst. Figure 3-8 shows the sample trace of a total of five calibration model parameters. For each parameter, the chains are mixed with each other well to be stationary and convergent, which indicates that the MCMC posterior distribution reached the convergence. A detailed trace plot of EPD is included in the figure as well.
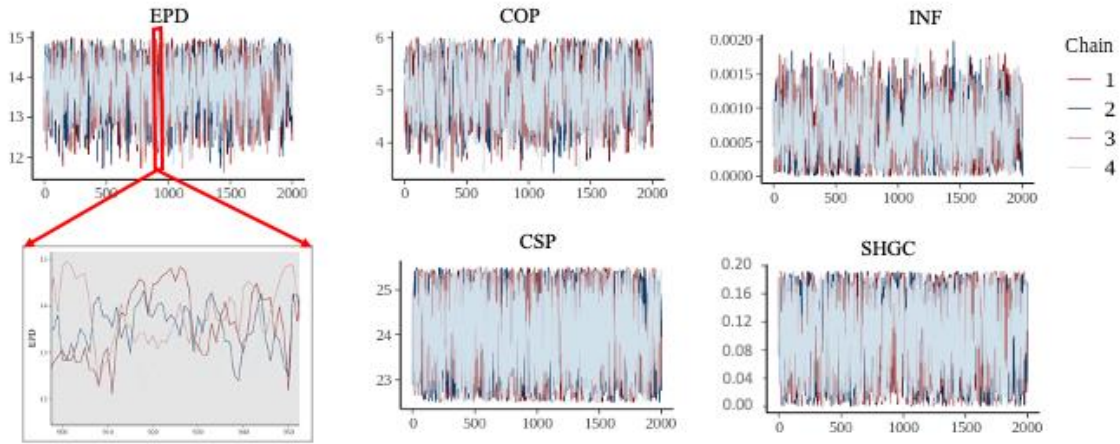
Figure 3-8 Trace plot of the calibration parameters: entire iterations of the fourth chain with detailed trace plot of equipment power density trace.

The Gelman-Rubin $\hat{R}$ evaluates the MCMC convergence by comparing the estimated between-chains and within-chain variances for each model parameter. Large Gelman-Rubin $\hat{R}$ values indicate a divergence. For a converged posterior distribution, $\hat{R}$ should be smaller than 1.1. The evolution of $\hat{R}$ of each parameter is shown in Figure 3-9. The $\hat{R}$ values of the parameters are between 1.00 to 1.06. The results of the trace plot and $\hat{R}$ values demonstrate that the iterations are convergent and all samples from the posterior distributions.
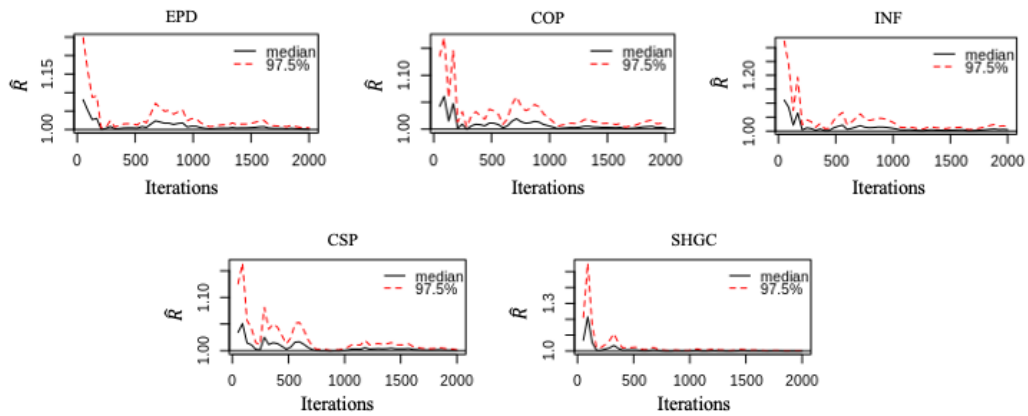

Figure 3-9 Gelman-Rubin evolution of calibration parameters.

3.3.5.4.2   Parameter estimation

The calibrated distribution of the annual total EUI is shown in Figure 3-10 (a). The dotted green line shows the measured annual total EUI of the target building, 565.4 MJ/m^2·year. The blue area is the annual total EUI distribution sampled from prior distributions of calibration model

parameters. Its confidence interval for 68% and 95% is (507.0, 590.5) and (465.2, 632.3), respectively. The dotted orange line is the mean value (549.0 MJ/m²·year) of posterior annual total EUI sampled using the posterior distributions of the calibration model parameters represented in the red area. The confidence interval of 68% and 95% of the posterior distribution of the annual total EUI are (521.8, 576.2) and (495.4, 602.6). After the Bayesian inference calibration, the standard deviation decreased to 65.3% from 41.8 to 27.3. The error rate of the annual total EUI of the measurement and the mean value of the posterior distribution is 2.9%.

The validation results are shown in Figure 3-10 (b). The measurement of annual total EUI by the red dot line is 546.8 MJ/m²·year, and the mean value of its posterior estimation in the blue line is 547.0 MJ/m²·year, and the error rate is 0.04%. The validated posterior distribution of annual total EUI is shown in the green area, and its confidence interval of 68% and 95% are colored by purple and orange (521.4, 576.1) and (494.9, 602.7), respectively.
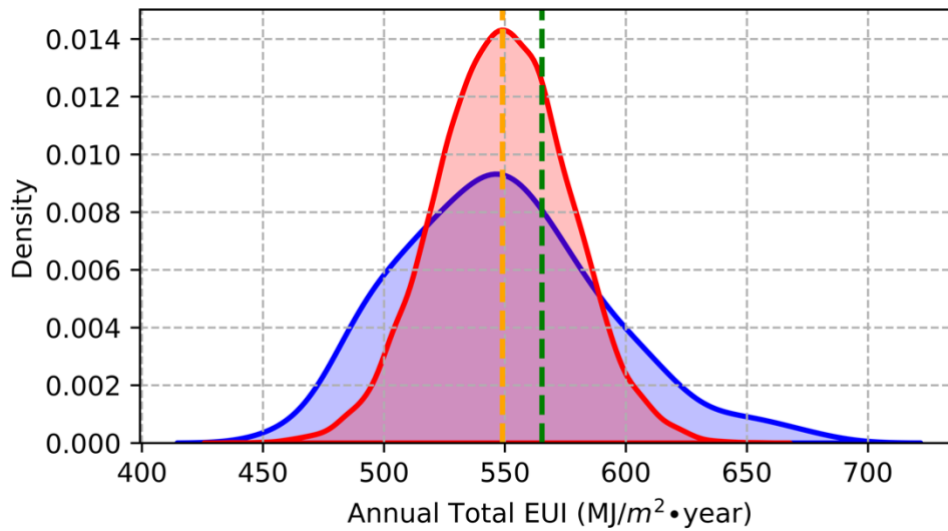
(a)
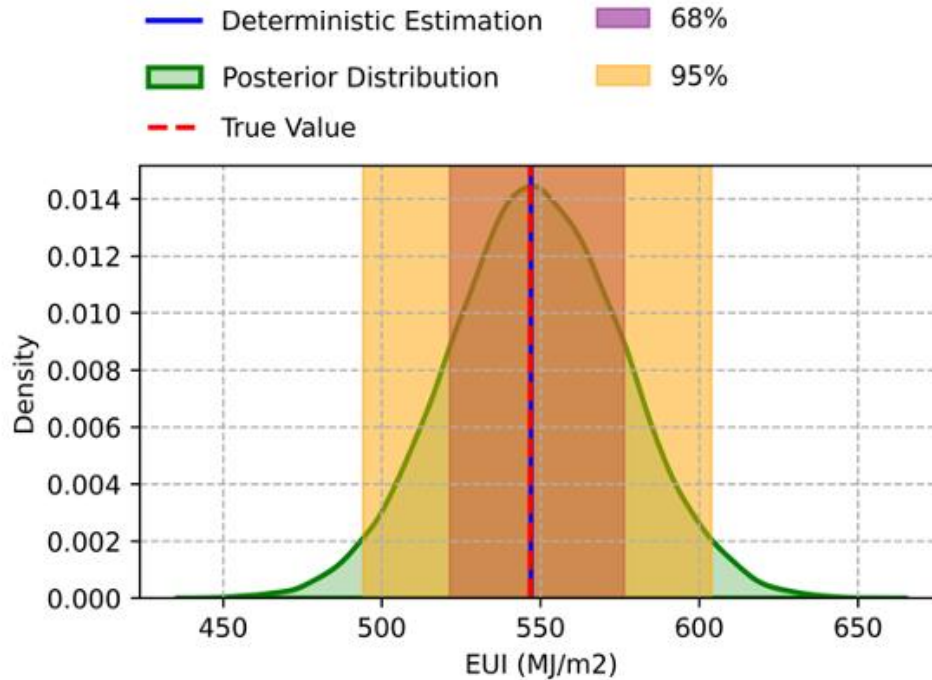
(b)

Figure 3-10 Distributions of annual total EUI.

((a): calibration using 2018 weather data; (b): validation using 2019 weather data)

The CVRMSE values of the monthly total EUI are illustrated in Figure 3-16. The calibration CVRMSE is 0.6%, and the validation CVRMSE is 0.5%, which is reasonable considering the monthly calibration tolerance of 15% required by ASHRAE Guideline 14 [125] and FEMP [127].

The distributions of five unknown parameters are shown in Figure 3-15: the CPN is 5. The details in Table 3-5 show that, for the COP and CSP, the error rate is 2.2% and 0.9%, respectively. For the parameter of EPD, its error rate is 9.3%. A larger range may cause this relatively higher error value. While for the INF, its error rate is 9.0%. For window SHGC, the error is 4.2%.

Table 3-5 Details about calibration parameters.

| Parameter | True Value | Prior Distribution | Posterior Distribution | | | | | | |
| | | Range with uniform distribution | Mean Value | Standard Deviation | Quantiles (%) | | | | |
					2.5	25	50	75	97.5
EPD	11.8	11-15	12.9	1.1	11.1	12.0	12.9	13.9	14.9
COP	4.5	3.3-6	4.6	0.8	3.4	4.0	4.6	5.3	5.9
INF	1.1E-3	0-2.0E-3	1.0E-3	5.8E-4	5.7E-5	5.2E-4	1.0E-3	1.5E-3	1.9E-3
CSP	22.7	22.5-28.5	22.5	0.02	22.5	22.5	22.5	22.5	22.6
WSHGC	9.6E-2	0-0.2	0.10	0.06	2.5E-3	0.04	0.09	0.15	0.19

3.4   Case 2: A real residential building

To demonstrate further the BIR-BEM calibration platform, we applied it to a real residential building. To avoid duplication, the details of how to prepare and run each module of the calibration platform are not included. However, the building information, calibration parameters, and results are shown below.

3.4.1   Calibration preparation

In this case study, a real building, Marina Tower (named "the MT" hereafter), located in Lusail city, was selected. The MT is a multi-apartment building with 19 stories (including two basements and a ground floor), as shown in Figure 3-13. The total floor area is 26,147.72 m^2. It is constructed at an orientation of 341.57 degrees from the North. The two basements are not cooled as they are used for parking. A summary of the building specifications is provided in Table 3-7. The building cooling energy is provided through a district cooling system. However, it is important to note that this study focuses on building cooling load, and due to building complexity, the HVAC system of the building was not modeled. Instead, the ideal cooling zone method was used to estimate cooling loads. The daily occupancy, equipment, and lighting power density fractions are given in Figure 3-14. They are based on ASHRAE 189.1-2009 typical schedules for apartment buildings. In this study, to demonstrate the proposed methods, the density fractions were not varied between weekdays and weekends. The same methods would be applicable when the variable density fractions can be considered. In fact, according to the information provided by the Qatar stakeholders, these constant fractions were reasonable for the study period of interest. The prior

distributions of selected calibration parameters are shown in Table 3-8. The measurements of monthly cooling consumption for the calibration are from August 2020 to July 2021.
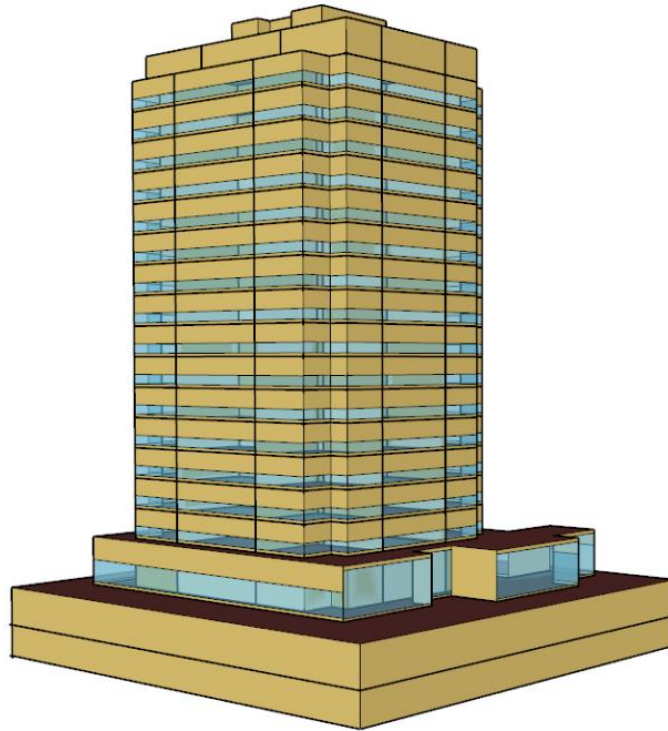

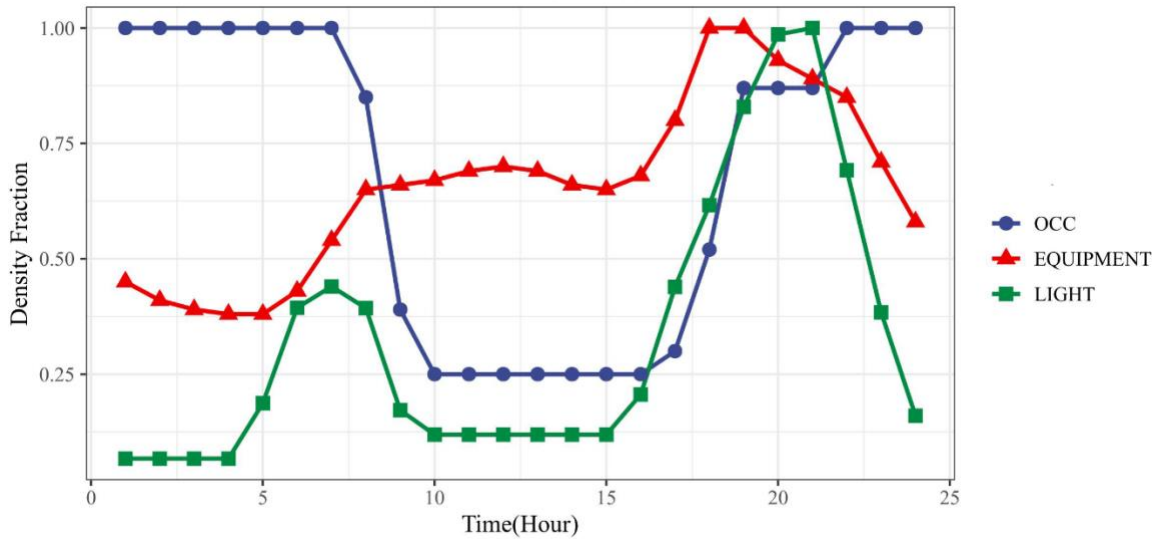Figure 3-11 EnergyPlus model of the real residential building.

Figure 3-12 Daily occupancy, lighting, and equipment density fractions.

Table 3-6 Floor plan summary.

Floor	Dimension (m×m)	Floor Height (m)	Function	WWR			
				Front	Rear	Left	Right
2nd Basement	60.70×58.33	3.9	Parking	/	/	/	/
1st Basement	60.70×58.33	4.7	Parking	/	/	/	/
Ground Floor	46.86×44.50	6.08	Lobby	46%	59%	87%	87%
Typical Floor(1st-15th)	35.80×31.50	3.8	Residential	31%	31%	32%	32%
16th Floor	35.80×23.00	4.06	Residential	31%	31%	32%	32%
Roof	21.48×11.46	3.8	Pump room & lift lobby	/	/	/	/

3.4.2 Results

Table 3-7 summarizes the prior ranges with uniform distribution of model parameters, including in the sensitivity analysis process, which was determined according to local or international building codes/standards [150,157,158]. The cooling setpoint appears to be the dominant parameter. Floor U-value, Solar reflectance of interior diffusing blinds roll, and window solar transmittance are the least influential parameters and were excluded from the further simulation. The first five important parameters are selected to use as independent variables in the MLR model and to be calibrated. Figure 3-11 shows the accuracy of the MLR Meta-Model indicated with R^2 and RES. By employing the developed MLR models in the MCMC process, the details of the posterior distributions of five calibration parameters are presented in Table 3-8.

The comparison between the simulated and measured monthly cooling consumption intensity is shown in Figure 3-12. The calculated CVRMSE is 13.95%, which is within the acceptable range of 15% based on the ASHRAE Guideline 14 and FEMP [125,127]. Compared to the previous case, the CVRMSE is higher because the measurements were collected during the COVID-19 pandemic with different occupancy profiles and schedules from those before the pandemic. The measured occupancy schedule and profile were not available due to privacy concerns. We think

the current accuracy is acceptable for demonstration purposes but could be improved further, given more measurement data.

Table 3-7 The sensitivity analysis results for the annual energy use intensity in Marina Tower.

| Parameter	Range of values	Unit	SRC	Random Forest	T-Value	SVI	Rank
Cooling setpoint	21-26	℃	0.70	165.80	168.74	31.07	1
Equipment power density	2-8	W/m²	0.39	102.19	94.47	18.05	2
Ventilation rate	0.0003–0.0006	m³/s· m²	0.36	97.07	85.95	16.75	3
Window SHGC	≤0.21	-	0.28	49.55	65.36	11.09	4
Lighting power density	3–6	W/m²	0.20	24.05	46.66	7.13	5
Infiltration rate	0.1–0.2	ACH	0.14	15.71	32.42	4.88	6
Window U-value	≤1.8	W/m²·K	0.10	15.57	22.83	3.74	7
Occupancy density	38–90	m²/person	0.09	7.54	20.99	2.98	8
Wall U-value	≤0.3	W/m²·K	0.09	3.17	20.62	2.63	9
Roof Insulation U-value	≤0.25	W/m²·K	0.02	2.13	3.90	0.60	10
Floor U-value	≤0.332	W/m²·K	0.02	0.99	3.94	0.53	11
Solar reflectance of interior diffusing blinds roll	0.4–0.8	/	0.01	0.32	3.22	0.40	12
Window Solar Transmittance	≤0.25	/	0.01	0.23	1.23	0.16	13
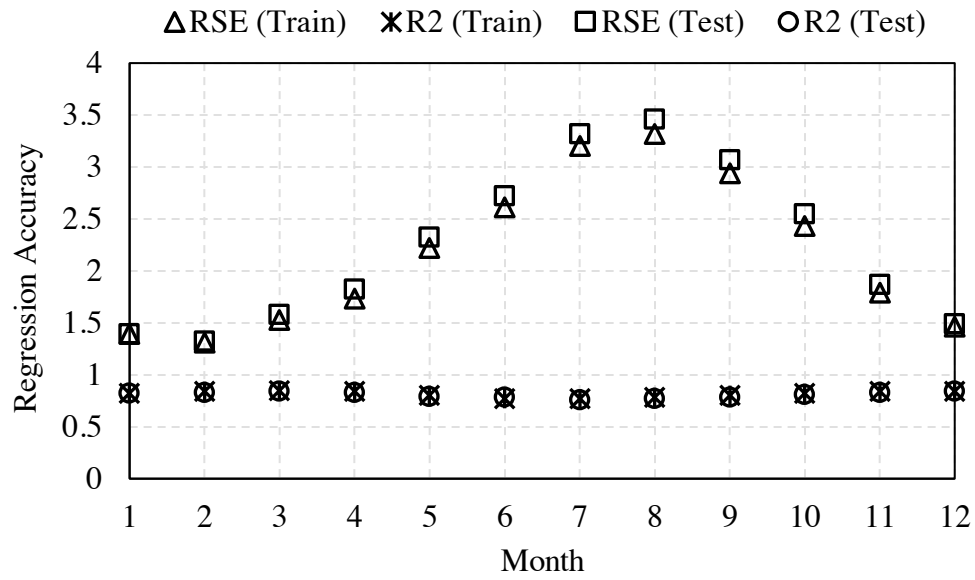
Figure 3-13 Results of regression analysis (Case 2).

Table 3-8 Posterior distributions of calibration parameters.

Parameter	Mean Value	Standard Deviation	Quantiles (%)				
			2.5	25	50	75	97.5
CSP	22.3	1.1	21.06	21.3	22.1	22.9	24.98
EPD	6.23	1.07	4.71	5.17	5.99	7.36	7.85
VEN	0.005	5.7E-5	0.000395	0.00048	0.00052	0.00058	0.000593
SHGC	0.11	0.06	0.01	0.05	0.11	0.17	0.19
LPD	4.94	1.1	3.03	4.20	5.55	5.74	5.95
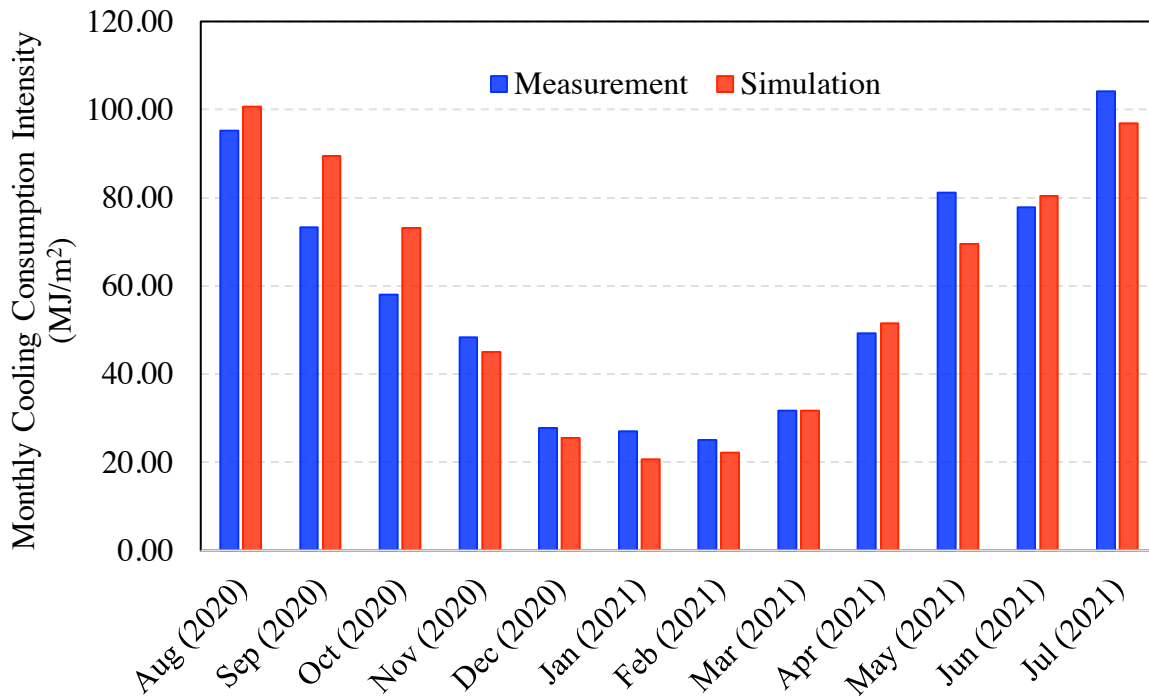
Figure 3-14 Monthly cooling energy consumption between simulations and measurement data.

3.5 Discussion

For the previous results in Section 3 and Section 4, the five calibration parameters are selected for the Bayesian inference. In this section, a comprehensive discussion about the calibration parameter number and its impact on the results of the essential steps of the Bayesian inference calibration is performed using Case 1. As suggested by Tian [110], for the Bayesian inference calibration using MLR, the calibration parameters should be less than ten. Therefore, a total of 10 cases were conducted, including different calibration parameter numbers from 1 to 10. For example, in case 3, three parameters with the most important impact are selected, namely EPD, COP, and INF, to repeat the procedure of Bayesian inference calibration. The weather data used for BEM calibration and validation and the selected sampler whose outputs are regarded as measurements maintained as constant in all 10 cases. The posterior distributions of the calibration parameters are shown in Figure 3-15. It shows that when the calibration parameter number is greater than 4, over-parameterization occurs, which means the calibration parameters are over the calibration capability. The comprehensive comparison, including MLR accuracy shown by R^2, calibration, and validation accuracy shown by CVRMSE, and computing time, were demonstrated in Figure 3-16. Please note

70

that the Gelman-Rubin values of all cases are within 1.07, which means that the MCMC iterations convergent for all cases.
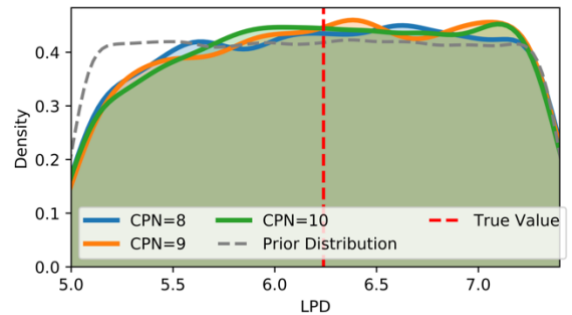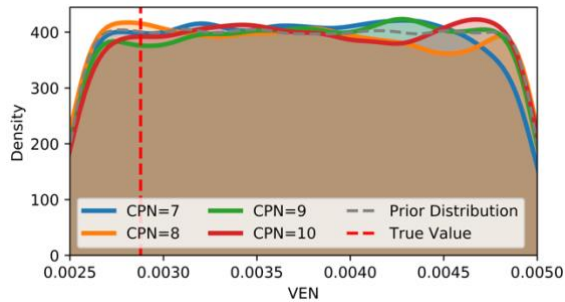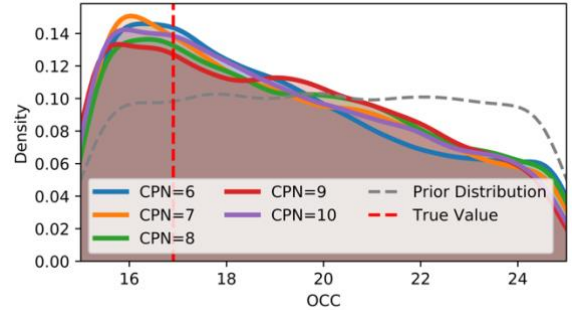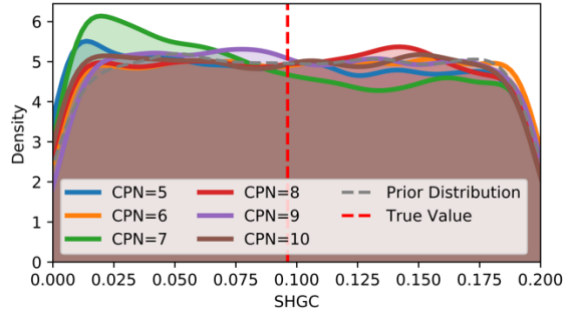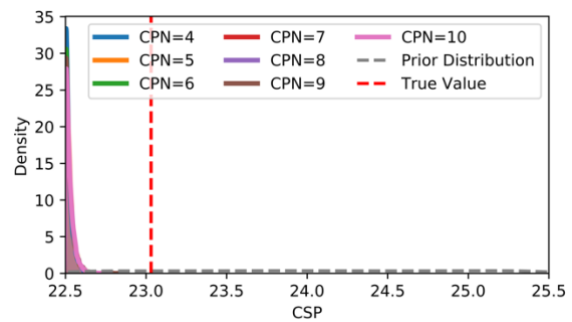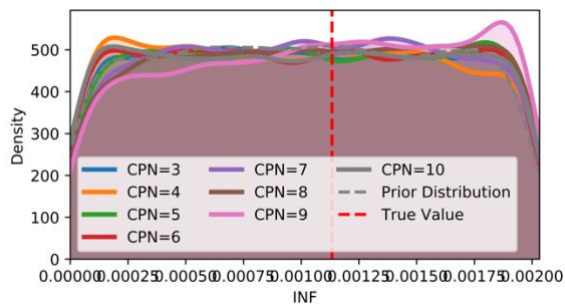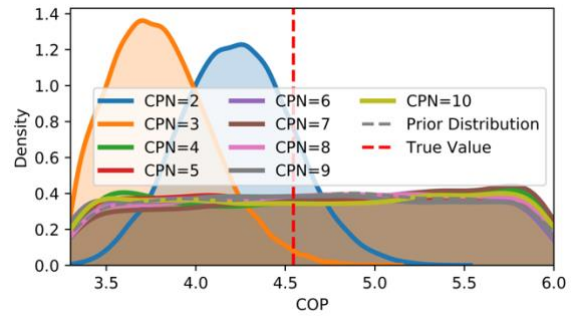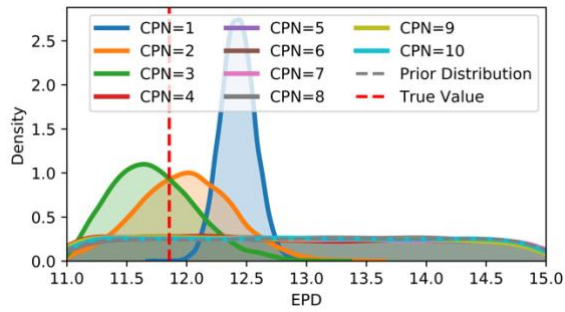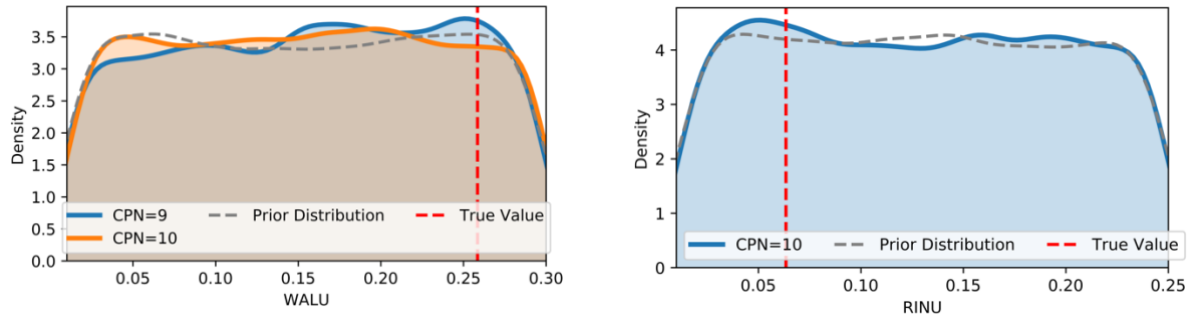
Note: CPN: calibrated parameter number.

Figure 3-15 Distribution of calibrated parameters by selecting different calibrated parameter numbers.

It shows that the relationship between the calibration parameter number and the accuracy of the MLR Meta-model seems a logarithmic pattern. When the number is less than 5, the average R^2 increases dramatically with the calibration parameter. After 5, R^2 reduces and becomes negligible after 8. Although the MLR model accuracy of the training set is slightly higher than the testing set, the trend will be disappeared with increasing the calibration parameter number. Besides, the calibration and validation performance estimated by CVRMSE was highly affected by the calibration parameter number. When the selected calibration parameter is less than 5, the accuracy of calibration and validation increases drastically, while when the calibration parameter number is greater than 5, the performance becomes stable. This observation can be explained by the Meta-model's accuracy. In MCMC, the monthly EUI computed by the MLR model was compared to the observations, searching for the optimal posterior distribution of the calibration parameter. If the Meta-model's accuracy is too low, the MCMC inference capability is limited to make the simulation data align with the measurements. When the accuracy of the Meta-model is sufficient, increasing calibration parameter numbers lead to higher calibration and validation performance. However, this impact may be negligible. Finally, without any doubt, the computing time of the MCMC process becomes longer with the increase of calibrated parameter number. The optimal calibration parameter number should be close to the intersection of CVRMSE performance and computing time with a high Meta-model accuracy and avoiding over-parameterization. Also, the optimal number should be chosen after the best results are shown. Therefore, the calibration parameter number of five seems optimal in this case.
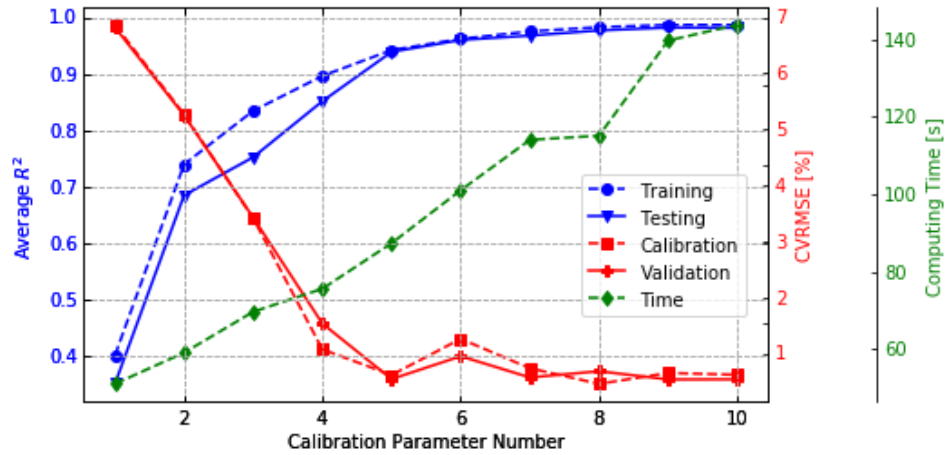
Figure 3-16 Comparison of Meta-model accuracy, calibration, validation performance, and computing time using different calibration parameter numbers.

3.6   Conclusions

In this paper, a new platform, BIR-BEM, was proposed for building energy model calibration based on Bayesian Inference. The platform was developed using the R language and provided a complete package of the programming environment for a systematic calibration process. Sensitivity analysis can also be conducted using BIR-BEM. The parameters to be calibrated can be selected from the sensitivity analysis results or user-defined. Compared to the conventional calibration platform, the Meta-model is developed and used in the MCMC process instead of the original BEM to reduce computing time. It can be applied to future analysis when numerous simulations are needed. The demonstration cases show that the value of CVRMSE can meet the 15% requirement from ASHRAE Guideline 14 [125] and FEMP [127], no matter for a synthetic office building or a real residential building. Besides, the calibration results are expressed in terms of uncertainty and probability. When the calibration parameter number is larger than 4, over-parameterization could occur, consistent with the previous study, such as Chong and Menberg [74]. When the calibrated parameter number was more than 5, the calibration and validation performance improved slightly, whereas the increase of computing time is almost linear for the MCMC process. For future work, the proposed BIR-BEM platform could be extended to other applications, such as building thermal performance and air quality analysis. The calibration of both the whole building and room levels is worth exploring too. Currently, only the EnergyPlus model can be coupled with the platform, and other BEM models could be integrated too. Monthly data

are used in the case studies for demonstration. High-resolution data can be applied in the future to investigate its impact on calibration performance and computational cost.

Chanpter 4   Bayesian Inference Calibration for   Building Thermal Predictions

With the increase in the frequency and duration of heatwaves and extreme temperatures, global warming has become one of the most critical environmental issues. Heatwaves pose significant threats to human health, especially for vulnerable groups. The heatwave during the summer of 2018 in Montreal, Canada, caused up to 53 deaths, with most lived-in buildings having no air-conditioning. Unlike energy models that mainly focus on energy performance, thermal models of builidngs emphasizes indoor thermal performance without a mechanical system. Developing such a model requires an understanding of the complex dynamics involved in the thermal performance of buildings. Detailed building parameters need to be specified, but they are challenging to determine in real life. The uncertainty assessment of the parameters estimates can make the results more reliable.

In this paper, a Bayesian-based calibration procedure is presented and applied to an educational building. First, the building was modeled in EnergyPlus based on an on-site visit and information collection. Second, a sensitivity analysis was performed to identify significant parameters affecting the errors between simulated and monitored indoor air temperatures. Then, a meta-model was developed and used during the calibration process instead of the original EnergyPlus model to decrease the requirement of computing load and time. Subsequently, the Bayesian inference theory was employed to calibrate the model on hourly indoor air temperatures in summer. Finally, the model was validated. This paper shown that the Bayesian calibration procedure can not only calibrate the model within the performance tolerance required by international building standards/codes, but also predict future thermal performance with a confidence interval, which makes it more reliable than deterministic calibration.[3]

4.1   Introduction
According to NASA, climate change is "a long-term change in the average weather patterns that have come to define Earth's local, regional and global climates." It refers to both human- and

---

[3] This chapter has been published as a peer-reviewed conference paper: Danlin Hou, Chang Shu, Lili Ji, Ibrahim Galal Hassan and Liangzhu (Leon) Wang (2021). "Bayesian Calibrating Educational Building Thermal Models to Hourly Indoor Air Temperature: Methodology and Case Study." ASME V&V 2021 Virtual Symposium, https://doi.org/10.1115/VVS2021-65268.

naturally produced warming and the effects it has on the planet [159]. Since the pre-industrial period (between 1850 and 1900), human activities are estimated to have increased Earth's global average temperature by about 0.78℃, a number that is currently rising by 0.2℃ per decade. The 20 warmest years have all occurred since 1981, and the 10 warmest have all occurred in the past 12 years [160].

In Canada, the annual average temperature has increased at approximately double the global mean rate [161]. As shown in Figure 4-1, from 1948 to 2018, there was an increasing trend in annual average temperature departures, with 1.7℃ of warming over that period (an average of annual values from 1961 to 1990 is used as a baseline). The consecutive 26 years from 1993 to 2018 saw annual average temperatures were above the reference value. In Canada, climate change brings more extreme heat, less extreme cold.

Four of the 10 warmest years on record have occurred in the last decade. The population in southern Canada accounts for 96.8% of the country's population. Quebec, the second most populous province, is home to 23.23% of the country's population, and so the impact of climate change in this province is worth studying.

In Montreal, heatwaves have become more frequent and severe. It has been reported that, during the heatwave in the summer of 2018, up to 53 deaths occurred, with most lived-in buildings have no air-conditioning, which is typical in a cold area. It has become challenging to predict the indoor environmental comfort in buildings without cooling systems and make them resilient to extreme heat.
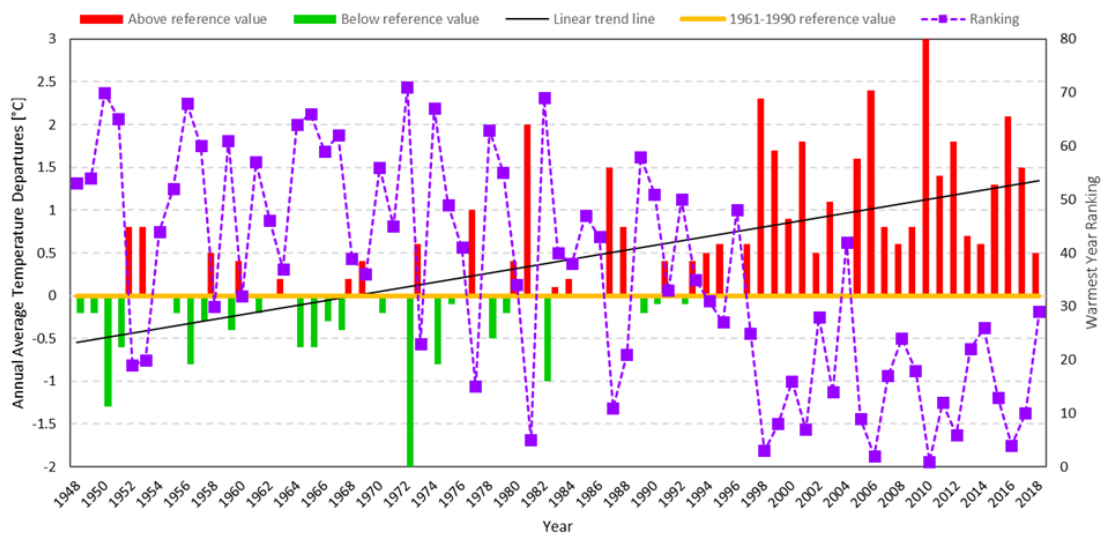
Figure 4-1 Canada annual average temperature departures and warmest year ranking.

Unlike energy models of buildings, thermal models focus on thermal performance instead of the building's energy performance. Developing such a model requires an understanding of the complex thermal dynamics in buildings. Detailed building parameters need to be specified, but they are challenging to determine in real life. Bayesian Inference statistics can be derived two hundred years ago and thrived prosperously recently with the development of computer techniques and advanced statistical theory. The first application of Bayesian Inference in building engineering was made by Heo to calibrate the building energy model and estimate the performance of retrofit conservations [33]. Since the uncertainties are considered during the calibration process, the calibration results are much more stable and close to the real ones, even if the measurements are limited. Moreover, the calibration outputs are presented with possibilities that can be regarded as a degree of belief to make them more reliable and comprehensive.

In this study, Bayesian inference was applied to the calibration of a thermal model of an educational building during summer, The entire systematic procedure is presented. The calibrated thermal model can be further used to estimate the effects of a variety of measures to combat heatwaves.

4.2 Methodology

In this study, Bayesian inference was applied to the calibration process. The systematic procedure is illustrated in Figure 4-2. The first step is the preparation of measurements. Modelers should be familiar with nature of the data, such as data types and the time resolution of measurements. The data should be clean to avoid negative impacts on the Bayesian Inference. A thermal model of the target building is then created based on the collected and audited building information. In the third step, unknown model parameters with ranges and distributions are defined, and parametric simulation is performed. The input-output dataset can be used for sensitivity analysis to identify the most important parameters of the building thermal model. In the fourth step, the input-output dataset can be used in the generation of a meta-model. The meta-model can replace the original building thermal model in the Bayesian calibration process to reduce the computing time, since several thousand simulations are needed. In the fifth step, Markov Chain Monte Carlo (MCMC) is employed to perform the Bayesian inference and align the simulation results to the measurements. Finally, the calibrated thermal model can be validated and further analyzed.

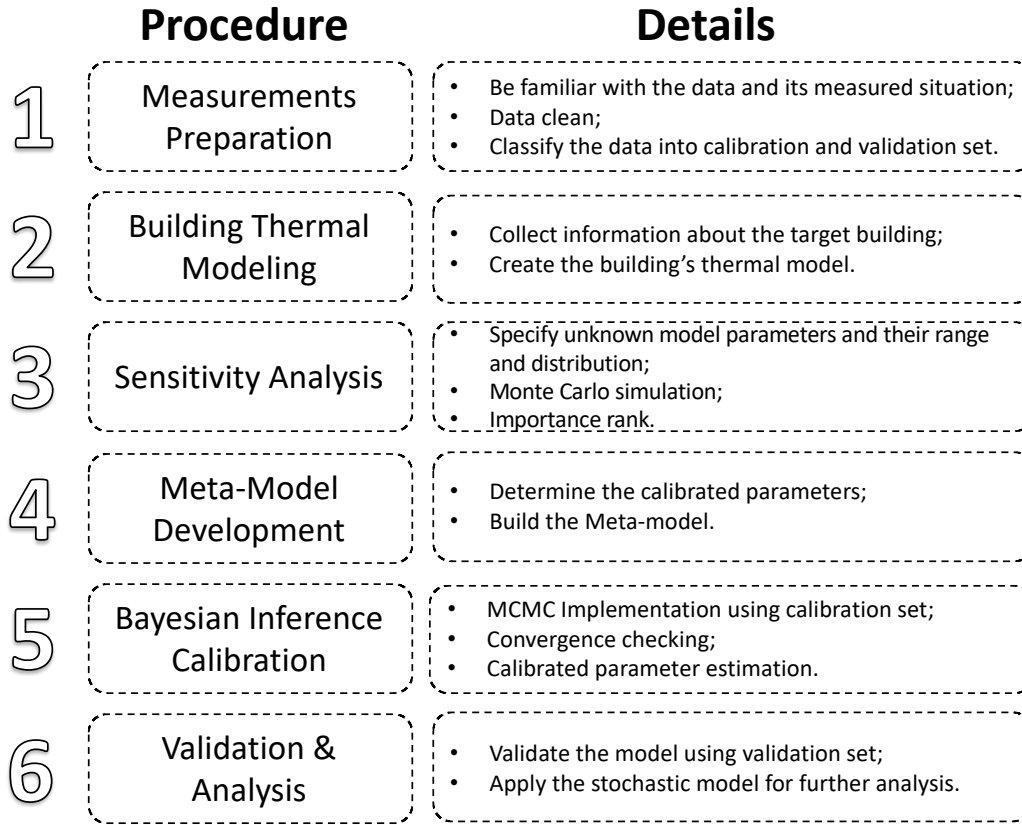| Procedure	Details
1 Measurements Preparation	• Be familiar with the data and its measured situation; • Data clean; • Classify the data into calibration and validation set.
2 Building Thermal Modeling	• Collect information about the target building; • Create the building's thermal model.
3 Sensitivity Analysis	• Specify unknown model parameters and their range and distribution; • Monte Carlo simulation; • Importance rank.
4 Meta-Model Development	• Determine the calibrated parameters; • Build the Meta-model.
5 Bayesian Inference Calibration	• MCMC Implementation using calibration set; • Convergence checking; • Calibrated parameter estimation.
6 Validation & Analysis	• Validate the model using validation set; • Apply the stochastic model for further analysis.

Figure 4-2 Systematic bayesian calibration process.

The results of the sensitivity analysis may vary with different combinations of sensitivity methods and outputs depending on the variety of fundamental algorithms and conditions for each sensitivity analysis method [109]. Lim and Zhai proposed a new sensitivity analysis index, the Sensitivity Value Index (SVI), to account for the differences in sensitivity analysis methods and target outputs [84]. Eq. 4-1 shows how SVI is used for recognizing and comparing the importance rankings from different sensitivity analysis methods through the normalization and aggregation process. In this study, three sensitivity analyses (SRC, Random forest variable importance, and T-value) were used.

$$\sum_{l=1}^{m} \frac{\sum_{j=1}^{k} \left(\frac{v_{i,j}}{\sum_{i=1}^{n} |v_{i,j}|} \right)}{m \cdot k^2} \times 100 = Sensitivity \ Value \ Index \ (SVI) \ (\%) \tag{4-1}$$

where v is the value from the sensitivity analysis, i is a parameter, n is the total number of the parameters (n=10 in this study), j is a sensitivity method, k is the total number of sensitivity

methods (k=3: SRC, Random forest variable importance, and T-value), l is the target output, and m is the total number of target outputs (m=1: special-averaged hourly indoor air temperature).

R^2 is used to define the performance of the Meta-model:

$$R^2 = 1 - \frac{\sum_{i=1}^{n}(\hat{y}_i - \bar{y})^2}{\sum_{i=1}^{n}(y_i - \bar{y})^2} \qquad (4\text{-}2)$$

where $\hat{y}_i$ is a predicted variable value for period i, y_i is an observed value for period i, $\bar{y}$ is the mean of the observed value, n is the sample size.

The performance of calibration and validation is estimated using the coefficient of variation with a root-mean-square error (CVRMSE):

$$CVRMSE = \frac{\sqrt{\frac{\sum_{i=1}^{n}(y_i - \hat{y}_i)^2}{n}}}{\bar{y}} \qquad (4\text{-}3)$$

The Hamiltonian Monte Carlo (HMC) sampling method was used for the MCMC. Five thousand steps of the HMC algorithms on each of four separate chains were explored in this study, giving a total of 20,000 samplers. One thousand samples were used during the "warming-up" stage to move chains toward the highest density area and tune the hyperparameters.

4.3 Case Study

A real school building in Montreal was selected for the demonstration of the calibration method. The building was built in 1930 and consists of three floors. It has no air conditioning. The site was visited in September 2019, and four rooms (#301, #302, #305, and #306) were selected from the different orientations on the top floor for field monitoring. It was found that rooms # 302 and #306 may have more severe overheating problems because they may have more prolonged exposure to solar irradiation.
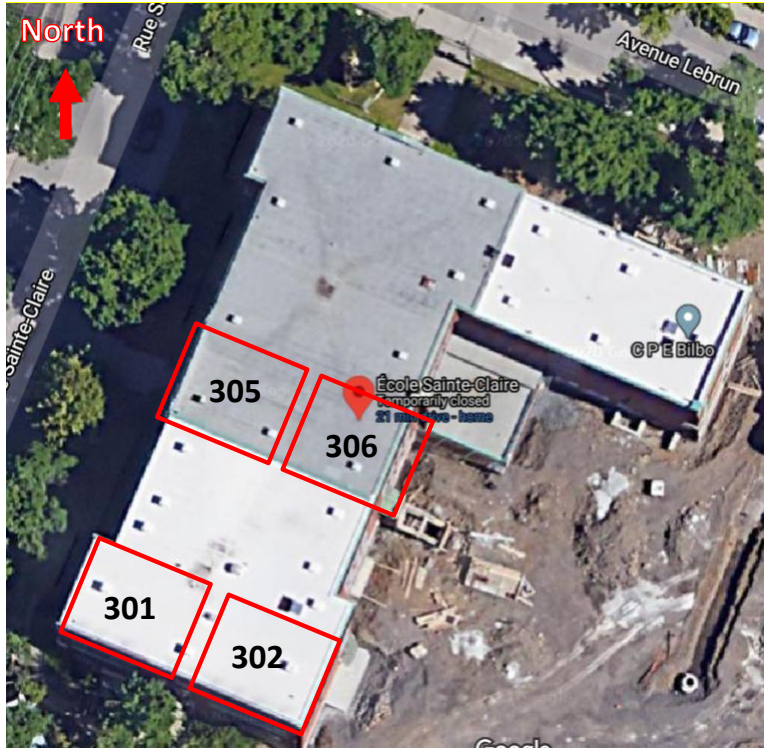
Figure 4-3 Top view of the building from google maps and the selected rooms for field monitoring.

The sensors for indoor thermal monitoring were attached to the rooms' internal walls at 1.7 m above the floor. The air temperature and relative humidity were monitored. Data from July 14 to July 31 (2020) and from August 1 to August 10 (2020) were used for the calibration and the validation of the building model, respectively. The weather data for the simulation were taken from a weather station mounted on the school's roof.

Figure 4-4 The energyplus building model.

The building model was generated by EnergyPlus, according to the building drawings. No internal heat was modeled, as the school was locked down during the measurement period due to the COVID-19 pandemic. The selected rooms were separated from other spaces as independent thermal zones so that the building model can capture the indoor condition of these rooms. For calibration, several model parameters were identified with reasonable ranges according to the current building codes [7] and the results of site visit. The 10 selected variables and their ranges are listed in Table 4-1. The selected parameters are related to the envelope (Wall Insulation U-Value, Roof Insulation U-Value, Wall Thermal Mass, Roof Thermal Mass), windows (Window U-Value, Window Solar Heat Gain Coefficient), internal walls (Internal Wall Conductivity, Partition Thermal Mass), infiltration, and curtain/blinds (Solar Reflectance of Interior Diffusing Blinds Roll).

Table 4-1 Selected building parameters and the ranges of the parameters for the calibration

Parameters	Symbol	Range	Unit
Wall Insulation U-Value	WALC	0.51-1.2	W/m^{2}K
Roof Insulation U-Value	RINU	0.15-0.30	W/m^{2}K
Internal Wall Conductivity	IWC	0.2-0.3	W/mK
Window U-Value	WINU	0.1-0.4	W/m^{2}K
Window SHGC	SHGC	0.60-0.76	-
Infiltration	INF	0.1-0.4	ACH
Solar Reflectance of Interior Diffusing Blinds Roll	SR	0.4-0.9	-
Wall Thermal Mass	WTM	150-350	KJ/K.m^2
Roof Thermal Mass	RTM	150-350	KJ/K.m^2
Partition Thermal Mass	PTM	150-350	KJ/K.m^2

4.4   Results and Discussion

4.4.1   Sensitivity analysis results

Table 4-2 shows the sensitivity analysis results with the importance ranks based on the spatial-averaged difference between hourly outdoor air temperature and indoor air temperature. As described in Section 2, the SVI takes into account the results from three sensitivity analysis methods (SRC, Random forest variable importance, and T-value). The most important parameter

is ranked as 1. It is concluded that, for educational buildings located in cold areas, the most dominant parameters are Solar Reflectance of interior diffusing blinds roll, Infiltration, Window Solar Heat Gain Coefficient, and Window U-value.

Table 4-2 SVI calculation and importance rank based on spatial-averaged hourly difference between outdoor and indoor air temperature

Parameters	Sensitivity Analysis Method			Sensitivity Value Index	Importance Rank
	SRC	Random Forest	T-Value		
Solar Reflectance of Interior Diffusing Blinds Roll	0.19	113.00	20.16	40.09	1
Infiltration	0.11	61.12	11.76	22.84	2
Window SHGC	0.06	28.09	5.95	11.25	3
Window U-Value	0.02	16.41	2.25	4.89	4
Roof Insulation U-Value	0.02	15.37	2.04	4.49	5
Wall Thermal Mass	0.02	16.76	1.74	4.22	6
Partition Thermal Mass	0.02	15.45	1.62	3.92	7
Internal Wall Conductivity	0.01	16.55	1.49	3.86	8
Roof Thermal Mass	9.6e-3	9.09	0.99	2.34	9
Wall Insulation U-Value	3.8e-3	14.33	0.38	2.09	10

The sensitivity analysis was conducted for each room, and the importance rank of each selected model parameter is presented in Figure 4-5. For most of the parameters, especially for the most dominant ones, the importance ranks are similar. However, for the parameters related to the internal walls, the importance ranks are different. This is due to the different areas of the internal walls of each room.
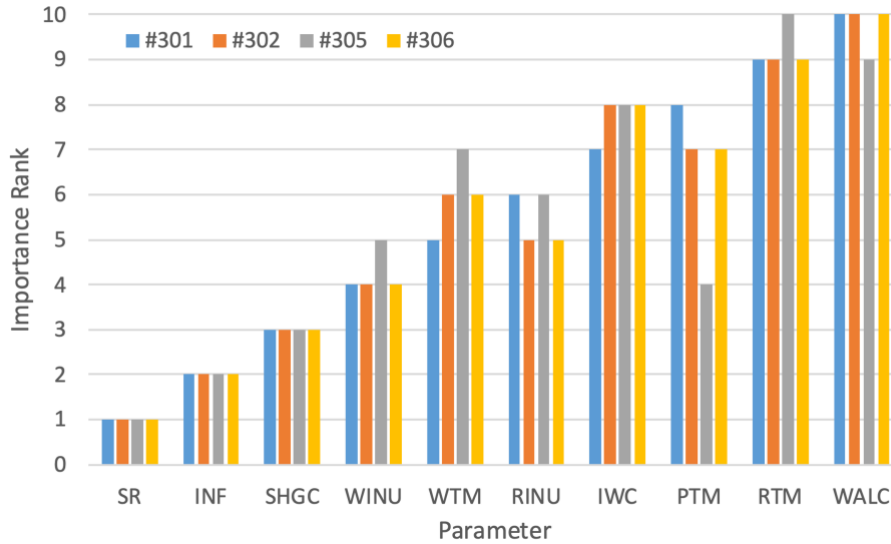
Figure 4-5 Importance rank based on hourly difference between outdoor and indoor air temperature for each room.

4.4.2 Meta -Model accur acy

A Meta-model (also called surrogate model) is a simplified representation or approximation (i.e., an emulator) of the simulator for saving computing time. Generally, the following models can be used as Meta-models in Bayesian inference to replace the original building models: multiple-linear regression (MLR) model [162], neural network (NN) [163], support vector machine (SVM) [164], multivariate adaptive regression splines (MARS) [165], and Gaussian process emulator (GPE) [166]. Lim and Zhai [84] estimated that, if MLR is employed to represent the original EnergyPlus simulation for a case study of a DOE reference medium-sized office building, the computing time can be reduced from 70 days to 2.2 minutes for an MCMC process with 100,000 iterations using a computer with an Intel Core CPU (i7-4790 3.6 GHz) and 12GB RAM. The calibration performance was still acceptable.

A MLR model is used in this study to generate the meta-model. The accuracy of the MLR model with different predictors is shown in Figure 4-6. Based on the sensitivity analysis results, when using spatially averaged hourly outdoor/indoor temperature difference as a reactor, the regression model becomes more accurate as the predictor number increases. Once the parameter number exceeds six, however, the accuracy is almost constant. The accuracy of the meta-model and its predictors can affect the calibration performance significantly. When too few predictors are selected, the meta-model accuracy is too low to represent the original building model. Therefore, the calibration results are not accurate. When too many predictors (calibration parameters) are

selected, the meta-model accuracy is high, but the over-parameterization may occur and reduce the calibration accuracy and reliability. Finally, the first four important parameters were chosen to generate the MLR model and used for the Bayesian calibration to balance the meta-model accuracy and calibration performance.
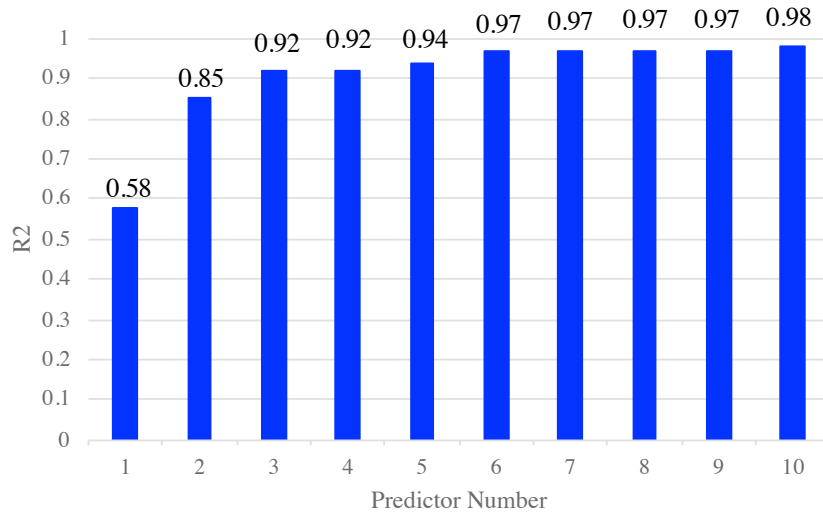

Figure 4-6 Multiple-linear regression model accuracy with variable predictor number.

### 4.4.3 Calibration performance

The four calibration parameters' distributions are shown in Figure 4-7, and the details are summarized in Table 4-3. The CVRMSE for calibration and validation is 6.62% and 8.52%, respectively, which meets the 30% requirement of ASHRAE Guideline 14 [125]. The simulated and observed spatially averaged temperature difference is presented in Figure 4-8. This difference is simulated using the MLR model. The blue dots represent the measurements. The red line represents the mean value of the predicted air temperature difference. The three pink lines with different transparent degrees represent different variable confidence intervals (68.3%, 95.5%, and 99.7%). The results are more reliable than conventional deterministic results, because the interval has an associated confidence level that proposes a range of plausible predicted values of the air temperature difference.
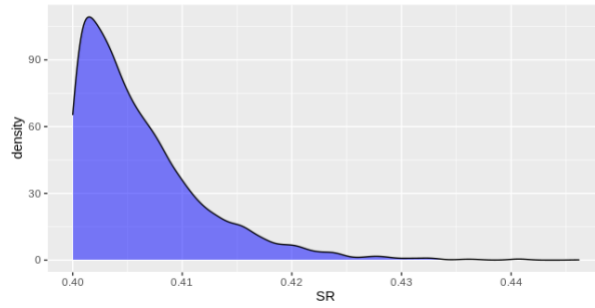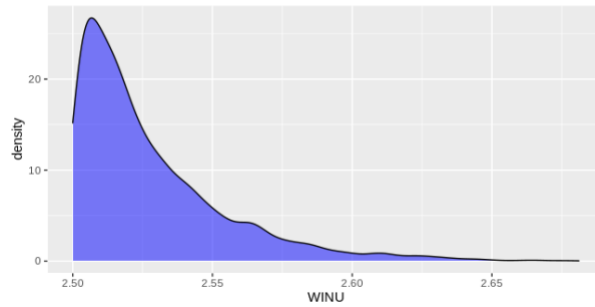
(a)   SOLAR REFLECTANCE OF INTERIOR DIFFUSING
BLINDS ROLL
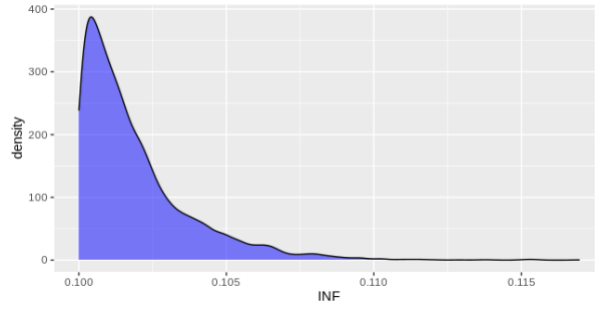
(B) INFILTRATION
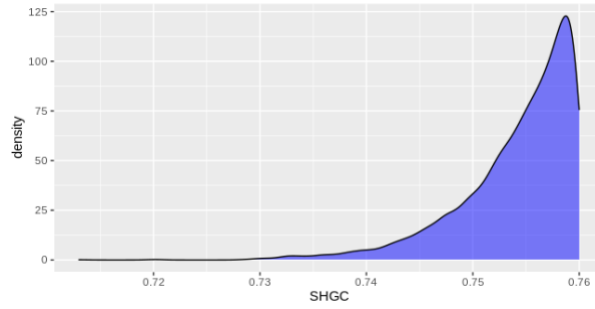
(C) WINDOW SHGC

(D) WINDOW U-VALUE

Figure 4-7 Distribution of calibrated parameters.

Table 4-3 Details about calibration parameters

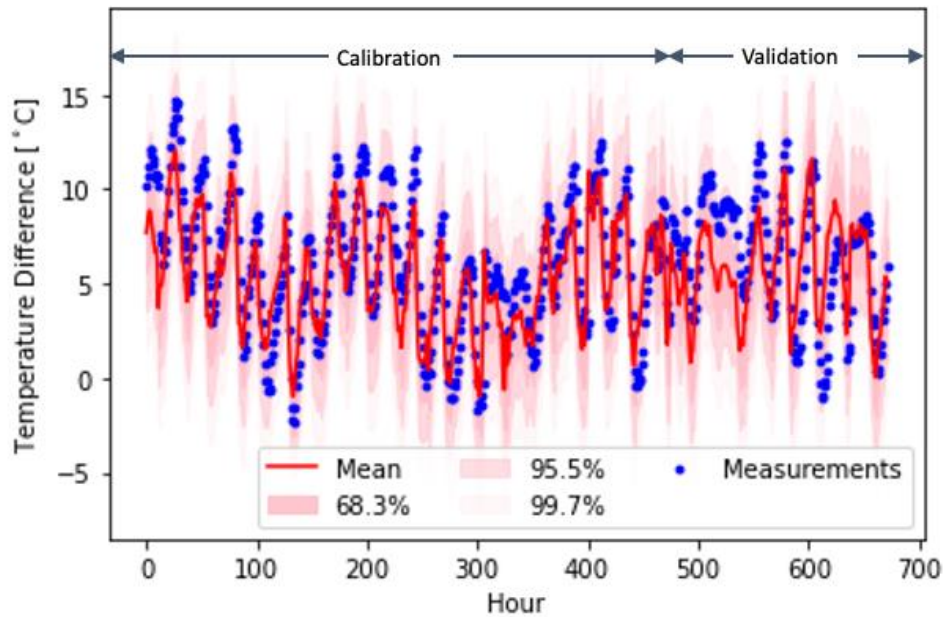| Parameter	Posterior Distribution						
	Mean Value	Standard Deviation	Quantiles (%)				
			2.5	25	50	75	97.5
Solar Reflectance	0.41	5.82e-3	0.40	0.40	0.40	0.41	0.42
Infiltration	0.10	1.93e-3	0.10	0.10	0.10	0.10	0.11
Window SHGC	0.75	5.29e-3	0.74	0.75	0.76	0.76	0.76
Window U-Value	2.53	2.74e-2	2.50	2.51	2.52	2.54	2.60

Figure 4-8 Comparison between simulated and observed spatial-averaged hourly indoor air temperature

4.5 Conclusions

In this study, Bayesian inference was applied to the calibration of the critical parameters used for thermal modeling of buildings. Using the Bayesian approach, the values of the calibrated parameters are outputs with the probabilities that reflects the inherent uncertainties. Based on the calibrated parameters, the model outputs are within the confidence interval. The calibrated thermal model can be used for evaluating the performance of the resilient measures during heatwaves. The results of the sensitivity analysis show that measures related to reducing solar heat gain, such as drawing curtains and using Low-E glass and high-performance windows, can decrease indoor air

temperature effectively. Moreover, infiltration is crucial. Increasing airtightness is another approach to avoid overheating. In the future, the model could be further calibrated from the spatially average level to the room level to explore the indoor environmental comfort performance.

Chanpter 5 Bayesian Inference Calibratio n for Building Environment Predictions

Ventilation rate plays a significant role in preventing the airborne transmission of diseases in indoor spaces. Classrooms are a considerable challenge during the COVID-19 pandemic because of large occupancy density and uncertain ventilation conditions. The indoor CO_2 level may be used as an index for indoor air quality. Thus, many schools start to use CO_2 meters, whereas they do not know how to interpret the data in terms of ventilation rates and possibly airborne transmission risks. Many uncertainties are also involved, including manually collected CO_2 readings, student numbers and schedules, and variable indoor and ambient conditions. This study investigated the CO_2 readings by the teachers in three schools by the sensitivity analysis and Bayesian calibration methods to identify uncertainties and calibrate key parameters. The outdoor ventilation rate with a 95% confidence was 1.96 ± 0.31ACH for Room 1 with mechanical ventilation and fully open window, 0.40 ± 0.08 ACH for Rooms 2, and 0.79 ± 0.06 ACH (occ1), 0.30 ± 0.04 ACH (occ2) for Room 3 with only windows open. A time-averaged CO_2 level < 450 ppm is equivalent to a ventilation rate > 10 ACH in all three rooms. We also defined the probability of the COVID-19 airborne infection risk associated with ventilation uncertainties. The outdoor ventilation threshold to prevent classroom COVID-19 aerosol spreading is between $3 - 8$ ACH, and the CO_2 threshold is around 500 ppm of a school day (< 8 hr) for the three schools.[4]

5.1 In troduction

Airborne transmission of relatively small aerosol droplets plays a dominant role in spreading SARS-CoV-2 (hereafter as COVID-19), especially in indoor spaces [167,168]. School classrooms pose a considerable challenge because of the large occupants' density, mandatory presence of students, and uncertain ventilation conditions of concern [169]. For example, in Quebec province, Canada, a partial lockdown was in effect for non-essential business, with many offices closed whereas primary and secondary schools open. The weekly school-related COVID-19 cases in Quebec at the end of August 2020 showed that schools accounted for 20% of the province's COVID-19 cases, while students and staffs account for about 18% of Quebec's population [170].

---

[4] This chapter has been submitted for publication in a peer-reviewed journal: Danlin Hou, Ali Katal and Liangzhu (Leon) Wang (2021). "Bayesian Calibration of Using CO2 Sensors to Assess Ventilation Conditions and Associated COVID-19 Airborne Aerosol Transmission Risk in Schools."

Statistical data shows that 1,781 schools had been observed with at least one positive case in Quebec since the beginning of the pandemic [171]. Therefore, the rate of COVID-19 transmission in schools was higher than the community transmission, and mitigation measures must be implemented in classrooms to reduce the infection risk.

Several studies revealed the significant impact of ventilation rate in reducing or preventing the airborne transmission of diseases in indoor environments [172]. There are different recommendations for the minimum required ventilation rate in indoor spaces to achieve an acceptable indoor air quality or preventing indoor airborne transmission. The United States Centers for Disease Control and Prevention (CDC) and World Health Organization (WHO) recommended a minimum ventilation rate of 12 air changes per hour (ACH) to prevent airborne transmission in health-care facilities [173,174]. The Harvard-CU Boulder Portable Air Cleaner Calculator [175] suggests a total of five ACH as a good ventilation condition for reducing airborne transmission risk in classrooms.

While recommendations are mainly based on the ventilation rate, it has been a challenge to quantify the outdoor air ventilation rate in a room. Indoor air CO_2 concentration is often considered a surrogate/indicator for the ventilation rate. For example, the Montreal school board (Centre de services scolaire de Montreal) stated in an open letter on December 14, 2020: "Establishments without a mechanical ventilation system should apply the window opening guidelines to ensure frequent air changes in our premises"; "Always to ensure good indoor air quality, we have also started measuring carbon dioxide (CO_2) in our establishments since November. In addition to this initiative, there are the CO_2 tests that must be carried out by all school service centers in Quebec before December 16. The level of CO_2 is a good indicator of the supply of fresh air in a room. Thus, following these tests, corrective measures will be put forward, if necessary." [176].

As a result, many school teachers started to measure CO_2 levels in their classrooms concerning ventilation conditions and safety. In an unofficial study by the teachers in Montreal's 25 classrooms, one-day CO_2 levels were recorded randomly throughout day [177] by CO_2 meters. It remains a question of how to interpret the CO_2 reading in terms of acceptable levels of ventilation and airborne transmission risk in classrooms. Meanwhile, these data are not continuously recorded but randomly measured during a day under variable student numbers, schedules, and indoor and outdoor conditions (temperature, pressure, and background CO_2 levels). The investigation of these combined parameters will need a scientific approach to consider the stochastic/random nature of

the problem. Persily [178] reviewed the relationship of indoor CO_2 concentration to ventilation rates, applications of indoor CO_2 levels to controlling outdoor air ventilation, and the role of indoor CO_2 levels in IAQ standards. It is stated that indoor CO_2 concentrations are clearly related to ventilation rate, but the relationship is complicated. In the literature, several studies used a transient CO_2 mass balance method and measured CO_2 levels to calculate the ventilation rate in different indoor environments such as classrooms and university libraries [179–181]. Batterman (2017) [181] estimated the CO_2 generation rate based on the age and assumed activity level for CO_2 calculation in mechanically ventilated classrooms. They then used the whole-day data to estimate the ventilation rate. However, the analysis was deterministic without sensitivities and uncertainties identified, and the proposed method was not validated by calculating the CO_2 levels at other time moments.

In summary, due to various factors affecting CO_2 levels, such as variable occupant numbers and outdoor conditions, and the unknown uncertainties of these factors, two types of questions have been recently raised about using CO_2 sensors to assess COVID-19 transmission risk [182]: 1). The CO_2 for Ventilation Assessment Question. When considering variable occupancy and dynamic surrounding environment, how can we relate CO_2 concentrations to ventilation rates with uncertainties taken into account? 2). The CO_2 for Risk Assessment Question. If CO_2 is used as an indicator for the COVID-19 airborne aerosol transmission risk associated with ventilation conditions, what are the CO_2 threshold levels to prevent spreading for ventilation-related risks with uncertainties quantified?

Both questions center around the uncertainties and associated sensitivity analysis of parameters. Sensitivity Analysis (SA) and calibration methods such as Bayesian Markov Chain Monte Carlo (MCMC) method [183] can be used along with measured indoor CO_2 concentrations to find the dominant parameters for the CO_2 levels such as ventilation rate and calibrate them. Bayesian MCMC is a calibration technique proposed in the twentieth century owing to the development of MCMC and modern computer. Its application to the computer models' calibration was systematically illustrated by Kennedy and O'Hagan [23]. From then on, the boom of Bayesian inference and calibration was signified. Now, Bayesian inference calibration has been utilized in various topics, such as environment [24–27], hydrology [28,29,184], transportation [31], and medicine research [32]. One of the early applications was conducted by Heo et al. [58] for building energy model calibrations for building research. In a recent review on Bayesian inference

90

calibration, Hou et al.[142] found that by propagating parameters using probabilistic analysis, Bayesian inference incorporates uncertainties into real systems' approximations by computer models. Combining multiple sources of information at different scales and with different reliabilities, the inadequacy of a model, revealed by the discrepancy between the predictions and observed data, can be corrected. Hou et al.[142] also found that 1) Bayesian calibration results are more stable and reasonable than conventional deterministic methods since the uncertainties are considered, especially when the measurements are qualitatively/quantitatively insufficient; 2) Bayesian inference calibration interprets results with a degree of belief by conducting quantitative stochastic analysis.

Therefore, to answer the "CO_2 for Ventilation Assessment" question, in this work, we investigated three classrooms from three schools in Montreal, Canada, to analyze CO_2 and ventilation rate, and estimate COVID-19 airborne aerosol infection risk. To estimate ventilation rate using the transient CO_2 mass balance model, we obtained the measurement data of transient CO_2 concentrations. We conducted a sensitivity analysis to find the dominant parameters for indoor air CO_2 concentration. The Bayesian MCMC method was then used with the three classrooms' measured CO_2 data to calibrate the dominant parameters and quantify the uncertainties. Calibrated ventilation rates inform the teachers of the ventilation conditions and air quality in their classrooms. Then we applied the calibrated model to various ventilation rates in each room to establish the connection between the ventilation rates and CO_2 levels at different exposure times.

On the other hand, calculation and adjusting the ventilation rate may not be enough for mitigating the airborne transmission of COVID-19 in classrooms because no definite ventilation and CO_2 thresholds have been agreed upon for COVID-19. Recommended ventilation rate or indoor air CO_2 level by some standards and agencies for indoor air quality conditions may not be enough to prevent indoor airborne transmission. For example, ASHRAE Standard 62-2001 [185] recommended a maximum CO_2 level of 1000 ppm in classrooms for acceptable indoor air quality, which may not be enough for preventing airborne transmission of diseases. The National Institute for Occupational Safety and Health (NIOSH) recommended a CO_2 level of 600-1500 ppm for schools and workplaces but only considered comfort and working efficiency [186]. The Wells-Riley model [187] can be used to calculate the indoor infection risk using calibrated ventilation rate. The basic reproductive ratio, R_{A0} (ratio between secondary infectious cases and source cases), is often applied and should be less than one to prevent spreading. Du et al. [172] studied the impact

of ventilation improvement on a real tuberculosis (TB) outbreak in under-ventilated university buildings. Their result showed that improving indoor ventilation to levels corresponding with CO_2 < 1000 ppm reduced 97% of TB infection risk.

Rudnick and Milton [188] derived an equation to estimate the indoor airborne infection transmission using indoor air CO_2 concentration. They calculated the critical rebreathed fraction of indoor air below which airborne propagation of typical respiratory infections will not occur. Several hypothetical cases were considered without actual measurement data. Peng and Jimenez [189] derived an analytical expression of CO_2-based risk proxies for COVID-19 and used it to estimate CO_2 level corresponding to an acceptable airborne risk level in different indoor environments. They showed that acceptable CO_2 level varies by over two orders of magnitude for various rooms and activities. It also depends on other factors, such as wearing face masks. No measurements and uncertainties were reported. Eykelbosh [182] reviewed several studies that used indoor CO_2 level in assessing the transmission risk and concluded that indoor air CO_2 level could only represent the ventilation condition. The infection risk does not depend only on the ventilation rate. Other factors such as wearing a face mask, using a portable air cleaner, and exposure time can also affect the infection risk. Therefore, to estimate the required ventilation rate and critical CO_2 level to prevent the transmission of COVID-19 aerosols in a classroom, it is crucial to know the actual room condition such as occupancy profile, activity type, and other parameters that affect the estimation of infection risk.

Therefore, to answer the "CO_2 for Risk Assessment" question, we employed the calibrated ventilation rate and actual room parameters to calculate the COVID-19 airborne transmission in the three classrooms using a modified Wells-Riley equation[190]. We compared the results with infection risks corresponding to the basic reproductive number to be one ($R_{A0} = 1$), and different ventilation rates and CO_2 threshold levels at various exposure durations.

5.2 Methodology

This section presents the models of CO_2 concentration, airborne infection risk, sensitivity analysis, and finally, the Bayesian calibration methods. Two well-mixed transient mass balance equations are solved to calculate indoor air CO_2 and COVID-19 quanta concentrations.

5.2.1 Indoor CO$_2$ concentration model

A well-mixed transient mass balance model is solved for the calculation of CO_2 concentration in the room.

$$V\frac{dC_{CO_2}}{dt} = G_s + \lambda_1 C_{oa} - \lambda_1 C_{CO_2} \qquad (5\text{-}1)$$

where V is the room volume (m^3); C_{CO_2} is the indoor air CO_2 concentration (mg/m^3); t is the time duration (s); G_s is the CO_2 generation rate by all occupants (mg/s), which depends on the age and activity level; λ_1 is the total outdoor air ventilation rate (m^3/s); and C_{oa} is the outdoor air CO_2 concentration (mg/m^3). The transient mass balance of Eq. 5-1 applies to solving arbitrary occupancy patterns and generation rates in classrooms. The solution of Eq. 5-1 is:

$$C_{CO_2} = \frac{G_s}{\lambda_1}\left(1 - e^{-\frac{\lambda_1}{V}t}\right) + \left(C_{CO_2,0} - C_{oa}\right)e^{-\frac{\lambda_1}{V}t} + C_{oa} \qquad (5\text{-}2)$$

where $C_{CO_2,0}$ is the observed initial CO_2 concentration at each occupancy phase, e.g., during a class or break session.

5.2.2 Airborne a erosol infection risk model

The probability of infection (PI) of a susceptible person in the room is calculated using the Wells-Riley formulation [190]. The method was first used by Jimenez et al. [191] for calculating infection risk in different indoor environments and is recently applied to the City Reduced Probability of Infection (CityRPI) model and used for city-scale infection risk analysis [192,193]. PI is a function of the number of quanta μ inhaled by the susceptible person (Eq. 5-3). We assumed that social distancing is maintained between all occupants, and the current study focuses on airborne aerosol transmission only. We used five assumptions for applying this model: i) there is only one infected person in the room who emits SARS-CoV-2 quanta with a constant rate, ii) the initial quanta concentration is zero, iii) the latent period of the disease is longer than the duration students stay in the classroom. Therefore, the quanta emission rate remains constant during the day, iv) the indoor environment is well-mixed, and v) the infectious quanta is removed as a first-order process by the ventilation, filtration, deposition on surfaces, and airborne inactivation. The PI in Eq. 5-3 is based on the attendance of one infected person in the room, so it calculates the probability that COVID-19 aerosols are transmitted from the infected person to a susceptible person in the room; therefore, it is a conditional probability of infection (PIcond).

93

$$PI_{cond} = 1 - e^{-\mu} \qquad (5\text{-}3)$$

The number of quanta inhaled by the susceptible person at the exposure time T is calculated by time-averaged quanta concentration.

$$\mu = C_{q,avg} \times B \times T \times (1 - f_m \times M_{in}) \qquad (5\text{-}4)$$

B is the inhalation rate (m^3/h); $C_{q,avg}$ is the time-average quanta concentration (q/m^3); T is the exposure time (h); f_m is the fraction of people in the room who wears the mask, and M_{in} is the inhalation mask efficiency. A well-mixed transient mass balance equation similar to Eq. 5-1 is solved to calculate the room's transient quanta concentration.

$$\frac{dC_q}{dt} = \frac{E}{V} - \lambda C_q \qquad (5\text{-}5)$$

where C_q is the indoor quanta concentration (q/m^3); E is the net quanta emission rate (h^{-1}); and λ is the first-order loss rate coefficient for quanta (h^{-1}). Assuming that the initial quanta concentration is zero at the beginning of the day, Eq. 5-5 is solved as follows:

$$C_q = \frac{E}{\lambda V}\left(1 - e^{-\lambda t}\right) \qquad (5\text{-}6)$$

Because of the change in the occupancy pattern during the day, the time-averaged quanta concentration is calculated using the Trapezoidal integration. E is calculated based on the number of infected people in the room N_{inf}, the fraction of people in the room with the mask f_m, exhalation mask efficiency M_{ex}, and quanta emission rate by one infected individual ER_q.

$$E = ER_q(1 - f_m \times M_{ex}) \times N_{inf} \qquad (5\text{-}7)$$

The first-order loss rate coefficient λ reflects several mechanisms: outdoor air ventilation λ_1, filtration λ_2, deposition on surfaces λ_3, and airborne inactivation λ_4.

$$\lambda = \lambda_1 + \lambda_2 + \lambda_3 + \lambda_4 \qquad (5\text{-}8)$$

λ_1 is the outdoor air change rate per hour (h^{-1}) through the HVAC system or opening windows. λ_2 is the in-room air filtration using portable air purifiers and/or duct filters in HVAC systems. λ_3 is the removal by gravitational settling. λ_4 is the inactivation/decay rate.

5.2.3 Sensitivity analysis approach

Both CO_2 and infection risk models include uncertain parameters such as ventilation rates and emission rates. Some of the uncertain parameters may impact the result's accuracy and should be calibrated by measurement data. Ideally, with sufficient measurements and computer resources, all the uncertain parameters should be included in the calibration parameters. In reality, limited by data quality/quantity or computer resources, only a few parameters may be available. Many parameters and inputs could also manifest different levels of uncertainties and significances on simulation outputs. So, it is impracticable and unnecessary to calibrate all parameters, but for dominant parameters only. Identifying these dominant parameters cannot merely rely on arbitrary parameter selections from modelers' knowledge but should be based on a scientific process, i.e., a sensitivity analysis.

To conduct a sensitivity analysis process, prior distributions and ranges of selected unknown parameters should be determined according to design code/standard, physical conditions, or modeler's knowledge. Then Monte Carlo (MC) simulation is employed to conduct parametric simulations by using Latin Hypercube Sampling (LHS) method [71], which achieves the convergence of parameter space with relatively fewer samples. The obtained input-output dataset is then employed to identify the dominant model parameters that strongly affect the outputs.

The importance ranking results may vary with different combinations of sensitivity methods and outputs depending on the variety of fundamental algorithms and conditions of each sensitivity analysis method [109]. To avoid the potential inconsistency caused by the variety of fundamental algorithms and conditions of each sensitivity analysis method, the sensitivity analysis method, sensitivity value index (SVI), proposed by Lim and Zhai [84]. Eq. 5-9 defines the SVI by the normalization and aggregation process for different sensitivity analysis methods.

$$\sum_{l=1}^{m} \frac{\sum_{j=1}^{k}\left(\frac{V_{i,j}}{\sum_{i=1}^{n}|V_{i,j}|}\right)}{m \cdot k} \times 100 = Sensitivity\ Value\ Index\ (SVI)\ (\%) \tag{5-9}$$

where $V_{i,j}$ is the value of a sensitivity analysis method, i is a parameter, n is the total number of the parameters, j is a sensitivity method, k is the total number of sensitivity methods, l is the target output, and m is the total number of target outputs. In this study, a total of 440 parametric simulations were conducted for the sensitivity analysis of the CO_2 concentration model [154].

5.2.4 Bayesian calibration and Markov Chain Monte Carlo (MCMC)

As the footstone of all Bayesian statistics, Bayes' theorem was first proposed by Reverend Thomas Bayes in his doctoral dissertation [21] and can be described as:

$$Posterior = \frac{Probability\ of\ the\ data\ \times Prior}{Average\ probability\ of\ the\ data} \tag{5-10}$$

The probability of an event is inferred based on the prior knowledge of conditions related to the event. Bayesian inference is one application of Bayes' theorem and can be written as:

$$p(\theta|y) = \frac{p(y|\theta) \cdot p(\theta)}{p(y)} \propto p(y|\theta) \cdot p(\theta) \tag{5-11}$$

where $p(\theta|y)$ is the posterior distribution of the unknown parameter θ based on known observation y. $p(y|\theta)$ is the likelihood function of observation conditional on the unknown parameter. $p(\theta)$ is the prior distribution of the unknown parameter which is the marginal probability that means it is irrespective of the outcome of another variable, and $p(y)$ is the probability of the observation that is marginal as well to normalize $p(y|\theta)$. Therefore, the posterior probability is proportional to the product of the prior probability and the likelihood.

In reality, it is impractical to apply the Bayesian inference for analytical solutions to all problems because the likelihood's integrals can be computationally expensive or sometimes impossible to be calculated. MCMC is a versatile approach to solve the parameter estimation problem with two components. One is the well-known Monte Carlo method. It is a computational algorithm to solve statistically challenging problems relying on repeated random samplings and approximate the target value (e.g., mean value) using the independent samples' results. The other is the Markov Chain method for solving a sequence of possible events. The probability of each event depends only on the state attained in the previous event. By combining MCMC and Bayesian inference, posterior distribution can be estimated efficiently.

Different MCMC algorithms can be classified into either a "random walking" group or a gradient-based group according to the acceptance-rejection criterion's adoption. In this study, Hamiltonian Monte Carlo (HMC) sampling method [156] was used for the MCMC. HMC is one typical representation of gradient-based approaches that uses the first-order gradient information to determine how to move to the right direction quickly. Five thousand steps of the HMC algorithms on each of four separate chains were explored in this study to make a total of 20,000 samplers. We

used one thousand samples during the "warming-up" stage to move chains toward the highest density area and tune sampler hyperparameters. For each room, the first 2/3 of measurements are used for the calibration, with the remaining for the validation of the model and their parameters developed. The measurement of (t-1) time step is used as the initial value of the CO_2 concentration model at t time step to obtain better results after comparing the results of using the first measurement as initial value for all time steps.

In this study, the Coefficient of Variance of Root Mean Squared Error (CVRMSE) (Eq. 5-12) and Normalized Mean Bias Error (NMBE) were used as indicators to estimate the calibration and validation performance.

$$CVRMSE \ (\%) = \frac{1}{\bar{y}} \sqrt{\frac{\sum_{i=1}^{n}(y_i - \hat{y}_i)^2}{n}} \times 100 \tag{5-12}$$

where $\hat{y}_i$ is a predicted variable value for period i, y_i is an observed value for period i, $\bar{y}$ is the mean of the observed value, and n is the sample size.

$$NMBE(\%) = \frac{1}{\bar{y}} \frac{\sum_{i=1}^{n}(y_i - \hat{y}_i)}{n} \times 100 \tag{5-13}$$

5.3   Case Study

In this study, three typical classrooms of three different schools in Montreal, Canada, were provided for calibration and infection risk analysis. Each classroom was monitored during a typical pandemic day, and occupants' information (students' age and number), ventilation system status, window status, and transient indoor CO_2 concentration were recorded. The CO_2 sensors' measurement range is zero to 5000 ppm with a resolution of 1 ppm, and school teachers manually calibrated the meters by following the manual. This is probably the most common way of calibrating CO_2 meters by a layperson. The brand and type of the CO_2 meters were provided. Thus, this study estimated the measurement accuracy from the previous study on similar types of meters to be $\pm(30 \ ppm + 5\% \times reading)$ [194]. The summary information is shown in Table 5-1 and Figure 5-1.

Table 5-1 Basic information about the measured classrooms.

Room NO.	Date	Volume (m^3)	MV	NV	Occupancy Number (student + adult)	Student age
1	Nov. 10, 2020	165	Y	Y	19 + 1	7
2	Nov. 6, 2020	236	N	Y	20 + 1	11
3	Nov. 9, 2020	236	N	Y	18 + 1	7

Notes: MV means mechanical ventilation; NV means natural ventilation.

Room 1 is equipped with a mechanical ventilation system, and CO_2 is between 500 ~ 1000 ppm, while for the non-mechanically ventilated Room 2 and Room 3, with windows open, the CO_2 reaches up to 1800 ppm. The CO_2 in Room 1 seems to indicate an acceptable level of air quality (<1000 ppm), and for Rooms 2 and 3, it is higher than the acceptable level of air quality requirements. The outdoor air temperature and pressure data were obtained from Environment and Climate Change Canada [195]. Other parameters required for the CO_2 calculation, such as outdoor air CO_2, generation rate, and outdoor air ventilation rate, are not available; therefore, we calibrate them using the CO_2 measurements.

The occupancy pattern of Room 1 and Room 2 was recorded, but no detailed occupancy record was available for Room 3. In the next part of Results, for room 3, a constant pattern (occ1) is used in which the value is from the recorded occupant number in the morning. Then another occupancy pattern (occ2), which is based on the recorded information in the morning and the trend of CO_2 measurements during the day, is proposed. The comparison of the impact of these two occupancy schedules is discussed later.
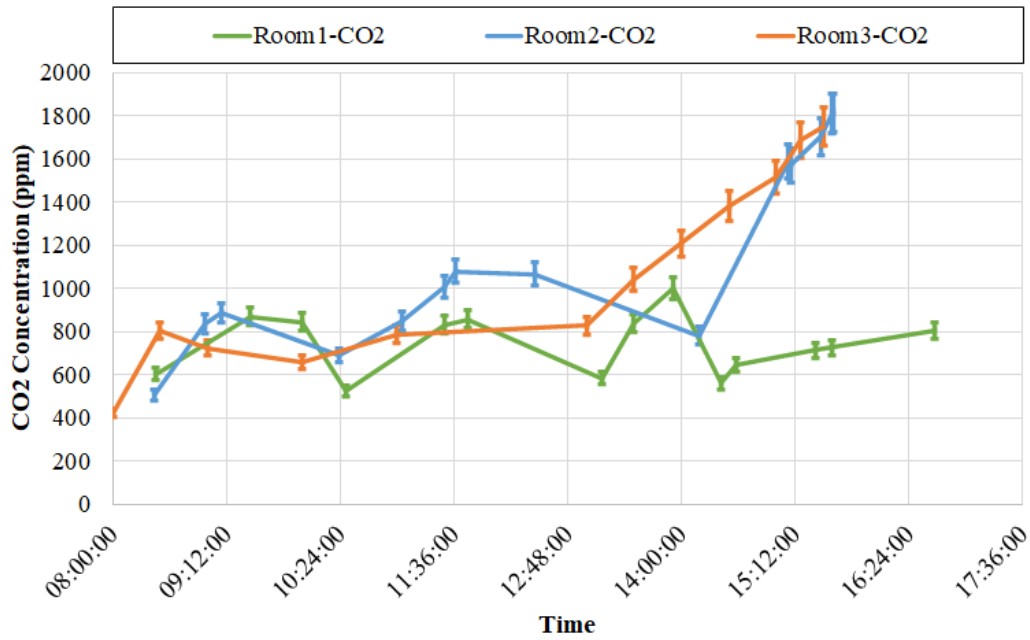
(a)
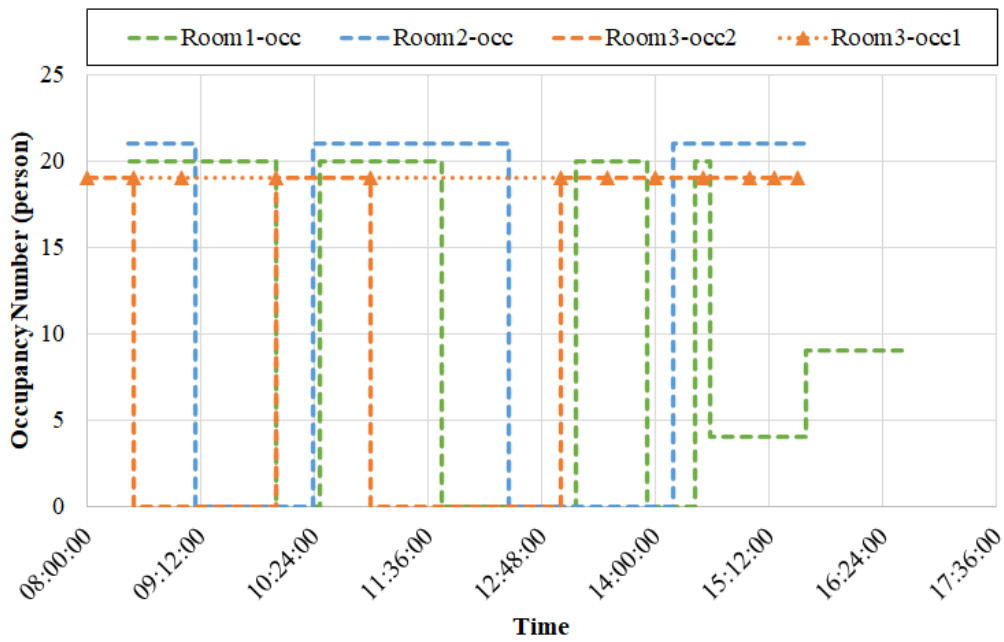
(b)
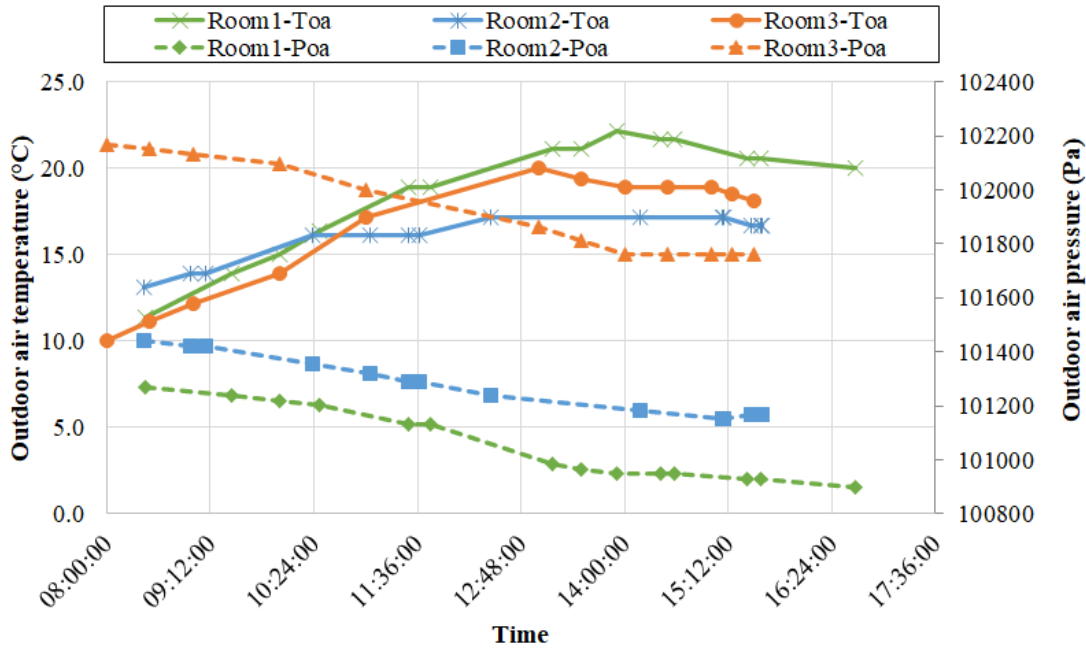
(c)

Figure 5-1 a) CO_2 concentration measurements, b) occupancy number profile, c) outdoor air temperature, and outdoor air pressure of all rooms.

5.4 Results

In this section, the sensitivity analysis finds the dominant parameters for the calculation of CO_2 concentrations. Then we use the Bayesian MCMC calibration to estimate the daily average ventilation rate using the CO_2 measurement data and occupancy patterns. We validated the CO_2 concentrations in the three rooms with the calibrated model and calculated CO_2 levels under different ventilation rates. Finally, we used the calibrated ventilation rate to estimate the infection risk in each classroom. We also find the ventilation rate and CO_2 level thresholds to avoid the airborne COVID-19 aerosol spread for different exposure times. The result presented for room3 is based on the constant occupancy assumption. The impact of occupancy schedule on the result is studied at the section 5.

5.4.1 CO_2 model sensitivity analysis

Outdoor/indoor pressure, outdoor/indoor air temperature, occupancy number, room volume, outdoor air ventilation rate, and CO_2 exhale rate are input parameters to predict CO_2 concentration. The ranges of selected model inputs/parameters were defined according to the references, codes,

100

and standards available for the sensitivity analysis. Table 5-2 shows the parameters with their sensitivity importance rankings: a smaller number indicates a more important/sensitive parameter.

Table 5-2 Sensitivity analysis with importance ranking for indoor CO_2 concentration.

Parameters	Symbol	Range	Reference	Sensitivity Analysis Method			Sensitivity Value Index	Importance Rank
				SRC	Random Forest	T-value		
Outdoor air ventilation rate (ACH)	λ_1	0.01~2 (non-mechanical); 1~5 (mechanical)	[196]	0.32	27.8	7.3	42.1	1
CO_2 generation rate per person (L/s·person)	G_1	0.002~0.01	[181,197]	0.18	10.1	4.1	20.2	2
Number of occupants (#)	N_{tot}	10~30	measured	0.06	4.6	1.4	7.5	3
Outdoor CO_2 (ppm)	C_{oa}	396~416	[181,198]	0.08	2.3	1.7	7.4	4
Outdoor pressure (kPa)	P_{oa}	100.5~102.5	[195]	0.05	0.7	1.2	4.6	5
Indoor pressure (kPa)	P_{in}	100.5~102.5	[195]	0.02	4.3	0.4	4.2	6
Indoor air temperature (℃)	T_{in}	18~25	[195]	0.04	1.9	0.8	4.0	7
Outdoor air temperature (℃)	T_{oa}	10~20	[195]	0.01	1.82	0.2	1.6	8

It is concluded that, for the classroom CO_2 levels, the most dominant parameters are outdoor air ventilation rate, CO_2 generation rate per person, number of occupants, and outdoor CO_2 concentration. Specifically, the outdoor air ventilation rate's SVI is two times the second important parameter. Some sensitive parameters are often known, such as occupant number, outdoor temperature, and pressure. So, they may not need to be calibrated. Therefore, we selected the outdoor air ventilation rate, CO_2 generation rate, outdoor CO_2 concentration, and indoor air temperature for the next step's model calibration. Indoor pressure was assumed to be identical to the outdoor pressure.

5.4.2   Calibration and validation performance

For the calibration of the CO_2 model, the Bayesian inference method was applied. For each occupancy phase (e.g., between every two measurements), we use the new measured CO_2 data as the initial condition for Eq. 5-2. The posterior distributions are shown in Figure 5-2 and Table 5-3. In each subplot, the red dash line represents the parameter's prior distribution in Table 5-2.
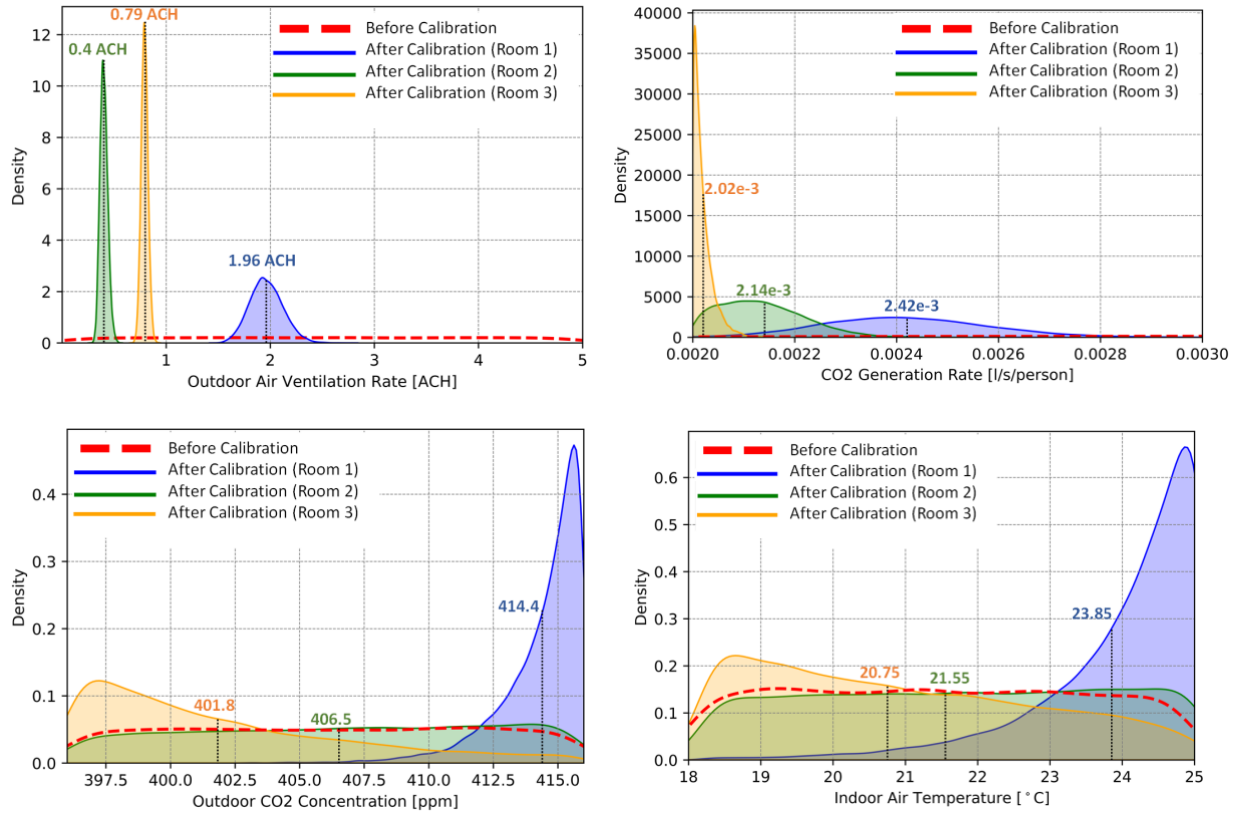

Figure 5-2 Distribution of calibrated parameters of the indoor CO_2 model.

The posterior distributions with the Bayesian calibration are indicated by blue, green, and orange for Rooms 1, 2, and 3, respectively. The calibrated outdoor ventilation rate is 1.96 ± 0.31 ACH for Room 1, 0.40 ± 0.08 ACH for Room 2, and 0.79 ± 0.06 ACH for Room 3. Here, the ventilation rate is expressed by the calibrated mean value followed by the uncertainty for a 95% confidence interval. Room 1 is both mechanically and naturally ventilated (i.e., open windows), so its ventilation rate is significantly higher than Rooms 2 and 3, with the outdoor air only from open windows. The results of Room 2 and Room 3 are closer since both are naturally ventilated with the same room volumes. The span of the posterior distribution of Room 1 is more significant because of its wider prior distribution range. For the parameters of CO_2 generation rate, outdoor CO_2 level, and indoor air temperature, Rooms 2 and 3 results are closer than Room 1 due to different ventilation modes.

Table 5-3 Calibrated parameters of the CO_2 model

| Room NO.	Prior Distribution	Posterior Distribution						
	Uniform Distribution Range	Mean Value	Standard Deviation	Quantiles (%)				
				2.5	25	50	75	97.5
Outdoor Air Ventilation Rate (ACH)								
Room 1	(1, 5)	1.96	0.16	1.67	1.85	1.96	2.07	2.29
Room 2	(0.01, 2)	0.40	0.04	0.33	0.38	0.40	0.43	0.48
Room 3		0.79	0.03	0.73	0.77	0.79	0.81	0.86
CO_2 Generation Rate [$\times 10^{-3}$ L/s/person]								
Room 1		2.42	0.16	2.12	2.30	2.41	2.52	2.75
Room 2	(2.0, 10.0)	2.14	0.08	2.01	2.07	2.13	2.19	2.32
Room 3		2.02	0.02	2.00	2.01	2.01	2.03	2.07
Outdoor CO_2 Concentration (ppm)								
Room 1		414.4	1.62	410.1	413.8	414.9	415.6	416.0
Room 2	(396, 416)	406.5	5.72	396.6	401.7	406.9	411.6	415.5
Room 3		401.8	4.89	396.2	397.9	400.4	404.7	414.1
Indoor Air Temperature (K)								
Room 1		297.0	1.13	293.8	296.6	297.4	297.9	298.1
Room 2	(291, 298)	294.7	2.03	291.4	293.0	294.8	296.6	298.0
Room 3		293.9	1.92	291.2	292.2	293.6	295.4	297.7

Using the mean value of the calibration parameters, we compared the simulation results and measurements of CO_2 in Figure 5-3. The simulation results show similar trends as the measurements. According to the American Society of Heating, Refrigerating, and Air-conditioning Engineers (ASHRAE) guideline 14 [199] and FEMP [127], when the CVRMSE and NMBE values are less than 30% and ±10% for transient data, the calibrated accuracy meet the requirements. The (CVRMSE, NMBE) of validation of Rooms 1-3 are $(15.3, 7.6)$, $(10.5, 6.1)$, and $(12.5, 12.3)$, respectively, which shows that the validated accuracy is acceptable.

(a)

(b)

104
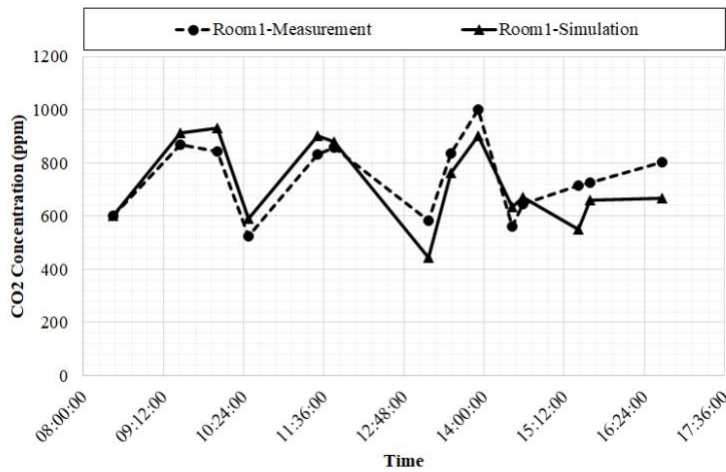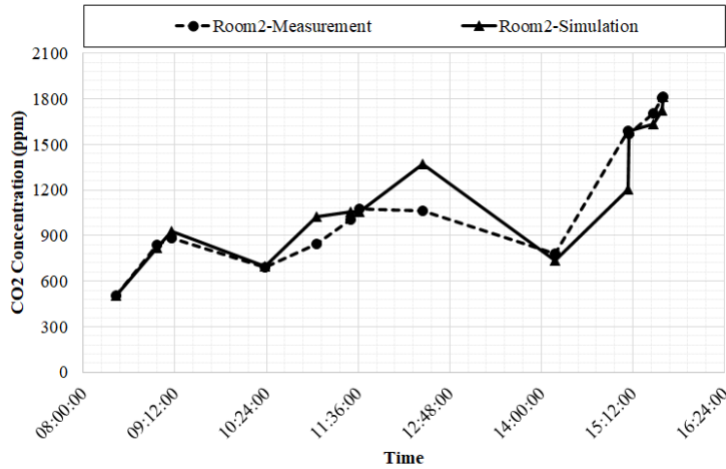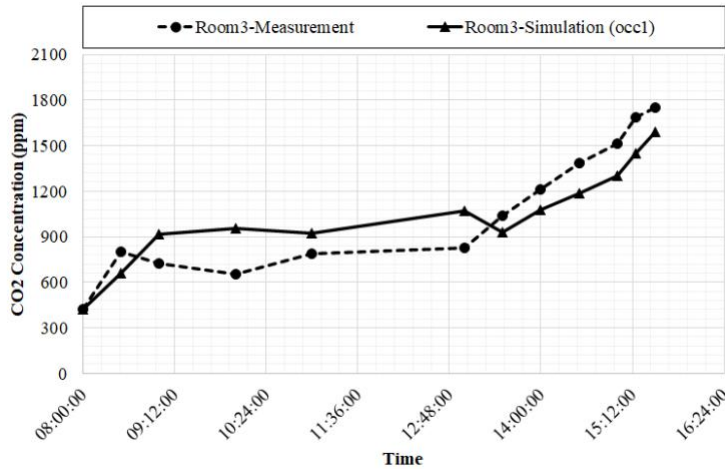
(c)

Figure 5-3 Comparison of simulated and measured CO_2 levels in three schools.

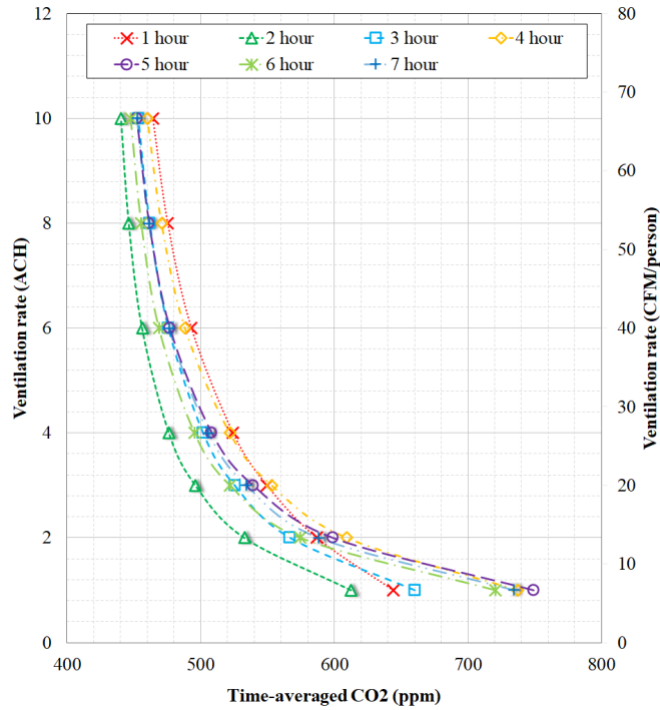5.4.3 CO_2 level and ventilation rate evaluations   [5]

The calibrated ventilation rates in all three classrooms are less than 2 ACH. The recommended ventilation rate for an indoor environment by Harvard-CU Boulder Portable Air Cleaner Calculator for Schools is at least 5 ACH. Therefore, the ventilation rate of all three classrooms seems inadequate. To relate the CO_2 levels and the ventilation rates, by using the calibrated CO_2 model, we calculated the outdoor air ventilation rate in ACH and CFM/person as a function of CO_2 levels at different exposure times in Figure 5-4. It helps teachers estimate the room ventilation rate directly based on the CO_2 sensors at different school hours. For example, for Room 1, when $CO_2 >$ 600 ppm, OA (outdoor air) < 5 ACH (24 CFM/person); $CO_2 >$ 800 ppm, OA < 2 ACH (9 CFM/person) at any time of the day. A CO_2 level less than 480 ppm indicates a ventilation rate greater than 10 ACH (48 CFM/person) at all times. For Room 2, the same CO_2 levels correspond to a lower ventilation rate than Room 1. For example, when $CO_2 >$ 600 ppm, OA < 2 ACH (13 CFM/person); $CO_2 <$ 440 ppm indicates that OA > 10 ACH (66 CFM/person). Room 1 shows a higher ventilation rate (ACH) for the same CO_2 level because of its smaller size. Room 3 ventilation rate at a specific CO_2 level is higher than Room 2 except the first hour because of constant occupancy. It seems the breaks indeed lower CO_2 levels significantly (thus infectious risk in schools). For Room 3, $CO_2 >$ 600 ppm indicates OA < 1.6 ACH (12 CFM/person). These results show that the indoor CO_2 could vary significantly in different classrooms even with the same ventilation rate because of different room sizes, occupants' number, and occupancy schedule. All

---

[5] Appreciate Dr. Ali Katal's work on section 5.4.3 and most of section 5.4.4.

three classrooms show that an indoor CO_2 lower than 450 ppm indicates a ventilation rate greater than 10 ACH, close to the recommended 12 ACH value to prevent airborne transmission in health-care facilities[173,174]. Note that here CO_2 is the exposure-time-averaged instead of the instantaneous level.
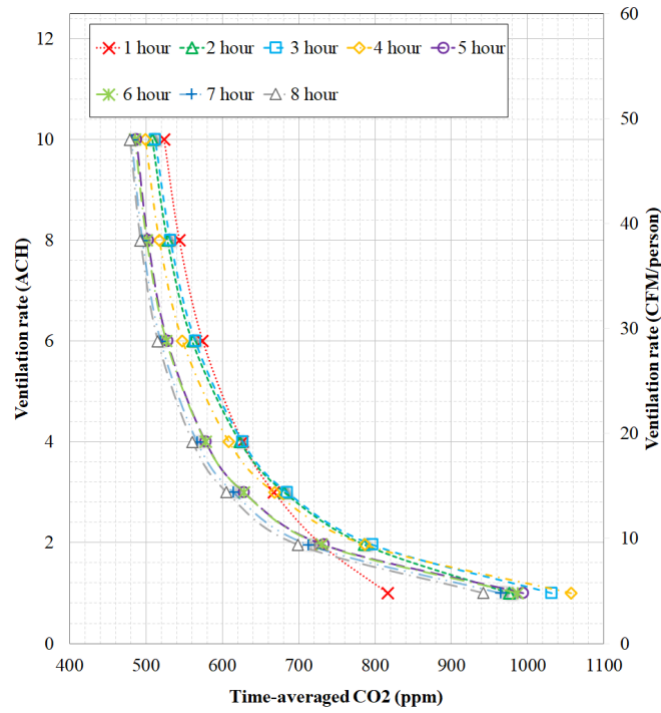
(a) Classroom #1

(b) Classroom #2
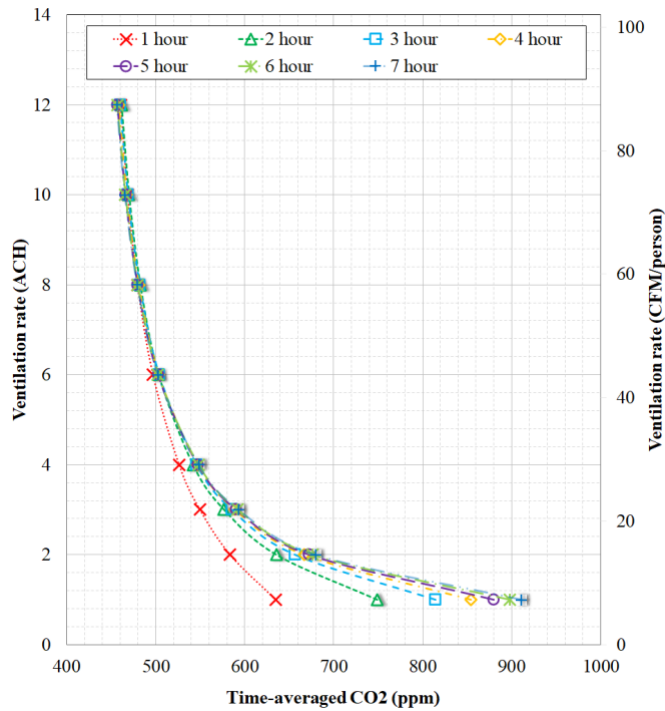
(c) Classroom #3

Figure 5-4 Relation of indoor CO_2 levels and ventilation rates for classrooms.

5.4.4　CO_2 level and i nfection risk evaluation　s[5]

To study CO_2 and airborne aerosol infectious risk relation, we first calculate the probability of infection risk with the posterior distribution of the ventilation rate obtained in Section 4.3. Here, the Bayesian MCMC analysis allows us to quantify the uncertainties of the ventilation rates to estimate airborne infectious risk by defining the probability of the infection risk: the probable range of the infection risk estimated in classrooms. Then, we evaluate different ventilation rates to identify the corresponding CO_2 threshold level, at which the reproductive number, $R_{A0} < 1$, at all exposure times. We estimate the infection risk and indoor air CO_2 threshold based on the actual room conditions. The recommended threshold could be used for other rooms under a similar condition.

Table 5-4 shows the input parameters for Eqs. 3-11 to calculate the COVID-19 airborne infection risk in classrooms. Actual room conditions with age and activity levels were used to determine breathing and quanta emission rates [200,201]. The quanta emission rate is based on the recommended values by Buonnano et al.[200,202]. All students wore a face mask in the classroom, and mask efficiency was selected based on students' typical mask type.

Table 5-4 Input parameters for calculation of infection risk in three classrooms.

| Parameter	Symbol (unit)	Room number		
		Room 1	Room 2	Room 3
Breath rate	$B\ (m^3/h)$	0.67	0.67	0.67
Mask fraction	f_m	1	1	1
Mask inhalation efficiency	M_{in}	30%	30%	30%
Mask exhalation efficiency	M_{ex}	50%	50%	50%
Quanta emission rate	$ER._q\ (q/h)$	27.55	27.55	27.55
Number of infected people	N_{inf}	1	1	1
Indoor air filtration rate	$\lambda_2(1/h)$	0	0	0
Deposition rate	$\lambda_3(1/h)$	0.3	0.3	0.3
Decay rate	$\lambda_4(1/h)$	0.62	0.62	0.62
Number of susceptible	N_{sus}	19	20	18

Figure 5-6 plots the transient PI_{cond} in three classrooms with the calibrated ventilation rates' posterior distribution. The orange line is the baseline of PI_{cond} calculated using the mean value of the posterior distribution of ventilation rate. The orange area is the estimated infection risk probability with a 95% confidence interval. For Rooms 1, 2, and 3, the mean PI_{cond} at the end of the day is around 14%, 14%, and 20%, respectively. The uncertain band of PI_{cond} in Room 1 is wider than other rooms because of the greater posterior range of mechanical ventilation rate. Meanwhile, breaks decrease the infection risk for all rooms. Therefore, to reduce infection risk,

frequent breaks are beneficial when increasing the classroom's ventilation rate is relatively harder to achieve.

The conditional PI is the ratio of the number of infections to susceptibles, $PI_{cond} = D/S$. The basic reproductive number (R_{A0}), defined by Rudnick and Milton [188], is the number of secondary infections when a single infected person is introduced in the room, and everyone in the room is susceptible. If $R_{A0} < 1$, then the infectious agent cannot spread in the population. For these three classrooms if PI_{cond} is smaller than $5.3\%, 5\%$, and 5.5%, it is expected that the community spread in the classrooms could be stopped. Figure 5-5 shows that, for Rooms 1 and 2, the conditional PI exceeds the level of $R_{A0} = 1$ at around two ~ three hours, while for Room 3 it exceeds the $R_{A0} = 1$ after 5 hours because of its occupancy condition.
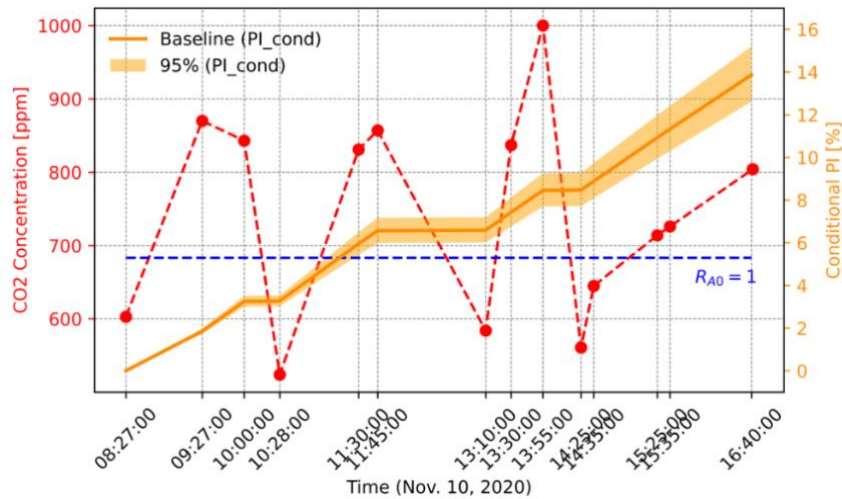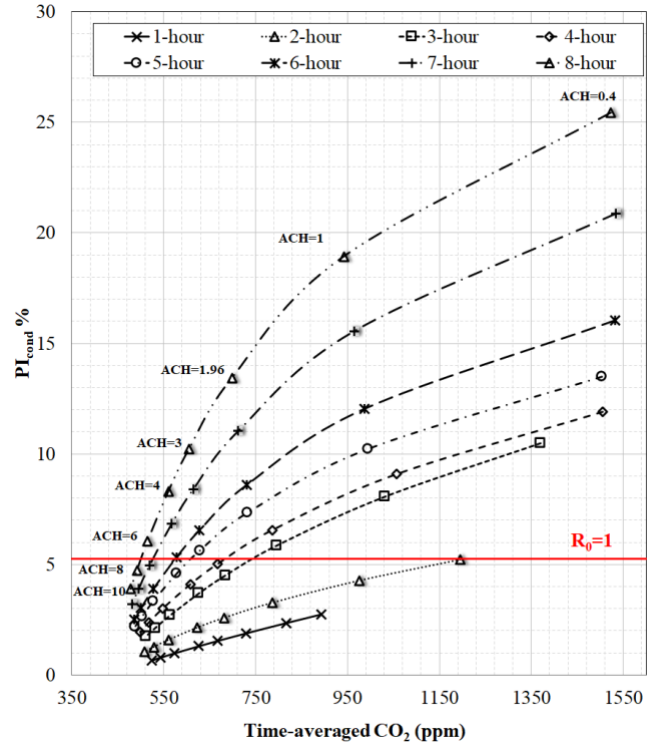

(a) Room 1
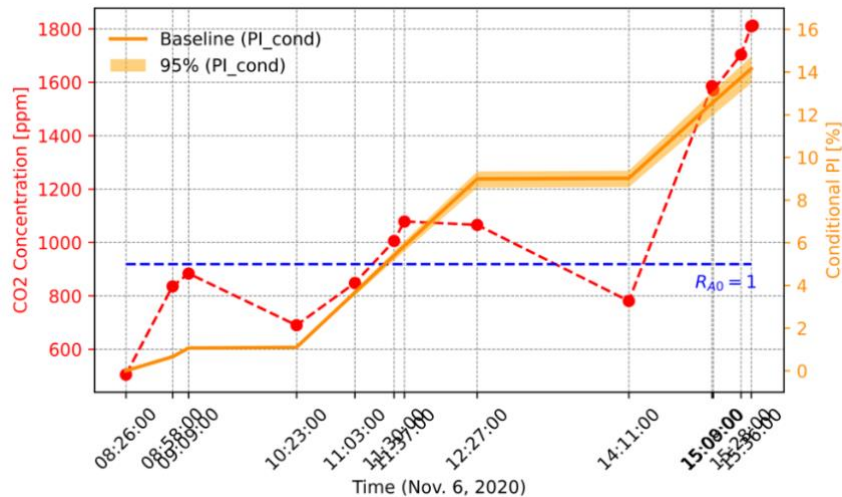
(b) Room 2
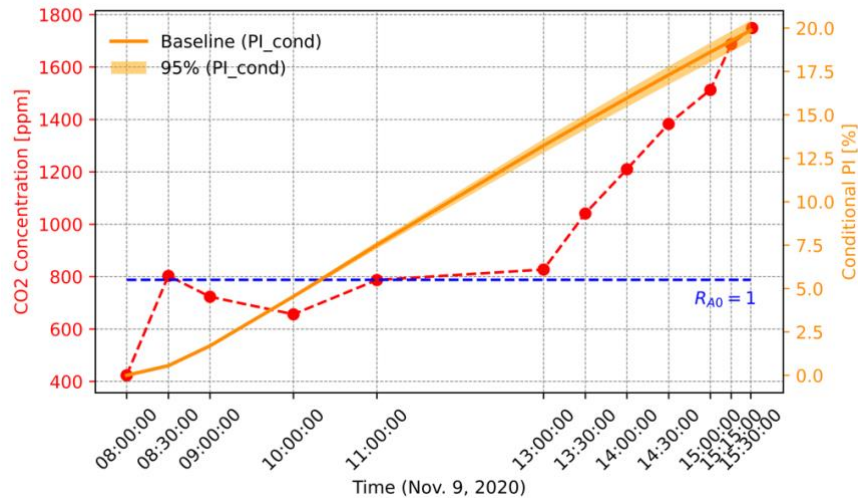
(c) Room 3

Figure 5-5 Probability of airborne infection risks in classrooms.

The relations among the required ventilation rates, corresponding CO_2 levels, and the COVID-19 airborne spreading risks are presented in Figure 5-6. At all exposure times, the indoor CO_2 and PI decrease with an increased ventilation rate. The ventilation rate threshold to prevent the spread (R_{A0}<1) at all exposure times is 8, 6, and 10 ACH for Rooms 1, 2, and 3, respectively. Room 1 requires a higher ventilation rate than Room2 primarily because of the smallest room size. Room 2 needs a lower ventilation rate than Room 3 because of several breaks during the day compared to constant occupancy of Room3. Therefore, the ventilation rate threshold depends on the occupancy schedule and the size of the room.

(a) Room 1

(b) Room 2

111
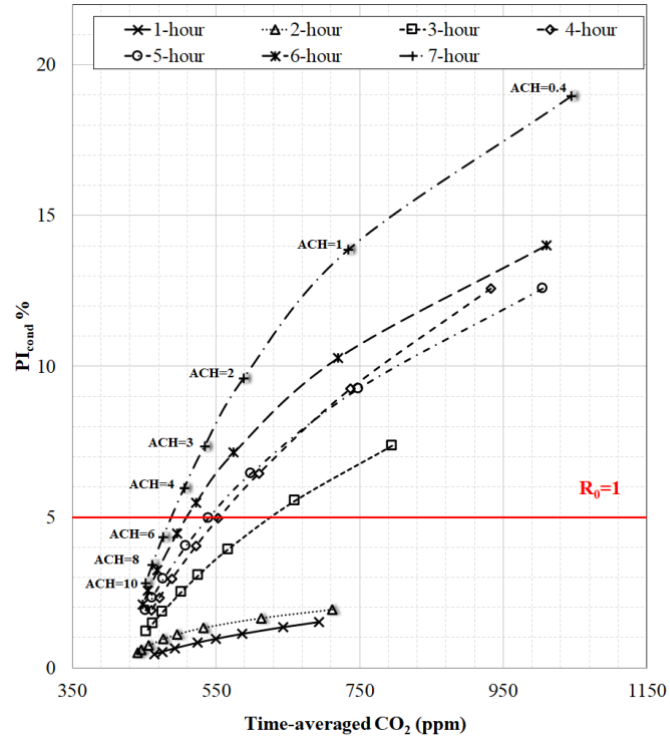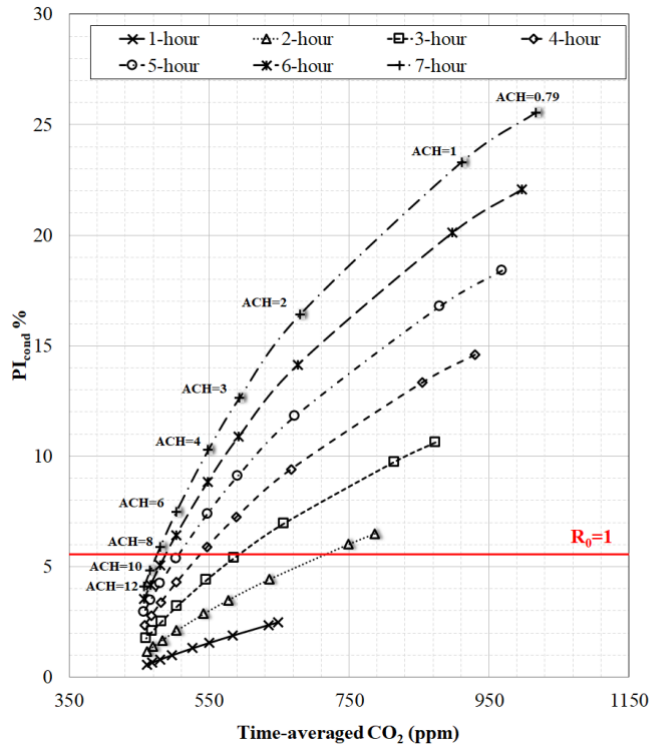
(c) Room 3

Figure 5-6 PI_{cond} and time-averaged CO_2 for different exposure times and ventilation rates.

On the other hand, we can find the indoor CO_2 thresholds for $R_{A0} < 1$ at different exposure times as shown in Figure 5-7. For example, the CO_2 threshold is around 980 ppm for a 2-hour exposure and around 490 ppm after 8 hours in Room 1. For Room 2, it decreases from 660 ppm (3-hour) to 505 ppm (7-hour), and for Room 3 first, it decreases from 790 ppm (2-hour) to 503 ppm (7-hour). Meanwhile, the threshold levels for 7 hours exposure are close for all classrooms, between 503-519 ppm. In comparison, Figure 5-7b and Figure 5-7c illustrate that the ventilation rate threshold (to prevent the spreading) increases with exposure time and is not a constant number because of the three rooms' different sizes and schedules.
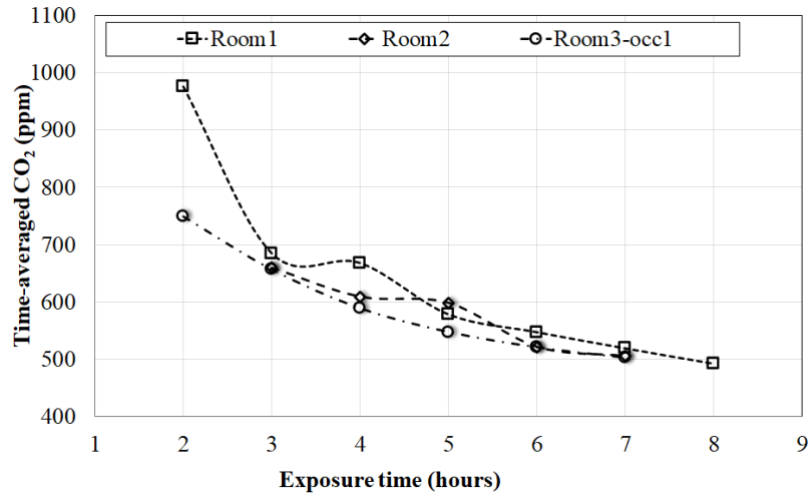
(a)
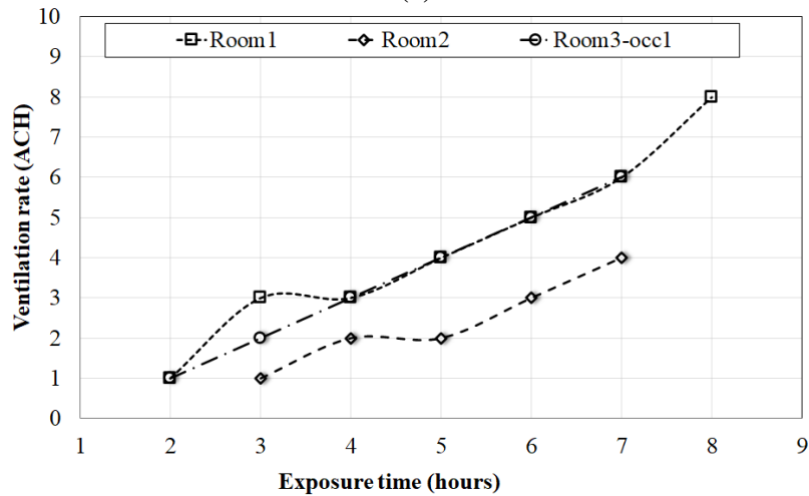
(b)
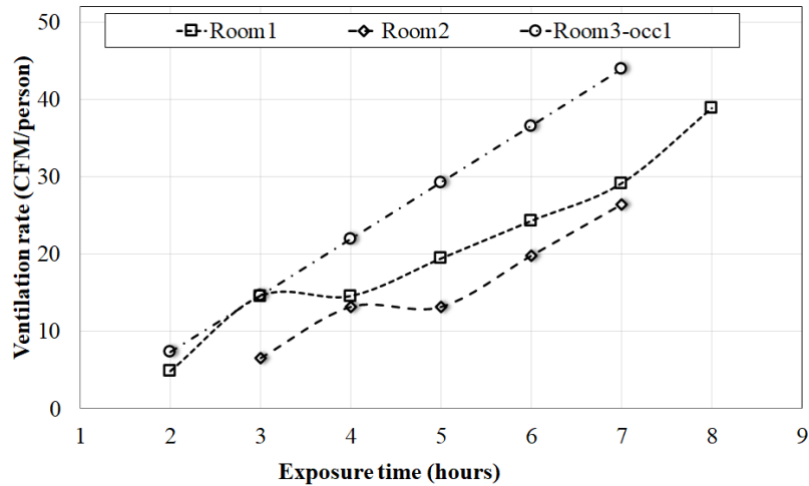
(c)

Figure 5-7 a) Time-averaged indoor CO_2 concentration thresholds, and b, c) outdoor ventilation rate thresholds with exposure times to prevent spreading.

In summary, the results of all three classrooms show that the ventilation rate threshold to prevent the airborne transmission of COVID-19 depends on several parameters such as room size, student schedules, and exposure time. The indoor CO_2 threshold seems to depend on exposure time mostly, and the time-averaged level of 500 ppm seems acceptable for all three classrooms.

5.5   Discussion

The sensitivity analysis results show that occupancy number is the third important model parameter of indoor CO_2 concentration model. The reliability of occupancy schedule can impact the calibration results of other model parameters. As mentioned above, for room 3, no dynamic occupancy schedule was recorded during the measured day, and the constant value of occupancy number (occ1) recorded in the morning was used. However, an occupancy schedule that considered actual situations is more reasonable. Therefore, based on the occupancy number recorded in the morning, the normal students' schedule, and the trend of the measured indoor CO_2 concentration, another occupancy schedule (occ2) is assumed. In this section, the impact of these two occupancy schedules on the calibration performance and infection risk is discussed.

The comparison of calibration results based on two occupancy schedules is summarized in Table 5-5 and Figure 5-8. By using occ2, the mean value of outdoor air ventilation rate, the most important parameter, decreases from 0.79 to 0.30 which is similar to the calibration result of Room 2 (0.40), with the narrow down of standard deviation. For the second important parameter, CO_2 generation rate, occ2 can decrease the standard deviation to make the results more informative. But no obvious difference in its mean value. For other two calibration parameters, results based on occ2 is close to the Room 2's results. The comparison between CO_2 measurements and simulations is shown in Figure 5-9. The occ2 occupancy schedule can reduce the (CVRMSE, NMBE) of validation from (12.5, 12.3) to (4.2, 2.8) to obtain a better result.

Table 5-5 Comparison of calibration details based on two occupancy schedules of Room 3

Calibration Parameter	Prior Distribution	Posterior Distribution (occ1/occ2)						
	Uniform Distribution Range	Mean Value	Standard Deviation	Quantiles (%)				
				2.5	25	50	75	97.5
Outdoor Air Ventilation Rate (ACH)	(0.01, 2)	0.79/ 0.30	0.03/ 0.02	0.73/ 0.26	0.77/ 0.29	0.79/ 0.30	0.81/ 0.32	0.86/ 0.35

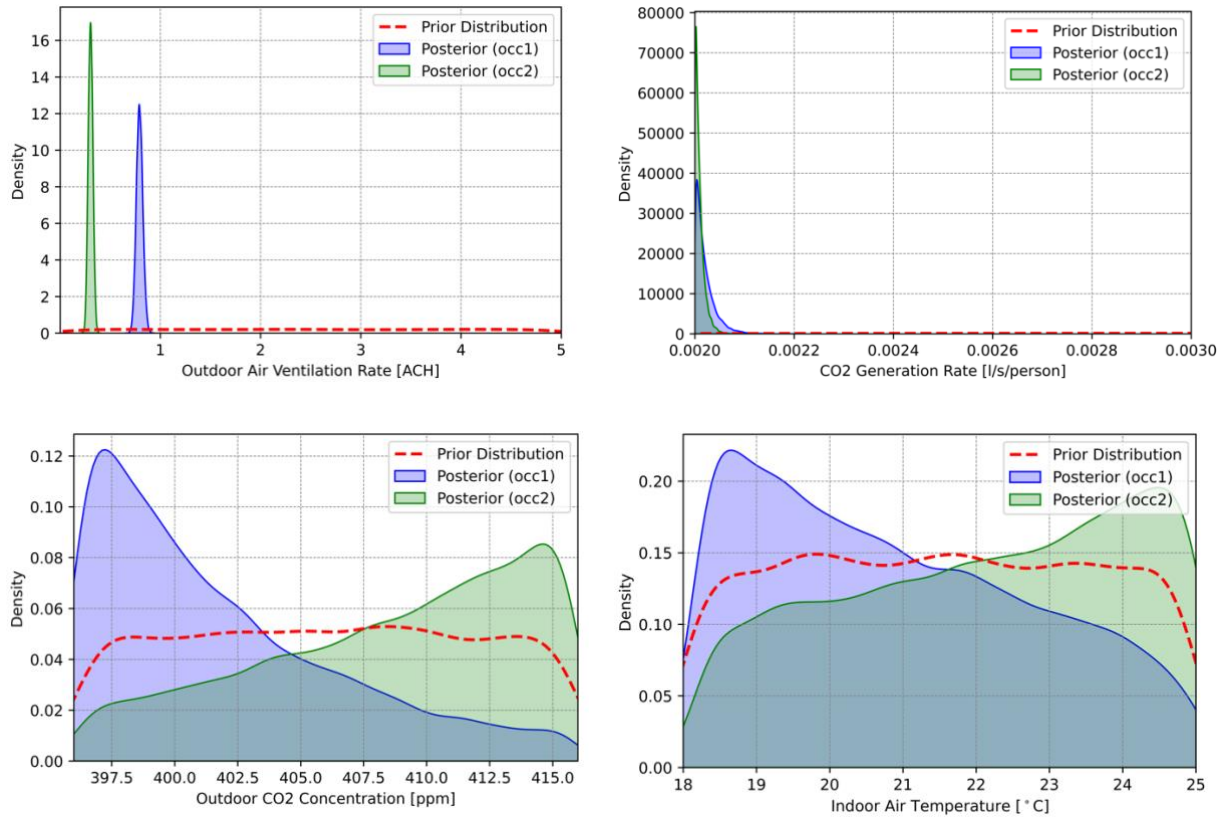| CO$_2$ Generation Rate [×10^{-3} L/s/person]	(2.0, 10.0)	2.02/ 2.01	0.02/ 0.01	2.00/ 2.00	2.01/ 2.00	2.01/ 2.01	2.03/ 2.01	2.07/ 2.04
Outdoor CO$_2$ Concentration (ppm)	(396, 416)	401.8/ 408.5	4.89/ 5.43	396.2/ 397.2	397.9/ 404.5	400.4/ 409.6	404.7/ 413.2	414.1/ 415.8
Indoor Air Temperature (K)	(18, 25)	20.9/ 22.1	1.92/ 2.00	18.2/ 18.4	19.2/ 20.4	20.6/ 22.3	22.4/ 23.9	24.7/ 25.0

Figure 5-8 Comparison of posterior distributions based on different occupancy schedules of Room 3
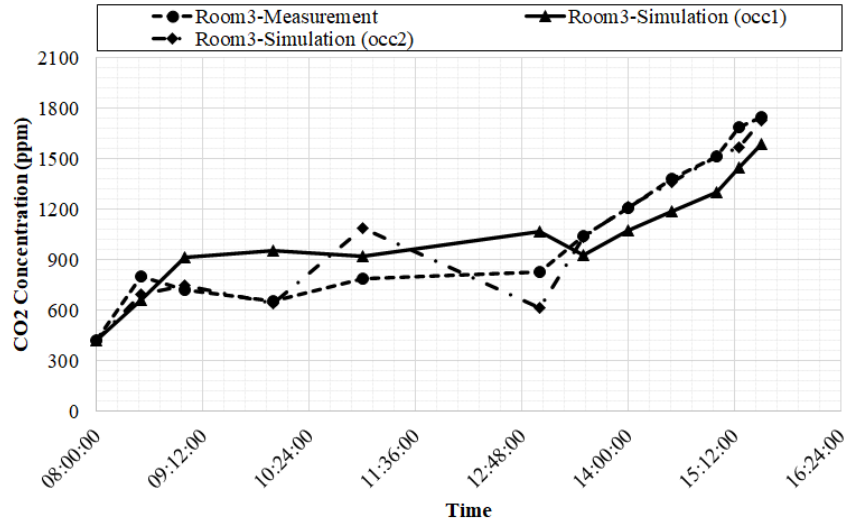
Figure 5-9 Comparison of CO_2 concentrations of Room 3.

5.6   Conclusions

The airborne transmission of COVID-19 is a major infection route in indoor spaces, especially with poor ventilation conditions, large occupancy density, and high exposure time, such as school classrooms. There are some recommended ventilation rates for acceptable indoor air quality or preventing airborne transmission in indoor spaces, but it is not easy to measure the actual room's ventilation rate. Indoor air CO_2 level can be used as an indicator for the ventilation rate, whereas it depends on several parameters that must be estimated. This study conducted a sensitivity analysis and a Bayesian inference calibration using measured indoor CO_2 and occupancy profiles in three school classrooms to identify the relations among CO_2 levels, ventilation rates, and airborne transmission risk indoors.

The results showed that the outdoor ventilation rate is the most significant parameter. The calibrated ventilation rate with a 95% confidence level is 1.96 ± 0.31 ACH for Room 1 with mechanical ventilation, and 0.40 ± 0.08 ACH and 0.79 ± 0.06 ACH (occ1), 0.30 ± 0.04 ACH (occ2) for Rooms 2 and 3 with windows open only. Based on the calibrated model, we established the correlations between the CO_2 levels and the ventilation rates. A time-averaged CO_2 lower than 450 ppm is equivalent to a ventilation rate greater than 10 ACH in all three rooms, close to the recommended 12 ACH value for a safe indoor environment against airborne transmission in hospitals. School teachers may use the proposed correlations to estimate the ventilation rates from the CO_2 readings at any time during the day.

116

Using the Bayesian calibration method, this study also proposed calculating the "probability" of the probability of infection risk based on the calibrated ventilation rate, which helps quantify the uncertainty of outdoor ventilation rates. Moreover, this study estimated the required ventilation rate threshold and the CO_2 threshold values to prevent the airborne aerosol spreading of COVID-19 as a function of exposure time in the classrooms. The ventilation threshold at all hours is 8, 6, and 10 ACH for Rooms 1, 2, and 3, respectively, and the CO_2 threshold is around 500 ppm at all exposure times (< 8 hr) of a school day for all classrooms. This threshold is significantly different from the recommended value of 1000 ppm for commonly acceptable indoor air quality conditions before the pandemic. This is reasonable because a pandemic air quality requirement must be more stringent. Therefore, it is recommended that the ventilation rate and indoor CO_2 concentration thresholds be reconsidered in indoor spaces, especially school classrooms, in the current pandemic. The limitation of the current study is that school teachers manually collected the CO_2 data, which are random with uncertainties. More and continuous data (e.g., minute intervals) could be collected when we are allowed access to actual schools in session, which will be our next step. This study's proposed method and simulation tools can be applied and further verified by our future work.

Chapnter 6   Other Calibration and Prediction   Method : Ensemble Kalman Filter

Bayesian Inference is capable of calibrating computer simulation models with uncertainty to make the results more reliable and robust. However, thousands of iterations are needed to sample the posterior distributions of calibration parameters. Computing cost is the distinct limitation. Compared to Bayesian Inference, another calibration and prediction method, Ensemble Kalman Filter, a data assimilation algorithm, which is used to weather forecast, has gained more attention recently. The model state can be updated by assimilating the information provided by measurements. The computing cost is lower the Bayesian Inference. Several studies investigated its applications to indoor air quality and fire forecast [203–206]. This chapter explored the performance of Ensemble Kalman Filter to calibrate a building model of free cooling from a hybrid ventilatin system. The potential approach of combining Ensemble Kalman Filter and Bayesian Inference is proposed in next chapter.[6]

Combining natural and mechanical ventilation, hybrid ventilation is an effective approach to reduce cooling energy consumption. Although most existing control strategies for HVAC systems with hybrid ventilation provide acceptable operation results, there still often exists a mismatch of demand and response from the systems of sensing, decision making and operating. Especially when using renewable energy sources, such as solar, and/or thermal storage, many energy-saving decisions need to be made before the actual events may happen. As a result, predictive-based controls are preferred and the future energy loads and saving potentials from renewable measures should be evaluated in a forecasted manner. Typical prediction simulation methods are developed for designs and analysis, which may not ensure the required accuracy for modeling future events. In this study, a novel data assimilation method originating from numerical weather prediction, Ensemble Kalman Filter (EnKF), was proposed and applied for the forecasting simulations of high-rise building cooling load and energy-saving potential from its hybrid ventilation system. Similar to an accurate short-term weather prediction process, the proposed EnKF method can ensure the simulation accuracy by combining numerical simulations and measured data for short-

---

[6] This chapter has been published as a peer-reviewed journal paper: Danlin Hou, Cheng-Chun Lin, Ali Katal and Liangzhu Leon Wang (2020). "Dynamic forecast of cooling load and energy saving potential based on Ensemble Kalman Filter for an institutional high-rise building with hybrid ventilation." Building Simulation, https://doi.org/10.1007/s12273-020-0665-7.

term forecasting of future events. In the EnKF algorithm, a simulation model is adjusted according to the measuring data to output more accurate predictive results of the cooling load reduction from a hybrid ventilation system. Based on these predictions, the supply air temperature can be adjusted and the duration of applying natural ventilation in real-time to maintain the desired comfort of building occupants with less energy consumption than existing strategies. The proposed forecasting model can be applied in real life and operate successfully when combined with smart building controls. Results show that by applying EnKF, the predicted air velocity can follow the measurements trend. Key parameters of EnKF, like Kalman fiter gain and the number of ensemble member, are discussed as well. By using localized Kalman filter, the average RMSE and CVRMSE can be decreased 46.4% and 53.5%, respectively. The predition accuracy will increase with the enlargement of the number of ensemble member.

6.1   Introduction

Accounting for nearly 40% of total global energy consumption and 33% of total greenhouse gas emissions [1], buildings play an important role in sustainable development and de-carbonization policies. In the context of migration to cities, increasing wealth, and changing lifestyles, occupants' desire for better indoor comfort is inevitably higher than before, which may result in an increase in building energy consumption. In this situation, smart buildings are becoming increasingly popular worldwide. One of the main objectives of a smart building is to maintain occupants' comfort level and reduce building energy consumption simultaneously.

In general, building energy-saving technologies are one of the focuses of many previous studies on smart buildings. In recent years, variable energy-saving technologies, such as ground and water source heat pump [207–209], heating, ventilation, air condition (HVAC) system with ice/thermal storages [210–212], renewable energy utilization [213,214], and demand response control strategies [215,216], are developed rapidly. Natural and hybrid ventilation systems are also effective approaches to obtaining free cooling [217–219]. A natural ventilation system can reduce air conditioning demand and improve thermal comfort by exploiting the ambient air as a heat sink [220]. The hybrid ventilation system can be adjusted between mechanical and natural ventilation using suitable control strategies leading to considerable energy savings [221]. Although various methods are utilized to estimate the performance of natural/hybrid ventilation on energy saving potential, almost none of them can predict the amount of free cooling and operate accordingly

under the real-time change of the environmental conditions. In reality, forecasting the performance of the natural/hybrid ventilation system and making flexible operational decisions based on future environmental information are very important and useful.

Integration with building energy-saving technologies and maintaining their adaptability are important topics in smart buildings. A smart building with strong adaptability should prepare the building for a particular event before it happens [6]. Model-based predictive controls (MPC) offer an explicit non-heuristic approach to reinforce the building's adaptability. With the rise of the concept of the Internet of Things (IoT) [10] and its development, buildings are equipped with sensors, monitors, cameras to make it much more convenient to gather real-time information internally and externally from a range of sources. This provides an alternative way to use dynamic characteristics of measurement data instead of its static application for better calibration and validation of a simulation model, which can then be used for better predictions and controls.

The major task of forecasting simulations is to update the model state to make sure it can predict future physical phenomenon with a certain lead time and reliability. In order to find the most promising model states, data assimilation provides a range of algorithms for model parameter estimation under consideration both of model uncertainty and measurement error. Data assimilation is typically a sequential time-stepping procedure, in which a previous model forecast is compared with newly received observations to obtain a more precise model forecast. It was first proposed by R. E. Kalman in 1960, as the presentation of Kalman filter which utilizes a recursive solution to find the most possible estimation of the true state with a dynamic model evolvement over time [222]. Kalman filter has been widely applied in building field research for a long time [223–225]. In order to develop data assimilation from linear system to nonlinear system, several variats of Kalman filter have been proposed. By using partial derivatives, Extended Kalman Filter (XKF) can linearize the nonlinear models [226]. Although its effectiveness has been proven in many applications, the error probability density is not fully considered in the linearization. In addition, the extra numeirical operations of the linearization can increase the computational burden drastically. Another popular development of data assimilation for nonlinear problems is four-dimensional variational assimilation (4D-Var) which is based on minimizing a cost function . In 4D-Var, manipulation of large matrices is needed to calculate the gradient of the cost function whichmakes it computationally intensive. In order to reduce the computational burden, Evensen proposed an affordable method, Ensemble Kalman Filter (EnKF) [227]. In the EnKF, Monte Carlo

method was used to generate ensemble members and calculate them separately to determine error statistics instead of direct calculation and storageof the evolution of the large error covariance matrices in XKF. The application of EnKF first appeared in the field of weather forecasting where the models are extremely high order and nonlinear with highly uncertain initial states and abundance of measurements [228,229]. Now it has expanded to many other fields owing to its simple conceptual formulation and feasible implementation [230–233]. In the research field of the building side, some applications of EnKF already existed [203–206]. However, these studies mainly focus on fire simulations in buildings. The potential of EnKF for other building aspects deserves to be further explored.

In this paper, EnKF is applied to the field of forecasting of energy load and energy-saving potential. Under the consideration of observation's impact, free cooling from a hybrid ventilation system could be forecasted accurately which could be used for further MPC control. In the following sessions, EnKF and its application in a high-rise institutional building with hybrid ventilation are introduced. The simulation results are then reported. In addition, key parameters in EnKF including localized Kalman Filter and the number of ensemble members, are discussed with more details.

6.2 Methodology

Ensemble Kalman Filter is a kind of data assimilation technique, which is capable of outputting more reliable forecasting, especially for a large-scale nonlinear dynamic system. It is developed and extended from classic Kalman Filter and Extended Kalman Filter. In EnKF, the error statistics could be predicted by using a stochastic or Monte Carlo method [234–236]. This estimation method can avoid the evolvment of cavariance matrix to reduce the computational burden dramatically. Owing to its simple conceptual formulation and feasible implementation, EnKF gained much more popularity and applications to variable research fields.

Considering a discrete-time nonlinear dynamic model

$$x_k = f(x_{k-1}, \Phi_{k-1}) + w_k \tag{6-1}$$

where $\Phi_{k-1} \in \mathbb{R}^m$ is the control vector, $w_k \in \mathbb{R}^n$ is a stationary zero-mean white noise process with covariance matrices Q_k, $x_k \in \mathbb{R}^n$. Subscript k and k-1 represent two sequential time steps. The measurement data corresponding to the mentioned model state can be expressed as

$$y_k = Hx_k + v_k \tag{6-2}$$

where the matrix H relates the model state x to the measurement y and can be an identity matrix I if x and y represent the same quantity. The $v_k \in \mathbb{R}^p$ is the observation noise and its corresponding covariance matrix is R_k. Moreover, x_0, w_k, and v_k are assumed to be uncorrelated.

The objective of EnKF is to approximate the model state x_k by using an optimal estimation x_k^a through combining measurements y_k. In general, the process of EnKF could be divided into two steps: forecast step and analysis step as shown in Figure 6-1.
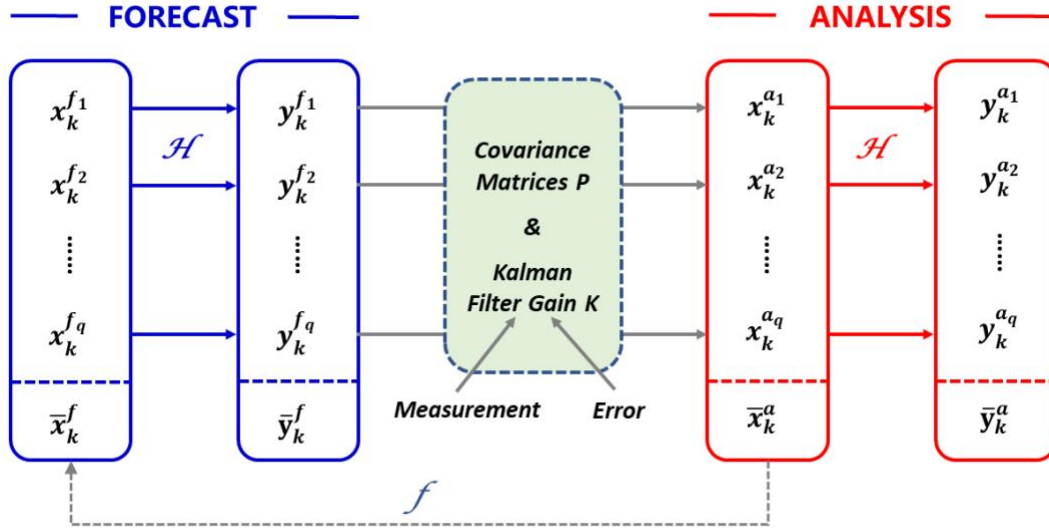

Figure 6-1 Data flowchart of EnKF.

For the forecast step, by perturbing the original state at time k, an ensemble of q forecasted state estimates was obtained with random sample errors. We define this ensemble as

$$X_k^f \triangleq (x_k^{f_1}, x_k^{f_2}, \dots, x_k^{f_q}) \tag{6-3}$$

where $X_k^f \in \mathbb{R}^{n \times q}$, and the superscript f_i refers to the ith forecast ensemble member.

Owing to the unavailability of the true state x_k, the mean value of ensemble members $\bar{x}_k^f \in \mathbb{R}^n$ is used to approximate it.

$$\bar{x}_k^f \triangleq \frac{1}{q} \sum_{i=1}^{q} x_k^{f_i} \tag{6-4}$$

$$x_k \doteq \bar{x}_k^f \tag{6-5}$$

Then the ensemble of the model error matrix $E_k^f \in \mathbb{R}^{n \times q}$ and the ensemble of the output error matrix $E_{yk}^f \in \mathbb{R}^{p \times q}$ are respectively defined as

$$E_k^f \triangleq (x_k^{f_1} - \bar{x}_k^f, x_k^{f_2} - \bar{x}_k^f, \dots, x_k^{f_q} - \bar{x}_k^f) \tag{6-6}$$

$$E_{yk}^f \triangleq (Hx_k^{f_1} - H\bar{x}_k^f, Hx_k^{f_2} - H\bar{x}_k^f, \dots, Hx_k^{f_q} - H\bar{x}_k^f) \tag{6-7}$$

The forecast state error covariance is denoted as

$$P_{xy_k}^f \triangleq \frac{1}{q-1} E_k^f (E_{y_k}^f)^T \tag{6-8}$$

$$P_{yy_k}^f \triangleq \frac{1}{q-1} E_{y_k}^f (E_{y_k}^f)^T \tag{6-9}$$

Here, $\frac{1}{q-1}$ is used to replace $\frac{1}{q}$ to make sure the estimation is unbiased [237].

Thus, the forecast ensemble mean value and the spread of the ensemble members around it are regarded as the best forecast estimate of the state and the error between the best estimate and the actual state, respectively.

For the analysis step, the classic Kalman Filter Gain expression K_k is used

$$K_k = P_{xy_k}^f (P_{yy_k}^f + R)^{-1} \tag{6-10}$$

Then the optimal estimation of the true state is calculated by

$$x_k^{a_i} = x_k^{f_i} + K_k (y_k - H\bar{x}_k^f) \tag{6-11}$$

$$\bar{x}_k^a = \frac{1}{q} \sum_{i=1}^{q} x_k^{a_i} \tag{6-12}$$

Finally, $\bar{x}_k^a$ can be used as x_{k-1} in Eq. 6-1 for the next time step forecast. Although the computational burden for Kalman filter gain K in EnKF is more affordable compared with conventional Kalman Filter, Eq. 6-4 implies that q parallel copies of the model have to be simulated. Therefore, the computational burden will become greater with the increase of the number of ensemble members. The estimation accuracy and computational burden need to be balanced in EnKF, which will be discussed in Section 4.

6.3 Case Study

As a case study, a typical institutional high-rise building (the EV building) of Montreal Canada is selected. In this section, firstly, more details about the EV building is described. Then a multi-zone model that is used to simulate EV building's energy performance is illustrated. Finally, how to forecast more reliable energy load and saving by using EnKF is introduced.

6.3.1 Description of the target building

The EV building is a 17-story institutional building with two main large facades facing approximately southwest and northeast, respectively. The building was designed and constructed for the use of a fan-assisted hybrid ventilation system (Figure 6-2). The 1st floor is underground and the 17th floor is used for mechanical purposes. At the roof of the building, there is a variable speed fan system whose maximum airflow of 40,000 L/s and is operated when needed to reinforce the natural ventilation. From the second floor to 16th floor, every three stories, there is an atrium (W×L×H = 9 m×12 m×12 m) at the middle of the southwest-facing part of the building. Each atrium connects to another through a 4 m^2 opening on the floor or slab with motorized dampers. Openings can be fully closed for fire protection purposes. Grills were set on these openings considering the safety and convenience. At facades facing southeast and northwest, openings were designed as inlets and outlets for the cool outdoor air and warm indoor air. With the motorized dampers equipped on the openings, the supply air rate of each opening could be controlled individually. With the help of a large window-to-wall ratio of around 50%, plenty of natural daylight and solar heat gains can be obtained. Simultaneously, the solar chimney effect is formed and will be reinforced when the hybrid ventilation is in operation. Due to the buoyancy with or without the fan-assistance, outdoor fresh air at a lower temperature is drawn into the building through the openings on facades and passes throughout the building through the openings on the floor of each atrium. After absorbing indoor heat, the warmed air is exhausted by the exhaust fan on the top. Free cooling is utilized during this process and less energy is consumed during cooling mode.
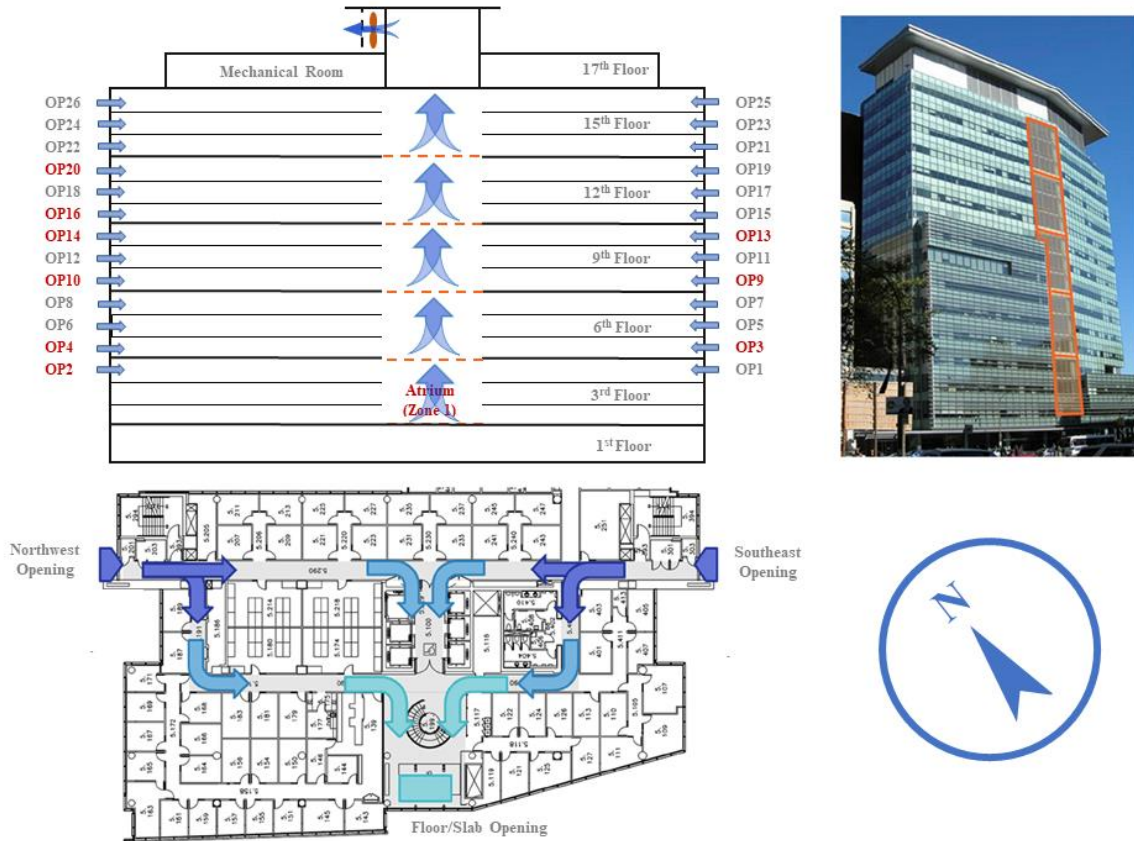
Figure 6-2 Schematic of the studied hybrid ventilation system in the EV building.

6.3.2 Multi-zone model

To simulate the target building and its hybrid ventilation system, in this study, a numeric model is developed using C++ based on a coupled thermal/airflow multi-zone network model [238]. The indoor environment of corridor areas of each floor and atriums could be simulated according to the actual service scope of the hybrid ventilation system. Equations about mass balance and energy conservation are used as governing ones to apply to each zone to calculate airflow rates and heat transfer strengths. By using the "fully-simultaneous" coupling strategy, the mass and energy balance equations for all zones are solved simultaneously. The input of the simulation model is building basic information, weather condition, fan status, occupant and equipment schedule, etc. The output of the simulation model is the fresh air velocity at openings, cooling load, free cooling and indoor air temperature of each zone. The mass conservation equation for each zone is

$$\frac{dm_i}{dt} = \sum_j F_{ji} + F_i \tag{6-13}$$

where F_{ji} is airflow rate (kg/s) between zones j and i; a positive value indicates flow from zone j to i and a negative value indicates flow from zone i to j. F_i (kg/s) defines sources and sinks that could add or remove air to or from the zone. m_i is the air mass flow rate in zone i (kg/s). The energy conservation equation for zone i is

$$\rho_i c_{pa} V_i \frac{dT_i}{dt} = \sum_{j:F_{ji}>0} F_{ji} c_{pa} T_j - \sum_{j:F_{ij}>0} F_{ij} c_{pa} T_i + S_i + \sum_k h_k A_k (T_{mk} - T_i) \qquad (6\text{-}14)$$

where T_j is the air temperature of zone j (k), S_i is heat gain in zone i (W). T_{mk} is the surface temperature of the thermal mass (ceiling, floor, or wall) that are connected to the zone i (K). h_k is convective heat transfer coefficient between the air and the thermal mass (W/m²·K), A_k is the corresponding surface area of the thermal mass (m²), and C_{pa} is the specific heat of the air (J/kg·K), ρ_i is the air density (kg/m³), and V_i is the air volume through the air dampers (m³).

The orifice airflow equation is used for the modeling of airflow through inlet dampers:

$$\dot{m} = C_d A \sqrt{2\rho_0 \Delta P_{ij}} \qquad (6\text{-}15)$$

where $\dot{m}$ is the mass flow rate in kg/s; ρ_0 is the outdoor air density, kg/m³; Δp is the pressure difference across the damper, Pa; A is the area (m²); C_d is the flow coefficient, which is related to the inlet flow resistance, and the ambient conditions play a key role in the simulation performance. The free cooling from fresh air through inlet dampers could be calculated as:

$$q = M \times c_{pa} \times (T_{exhaust} - T_0) \qquad (6\text{-}16)$$

where $T_{exhaust}$ is the temperature at exhaust and T_0 is the outdoor temperature, M is the total fresh airflow rate through the side dampers (kg/s), and c_{pa} is specific heat capacity.

6.3.3   EnKF combination

In general, the discharge flow coefficient C_d is determined empirically or experimentally. Inaccurate estimation could lead to a large mismatch between the actual situation and simulation states. Furthermore, the amount of free cooling and energy-saving potential would be inaccurate during the forecasting step. Since this key parameter changes according to environmental weather conditions, especially local wind speed, it is very difficult to set an accurate value. Therefore, in this paper, C_d is selected as the key parameter in the model state. Since both of measurement inaccuracy and model uncertainty are considered in EnKF, the updated C_d has a more comprehensive meaning rather than its original defined physical meaning.

Fresh air velocity is regarded as observations in EnKF. In order to obtain measurements of fresh air velocity through side openings, Hot-Wire anemometers were installed (Figure 6-2). The time-step of recording the data is 60 seconds. The measurement range of the airspeed is 0.2 ~ 25 m/s and the accuracy is ± (5%+0.1 m/s). Considering the uncertainty of the multi-zone model, finally, the measurement uncertainty R, required in Eq. (6-10) in EnKF is set as 10%. The number of ensemble member q is 60 which is discussed later.

The observed data of a typical day, from 8:00 to 14:00 on Aug 30th 2018 were employed, including the weather data (outdoor temperature, humidity, solar irradiation, wind direction and wind speed) collected from the weather station installed on the roof of the EV building, and measured air velocity near the selected openings shown in Figure 6-3. The initial indoor temperature is 24 ℃ and the time step of the simulation is 15 minutes.
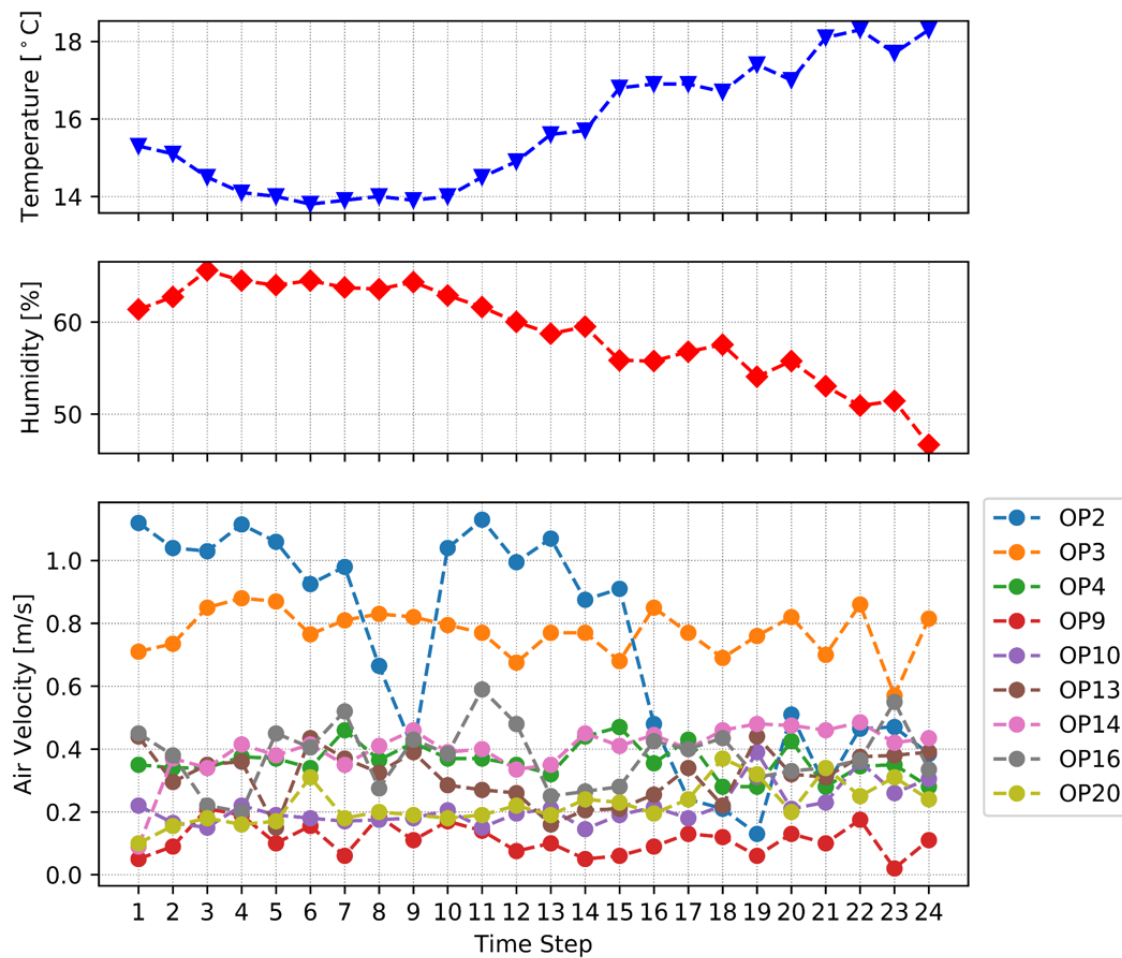

Figure 6-3 Selected weather inputs and air velocity measurements.

6.4 Simulation Results

By using the proposed method, the discharge coefficient C_d could be updated according to the environmental circumstances as shown in Figure 6-4. The air velocity both from the measurements and the EnKF simulation are shown in Figure 6-5. From the simulation result, it is obvious that the dynamic calibrated C_d followed the trend of the corresponding observations closely. When the air velocity is stable, the change of C_d is not obvious, e.g. for opening 16. However, if the air velocity changes dramatically, C_d starts to oscillate. Taking an example of opening 2, the air velocity could be roughly classified into two groups: around 1 m/s and 0.4 m/s. Therefore, the C_d values generated by EnKF have similar groups. Especially for the dramatic decrease in air velocity at the time step 8, it could be reflected by the C_d at time step 9. The difference between the average value of ensembles and the final output of EnKF displays the function of the Kalman Filter. The dynamic estimation of total C_d is shown in Figure 6-6. Since C_d is strongly influenced by environmental conditions, a stable value could not enable an accurate forecast simulation.
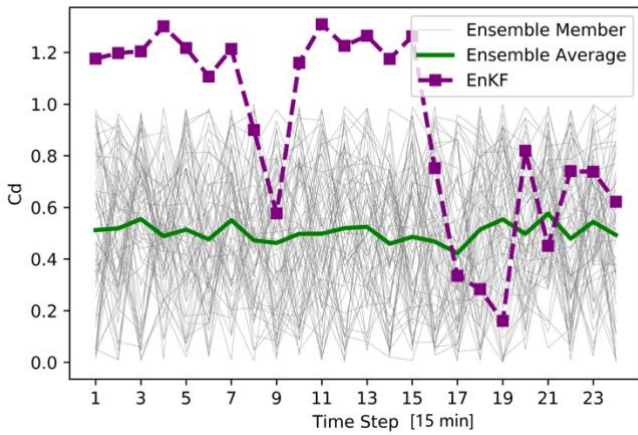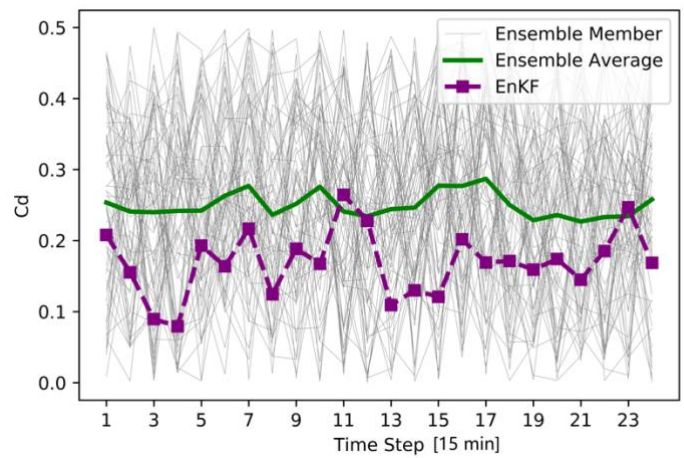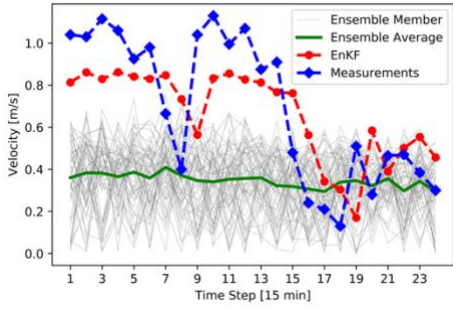

(a)   (b)
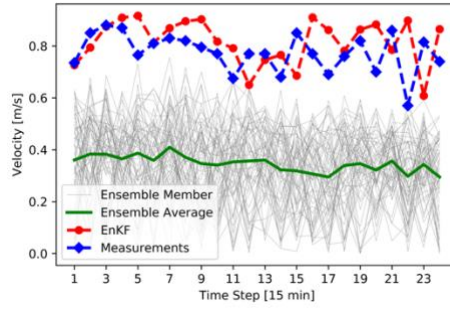
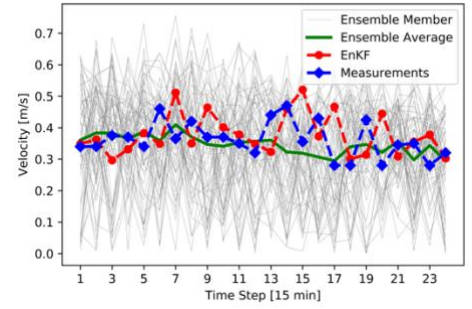Figure 6-4 Posteriori estimation of Cd: (a) Opening 2; (b) Opening 16.

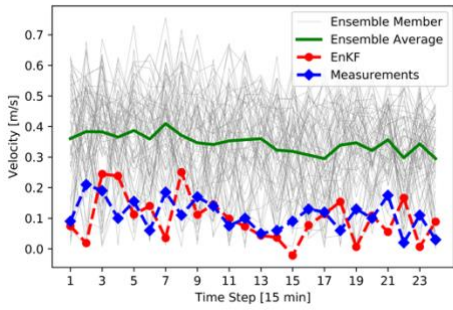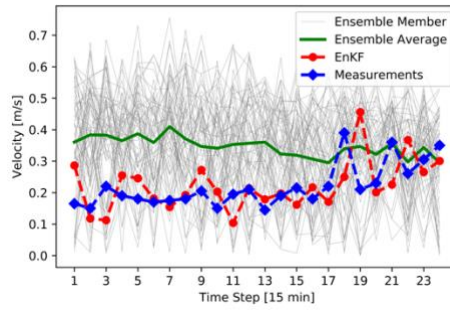OP 2   OP 3   OP 4

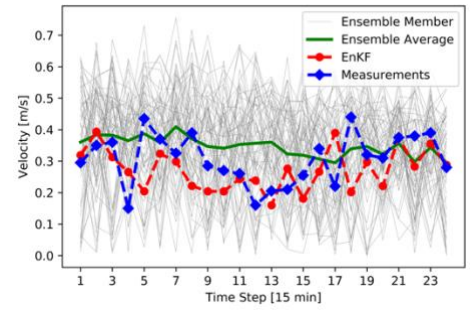OP 9   OP 10   OP 13
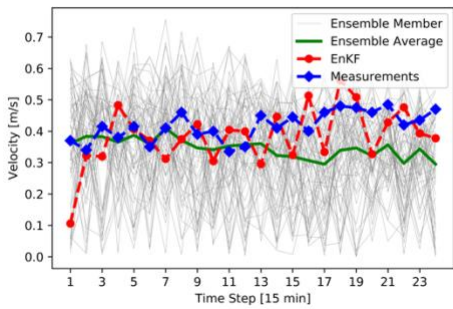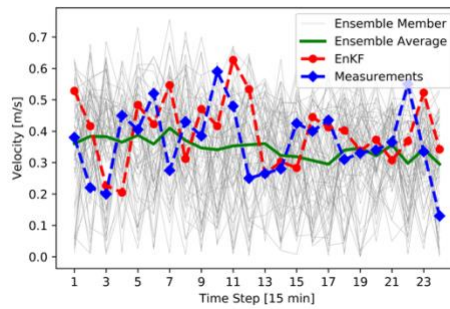
OP 14   OP 16   OP 20
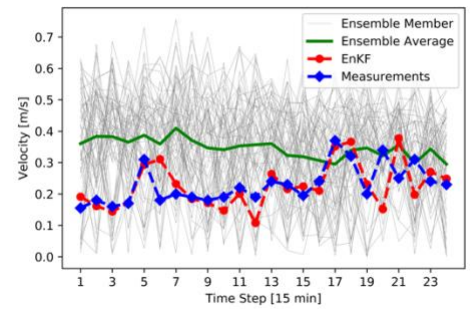
Figure 6-5 EnKF prediction of air velocity
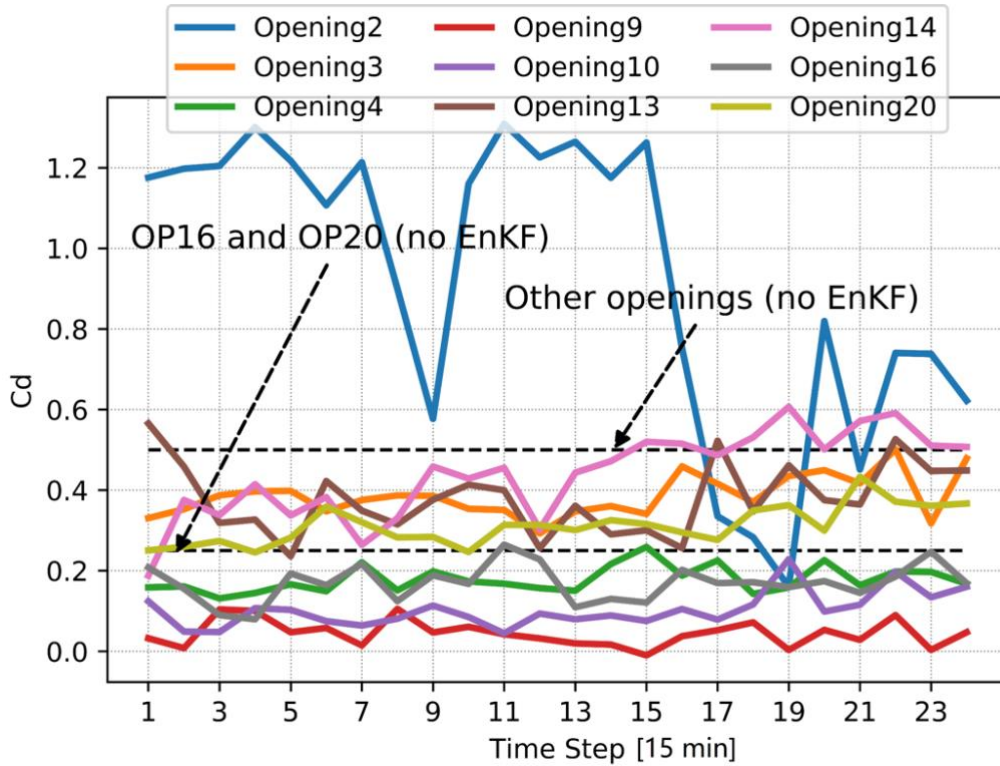
Figure 6-6 Dynamic estimations of C_d for all openings.

Figure 6-7 illustrates the results of building energy performance during the whole simulation period considering the COP is 3.5. The largest discrepancy of energy demand and potential energy saving by the hybrid ventilation system in each time step is 32.3% and 47.4%, respectively. This large difference will directly influence further on the control strategy.
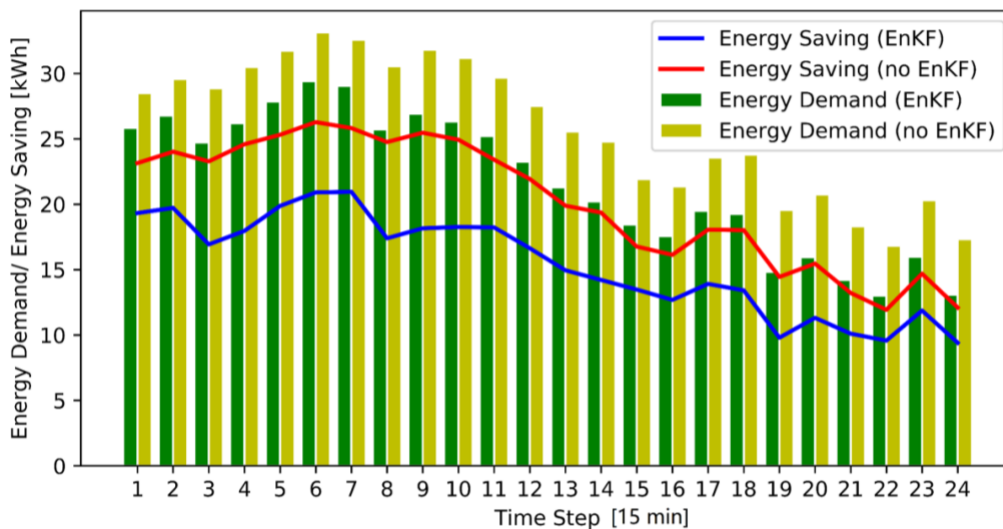
Figure 6-7 Simulated energy demand and saving potential.

6.5 Discussion of Key Parameters   in EnKF

In EnKF, the determination of several key parameters plays an important role in the assimilation performance including the simulation and observation error covariance, and the accuracy of the true states of the system. In addition, owing to the unique character of the building environment and its forecasting, the determination of these parameters can be totally different from that of other types of systems. In this section, the impact of spurious correlation and ensemble numbers will be discussed. The data used in this section is the same as in the case study.

To have a clear assessment of the model performance under different situations, three statistical indices are used, including the root mean square error (RMSE) (Eq. 6-17), the coefficient of variation with RMSE (CVRMSE) (Eq. 6-18), and the computing time.

$$RMSE = \sqrt{\frac{\sum_{i=1}^{n}(y_i - \hat{y}_i)^2}{n}} \tag{6-17}$$

$$CVRMSE = \frac{RMSE}{\bar{y}} \tag{6-18}$$

where $\hat{y}_i$ denotes a predicted variable value for period i, y_i is an observed value for period i, $\bar{y}$ is the mean of the observed value, and n is the sample size.

6.5.1 Spurious correlations and localization

In general, the correlation between the two physical states is influenced strongly by the spatial distance between them. The correlation possibility will become larger with distance shorten. In EnKF, the measurements are applied to approximating the error covariance matrix for the real model state with the neglection of the actual situation even though the certain model state is beyond the impact of some measurements. This kind of neglection can produce spurious correlations and lead to a significant underestimation of the true variance and filter divergence [239]. Therefore, the spurious correlations between the observations and model states should be avoided.

A formulate localization method was proposed by Houtekamer and Mitchell for EnKF [240]. In his study, a Schur-product θ is applied in the improvement of Kalman Filter Gain.

$$\theta = \begin{cases} -\dfrac{1}{4}d^5 + \dfrac{1}{2}d^4 + \dfrac{5}{8}d^3 - \dfrac{5}{3}d^2 + 1, 0 \le d \le 1 \\ \dfrac{1}{12}d^5 - \dfrac{1}{2}d^4 + \dfrac{5}{8}d^3 + \dfrac{5}{3}d^2 - 5d + 4 - \dfrac{2}{3d}, 1 \le d \le 2 \\ 0, 2 \le d \end{cases} \qquad (6\text{-}19)$$

$$d = \frac{|z|}{c} \qquad (6\text{-}20)$$

where z is the spatial distance between the location of the observation and a grid point. c is the distance to define the correlation scaling between two nodes. d is a dimensionless variable calculated by z and c. The correlation is assumed to be 1.0 when the distance is below c and gradually reduced to 0 when the distance increases to $2c$, as shown in Figure 6-8.
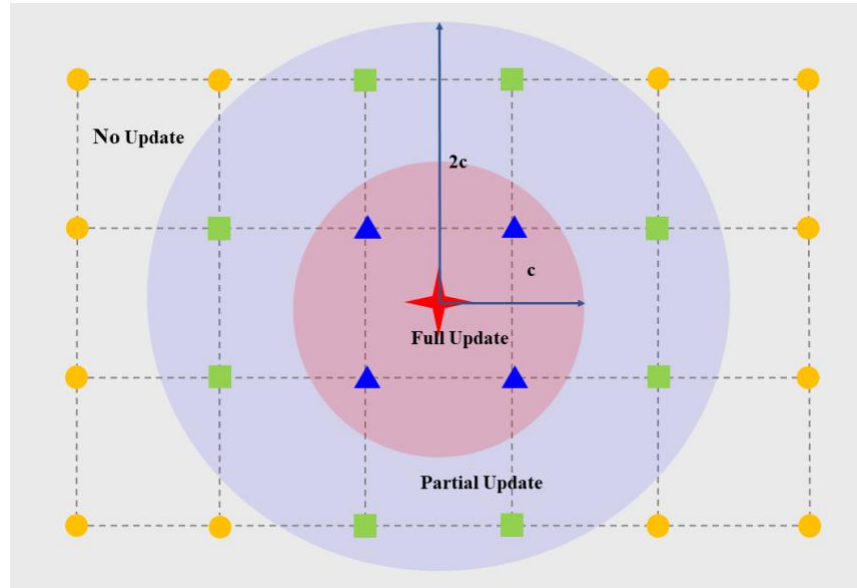
Figure 6-8 Illustration of localization of model states.

The localized Kalman Filter Gain can be determined as

$$K_k = \theta \circ P^f_{xy_k}(\theta \circ P^f_{yy_k} + R)^{-1} \qquad (6\text{-}21)$$

Figure 6-9 shows an air velocity comparison for opening 16 using the EnKF model with or without the localization improvement. As shown by the red line and blue line, the prediction using the localization method could follow the trend of actual measurements closely. The discrepancy between the prediction under localization and measurements is relatively small. While for the prediction represented by the green line, it is obvious that the trend is exaggerated. Without the localization, spurious correlations are mistakenly applied and finally result in an inaccurate

132

estimation of the discharge coefficient, the key parameter of the simulation model. For a total of 9 openings, the comparisons of RMSE and CVRMSE are shown in Figure 6-10. It is shown that the average RMSE of total 9 openings is decreased 46.4% (from 0.28 to 0.15), and the average CVRMSE is decreased 53.5% (from 1.01 to 0.47), which is a clear evidence of the improvement of the localization method.

Figure 6-9 Comparison of measured and predicted air velocity for Opening 16.
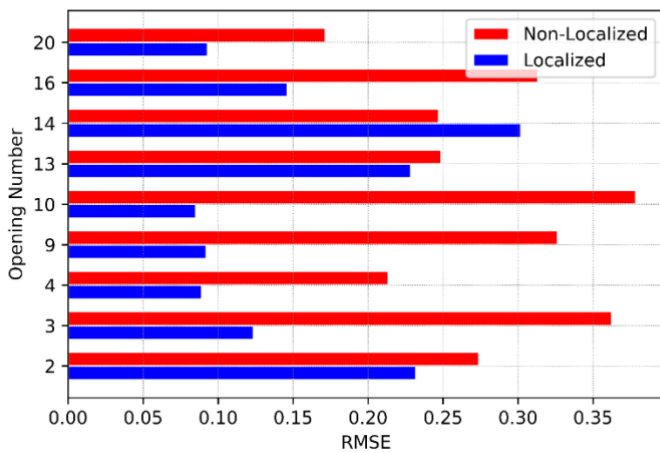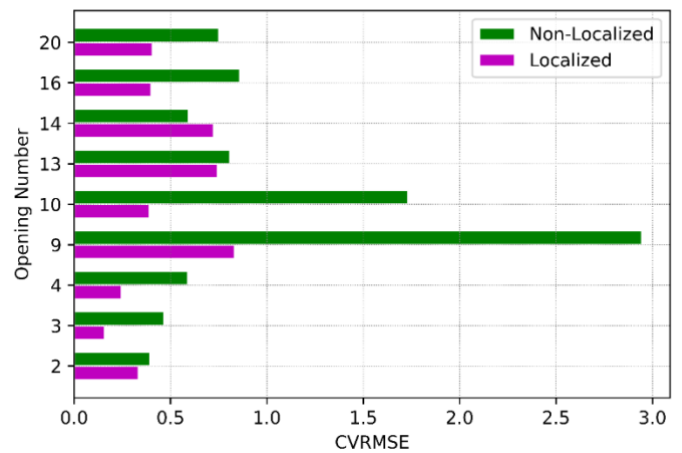
(a)   (b)
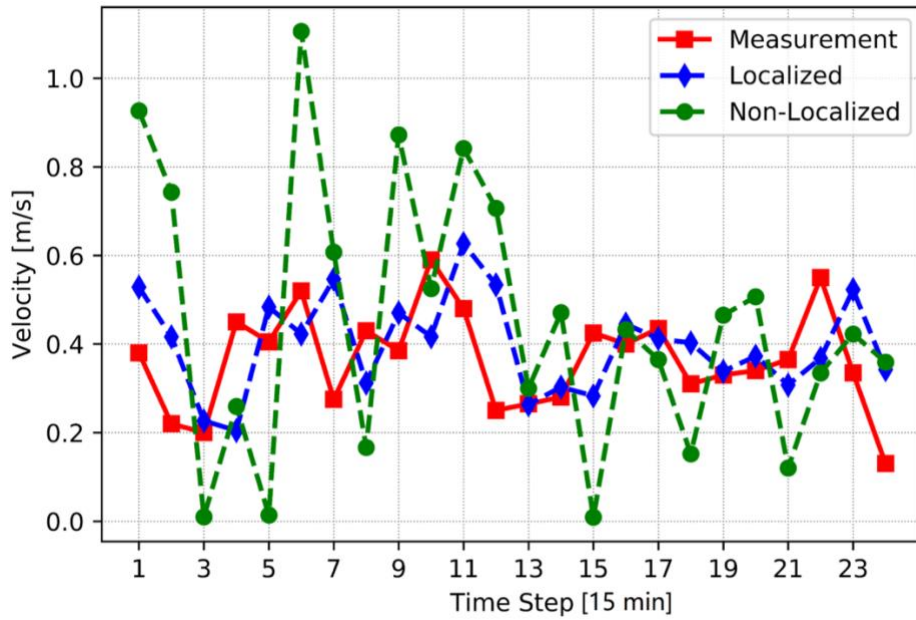
Figure 6-10 Comparisons of air velocity error with/without localization.

6.5.2   Number of Ensemble   member

It is often common for the Monte Carlo study that more accurate results can be obtained when larger ensemble members are applied. However, Eq. 6-4 implies that q parallel copies of the model have to be simulated which will affect the computational cost directly. Figure 6-11 shows the comparison of average RMSE and CVRMSE when different numbers of ensemble members are used for EnKF. Both of them increase dramatically with the decrease of ensemble numbers when it is less than 60, especially for the decrease from 20 to 10. On the other hand, the simulation time increased with the number of ensemble numbers (Figure 6-12). Considering both accuracy and computational cost, 60 ensemble members seem to be the best choice for the modeled hybrid ventilation system. It is noted that the increase of ensemble members seems not always generate a more accurate result. For example, the RMSE and CVRMSE values of 80 and 90 ensembles is higher than that of 70 ensembles. This may be related to the ensemble strategies which need further study.
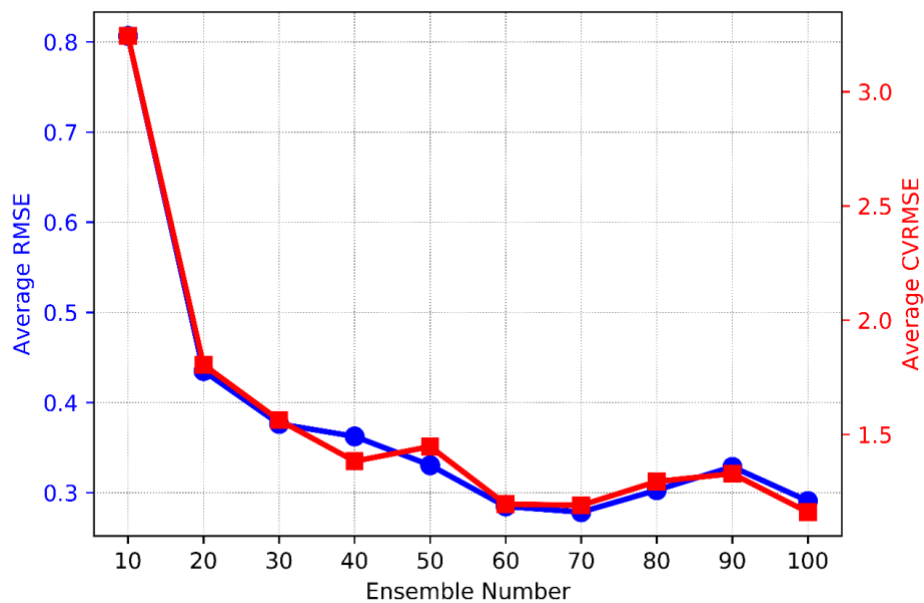
Figure 6-11 Velocity comparison of RMSE and CVRMSE with a variable number of ensemble members.
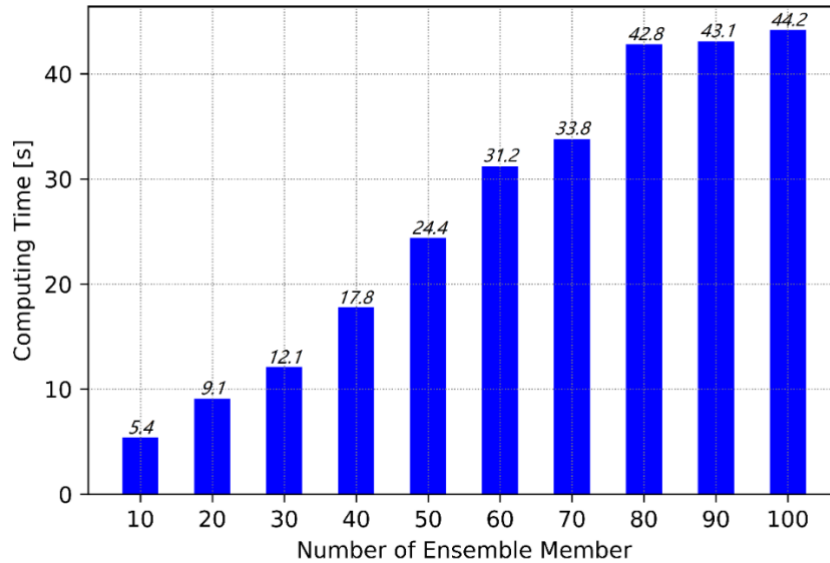
Figure 6-12 Computing time for each time step using different numbers of ensemble members.

6.6 Conclusions

In this paper, a data assimilation method, EnKF, was applied to forecasting the free cooling energy saving from a hybrid ventilation system of an institutional building. Since the discharge coefficient is highly impacted by the environmental condition, a constant value of this key parameter is not reasonable. By using the proposed data assimilation algorithm EnKF, the discharge coefficient can be calibrated dynamically. The predictability of a regular model can be improved by combining sensor measurement data. Then the spurious correlation and number of ensemble members, two important parameters in EnKF, were discussed. The results indicate that the spurious correlation can lead to a large difference between the observations and predictions. It can be avoided by the improvement of the Kalman Filter Gain using a localized method. Additionally, in general, a larger number of ensemble members can generate a more accurate prediction.

For a practical application, the proposed forecast EnKF model can be combined with the smart building operation and sensor systems, such as those based on IoT technologies, for the actual building HVAC systems. For our future work, other parameters in EnKF should be discussed to quantify their impact on EnKF performances. In addition, the observation strategy should also be investigated to obtain better forecasting with fewer sensor measurements. Finally, more

applications of EnKF to other dynamic building systems and their interactions with the surrounding environment may be explored.

Chanpter 7   Conclusion and Future Work

7.1   Conclusion s

This research established a new and comprehensive Bayesian Inference calibration platform to calibrate building energy and environment models. The results indicate that the proposed platform can improve the predictability of building energy models by considering uncertainties and absorbing information provided from measurements. Unlike other methods that calibrate models deterministically, the Bayesian models of this thesis can calibrate model parameters with probabilities. The models presented in this thesis provide more reliable and accurate predictions and require lower computational resources employing meta-models compared to other conventional methods.

For Bayesian Inference calibration, generally, thousands of iterations are needed to generate posterior distributions of calibration parameters. The computing cost is high. To compensate this weakness, another calibration and prediction method, Ensemble Kalman Filter, was studied. A general approach of forecasting the free cooling load of a hybrid ventilation system using EnKF is outlined. Results show that the EnKF can statistically update model parameters to maintain the forecasting accuracy and reliability for longer durations.

7.2   Contributions

The following is a list of significant findings and contributions from this thesis regarding building environment and energy model calibration and forecasting using Bayesian Inference and EnKF:

- A systematic review was conducted of building energy model calibration by Bayesian Inference. All studies on the topic were summarized. The theories of Bayesian Inference and Markov Chain Monte Carlo were discussed. A calibration framework was proposed based on the revision and extraction of previous studies with the authors' experience. The currently available tools for each step of the calibration were reviewed and assessed, and the most effective ones were recommended.

- A new auto-calibration platform using Bayesian Inference was developed. It is the only platform on which calibration can be conducted that considers uncertainties using Bayesian Inference. The proposed platform can complete the holistic calibration process, from the preparation of measurements to future analysis. The embedded sensitivity analysis module

can rank the importance of model parameters to help users determine the calibration parameters. In addition, it is the first calibration platform that can be used to develop a meta-model instead of the original building energy models. This can save a significant amount of computing time. The developed platform can be applied to building energy models, building thermal models, and indoor air quality models.

- The complicated relationship among the calibration parameters, calibration performance, and the meta-model's accuracy was explored. According to the results, the first five important parameters should be included in the calibration process.

- This research is among the first studies to use Bayesian Inference calibration for thermal predictions of buildings. The predictions with uncertainties are more reliable and robust.

- This research is the first study to use Bayesian Inference to estimate indoor air quality. The ventilation rate can be estimated with probability based on indoor CO_2 concentration. Then, the possibility of the probability of infection risk can be calculated. This is the first study to propose the idea of calculating the probabilities of infection risk with uncertainties.

- This thesis is the first study of use of numerical weather prediction models and data assimilation techniques, specifically EnKF, for forecasting simulations of the free cooling potential of a hybrid ventilation system. The proposed study method can be applied to real-time forecasting of the cooling load potential connecting to Internet of Things.

- EnKF is more flexible when the localization method is applied, especially when specific model parameters and model states are not highly correlated.

7.3   Future Work

The work undertaken in this thesis has highlighted exciting research questions and future investigations. Below are some of the recommendations for the future work.

- Develop a real-time automatic calibration platform

    One of the features of Bayesian Inference is that the accuracy and reliability can be increased by assimilating measurement data, which can be easily obtained from the Internet of Things. However, thousands of iterations are needed to sample the posterior distributions of the calibrated parameters. The issue of computing cost cannot be neglected when developing a real-time calibration platform. Compared to Bayesian Inference, the EnKF is a lightweight algorithm. The integration of EnKF and Bayesian Inference can

combine their strengths and avoid their weaknesses. In addition, the real-time Bayesian Inference & EnKF calibration platform can be developed for the web and a mobile application. An interactive map can be developed that is linked with GIS data. The workflow of the proposed platform is shown in Figure 7-1.
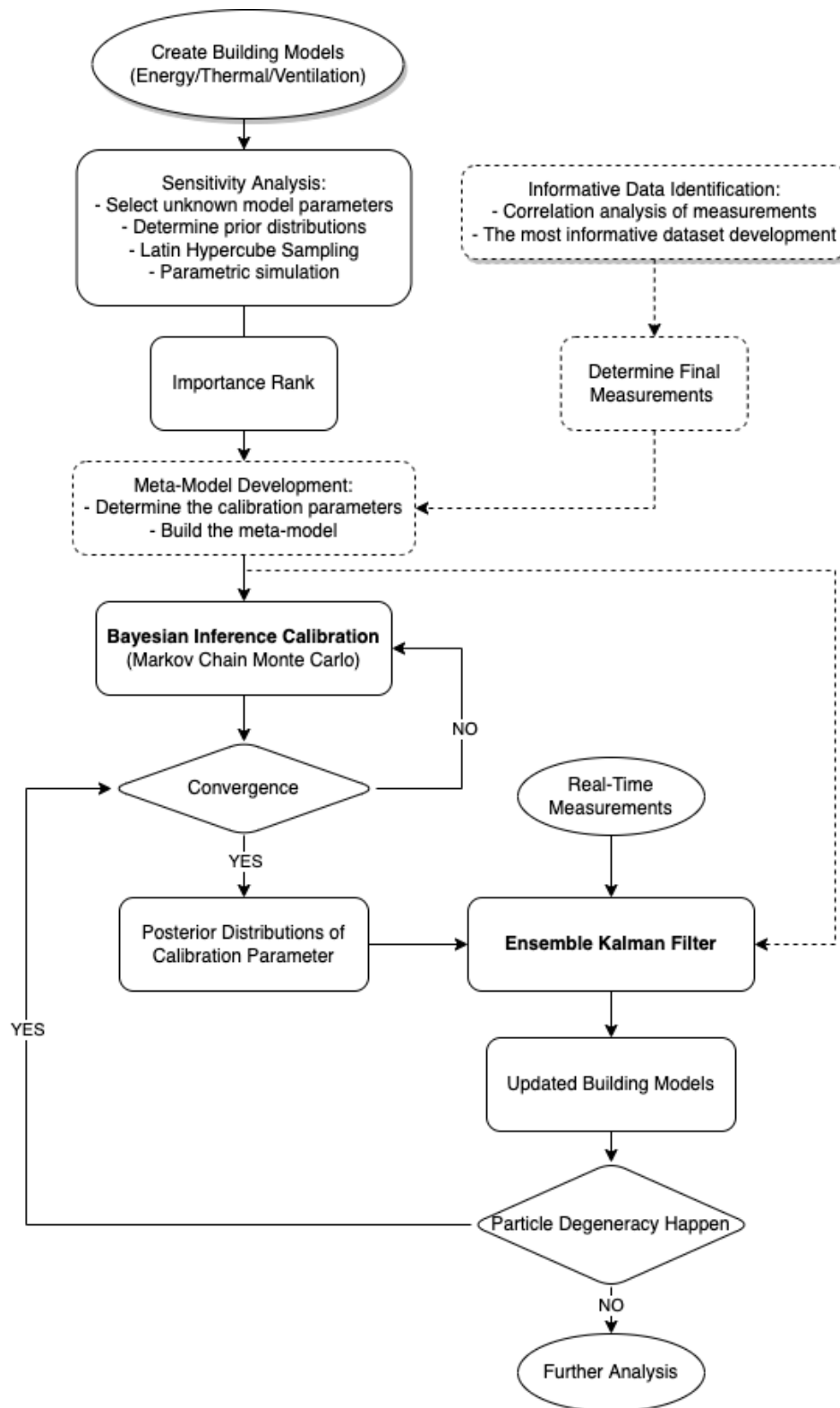
Figure 7-1 Overview of proposed real-time calibration workflow using Bayesian Inference and Ensemble Kalman Filter

- Improve interoperability with other   building simulation software

  Currently, only EnergyPlus can be coupled with the developed Bayesian Inference calibration platform for the modeling of building energy. However, other software is employed in building energy modeling. To make it more pupular, the proposed calibration platform should be able to work with more software.

  Taking an instance of CFD, its application is popular, but determining several vital inputs is difficult, especially for new users. The Bayesian Inference calibration may be used to investigate the suitable values of critical inputs.

- Calibrat e and predict at   the urban scale

  With rapid urbanization, building energy and environment models have been developed and applied at the district and city levels. It is more difficult, however, to calibrate city-scale models to guarantee acceptable accuracy. How to select the calibration parameters and what their values should be deserve in-depth studying. Bayesian Inference is a potential way to solve these issues. The proposed platform has been demonstrated for individual buildings but needs to be expanded for an urban scale.

- Reduce computing requirements

  Once the proposed platform is applied to the city level, the computing cost is high. Greater computing performance and longer computing time are needed. More research is therefore needed into organizing and classifying the data of many buildings. One solution is to group and classify similar individual buildings. Another solution is to work with a supercomputer. The platform should be modified to work on different operating systems.

- Develop a machine learning -based meta-model

  Machine learning approaches are more intelligent than conventional meta-models. Owing to the limitation of the MCMC package, only a few meta-models can be selected in the proposed Bayesian Inference platform. In the future, the available meta-model types should be more diverse, and machine learning methods can be included in the Meta-model module.

- Consider uncertainty from   occupancy behavior

  Occupancy behavior contributes significantly to uncertainties in building energy and environment modeling. Occupancy behavior is highly correlated with building type and function. Building schedules and occupancy density profiles have traditionally been simplified using steady and deterministic hourly schedules and peak loads. Further study

of the schedule model that takes into consideration uncertainty due to human behavior is required.

- Down scale from building level to room level

  In this thesis, the Bayesian Inference calibration works on a building level. In the future, the platform should be improved so that it can work at a room level.

- Compar e with other calibration methods

  The Bayesian Inference calibration approach can be compared to other methods to see where more improvements can be made.

References

[1]   Cuce E, Harjunowibowo D, Cuce PM. Renewable and sustainable energy saving strategies for greenhouse systems: A comprehensive review. Renew Sustain Energy Rev 2016;64:34–59. https://doi.org/10.1016/j.rser.2016.05.077.

[2]   U.S. Energy Information Administration. International Energy Outlook. Outlook 2019;0484:70–99. https://doi.org/https://www.eia.gov/outlooks/ieo/pdf/ieo2019.pdf.

[3]   U.S. Energy Information Administration. How much energy is consumed in U.S. buildings? 2019. https://www.eia.gov/tools/faqs/faq.php?id=86&t=1.

[4]   University BERC of T. China Building Energy Use 2018. 2018.

[5]   Rousselot M. Energy Efficiency Trends in Buildings. 2018.

[6]   Buckman AH, Mayfield M, Beck SBM. What is a smart building? Smart Sustain Built Environ 2014;3:92–109. https://doi.org/10.1108/SASBE-01-2014-0003.

[7]   Batty M, Axhausen KW, Giannotti F, Pozdnoukhov A, Bazzani A, Wachowicz M, et al. Smart cities of the future. Eur Phys J Spec Top 2012;214:481–518. https://doi.org/10.1140/epjst/e2012-01703-3.

[8]   Albino V, Berardi U, Dangelico RM. Smart cities: Definitions, dimensions, performance, and initiatives. J Urban Technol 2015;22:3–21. https://doi.org/10.1080/10630732.2014.942092.

[9]   Stuart Borlase. Smart Grids: Infrastructure, Technology, and Solutions. Taylor & Francis; 2013. https://doi.org/10.1007/978-1-4615-0981-3_11.

[10]   Gubbi J, Buyya R, Marusic S, Palaniswami M. Internet of Things (IoT): A vision, architectural elements, and future directions. Futur Gener Comput Syst 2013;29:1645–60. https://doi.org/10.1016/J.FUTURE.2013.01.010.

[11]   Tian W, Heo Y, de Wilde P, Li Z, Yan D, Park CS, et al. A review of uncertainty analysis in building energy assessment. Renew Sustain Energy Rev 2018;93:285–301. https://doi.org/10.1016/j.rser.2018.05.029.

[12]   Crawley DB, Lawrie LK, Winkelmann FC, Buhl WF, Huang YJ, Pedersen CO, et al.

EnergyPlus: Creating a new-generation building energy simulation program. Energy Build 2001. https://doi.org/10.1016/S0378-7788(00)00114-6.

[13] Chaudhary G, New J, Sanyal J, Im P, O'Neill Z, Garg V. Evaluation of "Autotune" calibration against manual calibration of building energy models. Appl Energy 2016;182:115–34. https://doi.org/10.1016/j.apenergy.2016.08.073.

[14] Coakley D, Raftery P, Keane M. A review of methods to match building energy simulation models to measured data. Renew Sustain Energy Rev 2014;37:123–41. https://doi.org/10.1016/j.rser.2014.05.007.

[15] Chaudhary G, New J, Sanyal J, Im P, O'Neill Z, Garg V. Evaluation of "Autotune" calibration against manual calibration of building energy models. Appl Energy 2016. https://doi.org/10.1016/j.apenergy.2016.08.073.

[16] Chong A, Xu W, Chao S, Ngo NT. Continuous-time Bayesian calibration of energy models using BIM and energy data. Energy Build 2019;194:177–90. https://doi.org/10.1016/j.enbuild.2019.04.017.

[17] Efficiency Valuation Organization. International Performance Measurement & Verification Protocol: concepts and options for determining energy and water savings 2010;1.

[18] Hansen SJ, Brown JW. Investment Grade Energy Audit: making smart energy choices. Lilburn, GA: Fairmont Press, Inc; 2004.

[19] Quan SJ, Li Q, Augenbroe G, Brown J, Yang PP-J. Urban data and building energy modeling: A GIS-based urban building energy modeling system using the urban-EPC engine. Plan. Support Syst. Smart Cities, 2015, p. 447--469.

[20] Gelman A, Carlin J, Stern H, Dunson D, Vehtari A, Rubin D. Bayesian data analysis. Chapman and Hall/CRC; 2013.

[21] Bayes TR. An Essay Towards Solving a Problem in the Doctrine of Chances. Philos Trans R Soc London 1763;53:370–418.

[22] Dani Gamerman, Hedibert F. Lopes. Markov Chain Monte Carlo: stochastic simulation for Bayesian inference. Chapman and Hall/CRC; 2006.

[23] Kennedy MC, O'Hagan A. Bayesian calibration of computer models. J R Stat Soc Ser B

(Statistical Methodol 2001;63:425–64. https://doi.org/10.1111/1467-9868.00294.

[24] Van Oijen M, Rougier J, Smith R. Bayesian calibration of process-based forest models: Bridging the gap between models and data. Tree Physiol 2005;25:915–27. https://doi.org/10.1093/treephys/25.7.915.

[25] Steel D. Bayesian Statistics in Radiocarbon Calibration. Philos Sci 2001;68:S153–64. https://doi.org/10.1086/392905.

[26] Lehuger S, Gabrielle B, Oijen M van, Makowski D, Germon JC, Morvan T, et al. Bayesian calibration of the nitrous oxide emission module of an agro-ecosystem model. Agric Ecosyst Environ 2009. https://doi.org/10.1016/j.agee.2009.04.022.

[27] Arhonditsis GB, Papantou D, Zhang W, Perhar G, Massos E, Shi M. Bayesian calibration of mechanistic aquatic biogeochemical models and benefits for environmental management. J Mar Syst 2008. https://doi.org/10.1016/j.jmarsys.2007.07.004.

[28] Kuczera G, Kavetski D, Renard B, Thyer M. A limited-memory acceleration strategy for MCMC sampling in hierarchical Bayesian calibration of hydrological models. Water Resour Res 2010;46:1–6. https://doi.org/10.1029/2009WR008985.

[29] Hall JW, Manning LJ, Hankin RKS. Bayesian calibration of a flood inundation model using spatial data. Water Resour Res 2011;47:1–14. https://doi.org/10.1029/2009WR008541.

[30] Tianfang Xu, Albert J. Valocchi. A Bayesian approach to improved calibration and prediction of groundwater models with structural error 2015;51:9290–311. https://doi.org/10.1002/2015WR017200.A.

[31] Van Hinsbergen CPIJ, Van Lint HWC, Hoogendoorn SP, Van Zuylen HJ. Bayesian calibration of car-following models. IFAC Proc. Vol., 2009. https://doi.org/10.3182/20090902-3-US-2007.0049.

[32] Whyte S, Walsh C, Chilcott J. Bayesian calibration of a natural history model with application to a population model for colorectal cancer. Med Decis Mak 2011;31:625–41. https://doi.org/10.1177/0272989X10384738.

[33] Heo Y. Bayesian Calibration of Building Energy Models for Energy Retrofit Decision-Making Under Uncertainty 2011:1–116.

[34] Sadeghi SA, Lee S, Karava P, Bilionis I, Tzempelikos A. Bayesian classification and inference of occupant visual preferences in daylit perimeter private offices. Energy Build 2018;166:505–24. https://doi.org/10.1016/j.enbuild.2018.02.010.

[35] Lee S, Karava P, Tzempelikos A, Bilionis I. Inference of thermal preference profiles for personalized thermal environments with actual building occupants. Build Environ 2019;148:714–29. https://doi.org/10.1016/j.buildenv.2018.10.027.

[36] Carstens H, Xia X, Yadavalli S. Bayesian energy measurement and verification analysis. Energies 2018;11:1–20. https://doi.org/10.3390/en11020380.

[37] Liu Y, Qin H, Zhang Z, Pei S, Jiang Z, Feng Z, et al. Probabilistic spatiotemporal wind speed forecasting based on a variational Bayesian deep learning model. Appl Energy 2020;260:114259. https://doi.org/10.1016/j.apenergy.2019.114259.

[38] Liu Y, Qin H, Zhang Z, Pei S, Wang C, Yu X, et al. Ensemble spatiotemporal forecasting of solar irradiation using variational Bayesian convolutional gate recurrent unit network. Appl Energy 2019;253:113596. https://doi.org/10.1016/j.apenergy.2019.113596.

[39] Zhang C, Butepage J, Kjellstrom H, Mandt S. Advances in Variational Inference. IEEE Trans Pattern Anal Mach Intell 2019;41:2008–26. https://doi.org/10.1109/TPAMI.2018.2889774.

[40] Chong A, Lam KP, Pozzi M, Yang J. Bayesian calibration of building energy models with large datasets. Energy Build 2017;154:343–55. https://doi.org/10.1016/j.enbuild.2017.08.069.

[41] Kim YJ, Kim KC, Park CS, Kim IH. Deterministic vs. Stochastic Calibration of Energy Simulation Model for an Existing Building. Proceeding ASim 2014, 2014.

[42] Pavlak GS, Florita AR, Henze GP, Rajagopalan B. Comparison of traditional and bayesian calibration techniques for gray-box modeling. J Archit Eng 2014;20. https://doi.org/10.1061/(ASCE)AE.1943-5568.0000145.

[43] Kim YJ, Park CS. Stepwise deterministic and stochastic calibration of an energy simulation model for an existing building. Energy Build 2016. https://doi.org/10.1016/j.enbuild.2016.10.009.

[44]   Zhang Z, Chong A, Pan Y, Zhang C, Lam KP. Whole building energy model for HVAC optimal control: A practical framework based on deep reinforcement learning. Energy Build 2019;199:472–90. https://doi.org/10.1016/j.enbuild.2019.07.029.

[45]   Rouchier S, Rabouille M, Oberlé P. Calibration of simplified building energy models for parameter estimation and forecasting: Stochastic versus deterministic modelling. Build Environ 2018;134:181–90. https://doi.org/10.1016/j.buildenv.2018.02.043.

[46]   Muehleisen RT, Bergerson J. Bayesian Calibration-What, Why And How. 4th Int High Perform Build Conf 2016:167.

[47]   Riddle M, Muehleisen RT. A guide to Bayesian calibration of building energy models. 2014 ASHRAE/IBPSA-USA   Build   Simul   Conf   2014:276–83. https://doi.org/10.13140/2.1.1674.9127.

[48]   Lim H, Zhai ZJ. Review on stochastic modeling methods for building stock energy prediction. Build Simul 2017;10:607–24. https://doi.org/10.1007/s12273-017-0383-y.

[49]   McElreath R. Statistical rethinking: A Bayesian course with examples in R and Stan. Chapman and Hall/CRC; 2018.

[50]   Lim H. Prediction of Urban-Scale Building Energy Performance with a Stochastic-Deterministic-Coupled Approach. University of Colorado at Boulder, 2017.

[51]   Booth AT, Choudhary R, Spiegelhalter DJ. Handling uncertainty in housing stock models. Build Environ 2012;48:35–47. https://doi.org/10.1016/j.buildenv.2011.08.016.

[52]   Booth AT, Choudhary R, Spiegelhalter DJ. A hierarchical bayesian framework for calibrating micro-level models with macro-level data. J Build Perform Simul 2013;6:293–318. https://doi.org/10.1080/19401493.2012.723750.

[53]   Tian W, Choudhary R. A probabilistic energy model for non-domestic building sectors applied to analysis of school buildings in greater London. Energy Build 2012;54:1–11. https://doi.org/10.1016/j.enbuild.2012.06.031.

[54]   Yamaguchi Y, Suzuki Y, Choudhary R, Booth A. Urban-scale energy modeling of food supermarket considering uncertainty. Proc. BS, 2013.

[55]   Booth AT, Choudhary R. Decision making under uncertainty in the retrofit analysis of the

UK housing stock: Implications for the Green Deal. Energy Build 2013;64:292–308. https://doi.org/10.1016/j.enbuild.2013.05.014.

[56] Booth A, Choudhary R. Calibrating micro-level models with macro-level data using bayesian regression analysis. Proc Build Simul 2011 12th Conf Int Build Perform Simul Assoc 2011:641–8.

[57] Heo Y, Augenbroe G, Choudhary R. Risk Analysis of Energy-Efficiency Projects Based on Bayesian Calibration of Building Energy Models. 12th Conf. Int. Build. Perform. Simul. Assoc., 2011, p. 2579–86.

[58] Heo Y, Choudhary R, Augenbroe GA. Calibration of building energy models for retrofit analysis under uncertainty. Energy Build 2012;47:550–60. https://doi.org/10.1016/j.enbuild.2011.12.029.

[59] Heo Y, Augenbroe G, Choudhary R. Quantitative risk management for energy retrofit projects. J Build Perform Simul 2013;6:257–68. https://doi.org/10.1080/19401493.2012.706388.

[60] Heo Y, Graziano DJ, Guzowski L, Muehleisen RT. Evaluation of calibration efficacy under different levels of uncertainty. J Build Perform Simul 2015;8:135–44. https://doi.org/10.1080/19401493.2014.896947.

[61] Heo Y, Augenbroe G, Graziano D, Muehleisen RT, Guzowski L. Scalable methodology for large scale building energy improvement: Relevance of calibration in model-based retrofit analysis. Build Environ 2015;87:342–50. https://doi.org/10.1016/j.buildenv.2014.12.016.

[62] Tian W, Yang S, Li Z, Wei S, Pan W, Liu Y. Identifying informative energy data in Bayesian calibration of building energy models. Energy Build 2016;119:363–76. https://doi.org/10.1016/j.enbuild.2016.03.042.

[63] Choudhary R. Energy analysis of the non-domestic building stock of Greater London. Build Environ 2012;51:243–54. https://doi.org/10.1016/j.buildenv.2011.10.006.

[64] Choudhary R, Tian W. Influence of district features on energy consumption in non-domestic buildings. Build Res Inf 2014;42:32–46. https://doi.org/10.1080/09613218.2014.832559.

[65] Kim YJ, Yoon SH, Park CS. Stochastic comparison between simplified energy calculation

and dynamic simulation. Energy Build 2013;64:332–42. https://doi.org/10.1016/j.enbuild.2013.05.026.

[66]   Kim YJ, Ahn KU, Park CS. Decision making of HVAC system using Bayesian Markov chain Monte Carlo method. Energy Build 2014;72:112–21. https://doi.org/10.1016/j.enbuild.2013.12.039.

[67]   Kim YJ. Challenging issues in stochastic calibration based on bayesian paradigm for building energy model. Int J Smart Home 2015;9:127–42. https://doi.org/10.14257/ijsh.2015.9.5.13.

[68]   Manfren M, Aste N, Moshksar R. Calibration and uncertainty analysis for computer models - A meta-model based approach for integrated building energy simulation. Appl Energy 2013;103:627–41. https://doi.org/10.1016/j.apenergy.2012.10.031.

[69]   Li Q, Gu L, Augenbroe G, Jeff Wu CF, Brown J. A Generic approach to calibrate building energy models under uncertainty using Bayesian inference. 14th Int Conf IBPSA - Build Simul 2015, BS 2015, Conf Proc 2015:2913–21.

[70]   Li Q, Gu L, Augenbroe G, Jeff Wu CF, Brown J. Calibration of dynamic building energy models with multiple responses using Bayesian inference and linear regression models. Energy Procedia 2015;78:979–84. https://doi.org/10.1016/j.egypro.2015.11.037.

[71]   Li Q, Augenbroe G, Brown J. Assessment of linear emulators in lightweight Bayesian calibration of dynamic building energy models for parameter estimation and performance prediction. Energy Build 2016;124:194–202. https://doi.org/10.1016/j.enbuild.2016.04.025.

[72]   Chong A, Lam KP. Uncertainty analysis and parameter estimation of HVAC systems in building energy models. 14th Int Conf IBPSA - Build Simul 2015, BS 2015, Conf Proc 2015:2788–95.

[73]   Chong A, Poh Lam K. A Comparison of MCMC Algorithms for the Bayesian Calibration of Building Energy Models. 15th IBPSA Conf 2017:494–503.

[74]   Chong A, Menberg K. Guidelines for the Bayesian calibration of building energy models. Energy Build 2018;174:527–47. https://doi.org/10.1016/j.enbuild.2018.06.028.

[75]   Chong A, Xu W, Chao S, Ngo NT. Continuous-time Bayesian calibration of energy models

using BIM and energy data. Energy Build 2019;194:177–90. https://doi.org/10.1016/j.enbuild.2019.04.017.

[76] Henze GP, Pavlak GS, Florita AR, Dodier RH, Hirsch AI. An energy signal tool for decision support in building energy systems. Appl Energy 2015;138:51–70. https://doi.org/10.1016/j.apenergy.2014.10.029.

[77] Braulio-Gonzalo M, Juan P, Bovea MD, Ruá MJ. Modelling energy efficiency performance of residential building stocks based on Bayesian statistical inference. Environ Model Softw 2016;83:198–211. https://doi.org/10.1016/j.envsoft.2016.05.018.

[78] Kang Y, Krarti M. Bayesian-Emulator based parameter identification for calibrating energy models for existing buildings. Build Simul 2016;9:411–28. https://doi.org/10.1007/s12273-016-0291-6.

[79] Zhao F, Lee SH, Augenbroe G. Reconstructing building stock to replicate energy consumption data. Energy Build 2016;117:301–12. https://doi.org/10.1016/j.enbuild.2015.10.001.

[80] Sokol J, Cerezo Davila C, Reinhart CF. Validation of a Bayesian-based method for defining residential archetypes in urban building energy models. Energy Build 2017;134:11–24. https://doi.org/10.1016/j.enbuild.2016.10.050.

[81] Kristensen MH, Choudhary R, Petersen S. Bayesian calibration of building energy models: Comparison of predictive accuracy using metered utility data of different temporal resolution. Energy Procedia 2017;122:277–82. https://doi.org/10.1016/j.egypro.2017.07.322.

[82] Kristensen MH, Choudhary R, Pedersen RH, Petersen S. Bayesian Calibration Of Residential Building Clusters Using A Single Geometric Building Representation. Proc 15th IBPSA Conf 2017:1294–303.

[83] Lim H. Prediction of Urban-Scale Building Energy Performance with a Stochastic-Deterministic-Coupled Approach 2017.

[84] Lim H, Zhai ZJ. Comprehensive evaluation of the influence of meta-models on Bayesian calibration. Energy Build 2017;155:66–75. https://doi.org/10.1016/j.enbuild.2017.09.009.

[85]   Lim H, Zhai Z (John). Influences of energy data on Bayesian calibration of building energy model. Appl Energy 2018;231:686–98. https://doi.org/10.1016/j.apenergy.2018.09.156.

[86]   Menberg K, Heo Y, Choudhary R. Efficiency and Reliability of Bayesian Calibration of Energy Supply System Models University of Cambridge , Department of Engineering , Cambridge , UK , University of Cambridge , Department of Architecture , Cambridge , UK , 2017:1594–603.

[87]   Menberg K, Heo Y, Choudhary R. Influence of error terms in Bayesian calibration of energy system models. J Build Perform Simul 2019;12:82–96. https://doi.org/10.1080/19401493.2018.1475506.

[88]   Yuan J, Nian V, Su B. A Meta Model Based Bayesian Approach for Building Energy Models Calibration. Energy Procedia 2017;143:161–6. https://doi.org/10.1016/j.egypro.2017.12.665.

[89]   Yuan J, Nian V, Su B, Meng Q. A simultaneous calibration and parameter ranking method for building energy models. Appl Energy 2017;206:657–66. https://doi.org/10.1016/j.apenergy.2017.08.220.

[90]   Yuan J, Nian V, Su B. Evaluation of cost-effective building retrofit strategies through soft-linking a metamodel-based Bayesian method and a life cycle cost assessment method. Appl Energy 2019;253:113573. https://doi.org/10.1016/j.apenergy.2019.113573.

[91]   Raillon L, Ghiaus C. An efficient Bayesian experimental calibration of dynamic thermal models. Energy 2018;152:818–33. https://doi.org/10.1016/j.energy.2018.03.168.

[92]   Zhang Z, Chong A, Poh Lam K, Pan Y, Zhang C, Lu S. A Deep Reinforcement Learning Approach to Using Whole Building Energy Model For HVAC Optimal Control ASHRAE Multidisciplinary Task Group on Occupant Behavior in Buildings View project International Energy Agency Energy in Buildings and Communities Program 2018.

[93]   Chen S, Friedrich D, Yu Z, Yu J. District Heating Network Demand Prediction Using a Physics-Based Energy Model with a Bayesian Approach for Parameter Calibration. Energies 2019;12:3408.

[94]   Rysanek AM, Fonseca JA, Schlueter A. Bayesian calibration of a building energy model by stochastic optimisation of root-mean square error. Prepr Submitt to Appl Energy 2019.

151

https://doi.org/https://doi.org/10.3929/ethz-b-000349836.

[95]   Yi DH, Kim DW, Park CS. Parameter identifiability in Bayesian inference for building energy models. Energy Build 2019;198:318–28. https://doi.org/10.1016/j.enbuild.2019.06.012.

[96]   Ahmadi S, Fakehi A hossien, vakili A, Haddadi M, Iranmanesh SH. A hybrid stochastic model based Bayesian approach for long term energy demand managements. Energy Strateg Rev 2020;28:100462. https://doi.org/10.1016/j.esr.2020.100462.

[97]   Zhu C, Tian W, Yin B, Li Z, Shi J. Uncertainty calibration of building energy models by combining approximate Bayesian computation and machine learning algorithms. Appl Energy 2020;268:115025. https://doi.org/10.1016/j.apenergy.2020.115025.

[98]   Zhu C, Tian W, Wilde P De, Yin B. Approximate Bayesian Computation in Parameter Estimation of Building Energy Models. Springer Singapore; 2020. https://doi.org/10.1007/978-981-13-9528-4.

[99]   Metropolis N, Rosenbluth WA, Rosenbluth NM, Teller HA, Teller E. Equation of State Calculations by Fast Computing Machines. Jounal Chem Phys 1953;21:1087–92.

[100] Geman S, Geman D. Stochastic Relaxation, Gibbs Distributions, and the Bayesian Restoration of Images. IEEE Trans Pattern Anal Mach Intell 1984;PAMI-6.

[101] Hoffman DM, Gelman A. The No-U-Turn Sampler: Adaptively Setting Path Lengths in Hamiltonian Monte Carlo. J Mach Learn Res 2014;15:1593–623.

[102] Ihaka R, Gentleman R. R: a language for data analysis and graphics. J Comput Graph Stat 1996;5:299--314.

[103] Team RC. R: A language and environment for statistical computing 2013.

[104] Winkelmann FC, Birdsall BE, Buhl WF, Ellington KL, Erdem AE, Hirsch JJ, et al. DOE-2 supplement: Version 2.1E. United States: 1993.

[105] Klein SA. TRNSYS-A transient system simulation program. Univ Wisconsin-Madison, Eng Exp Stn Rep 1988:38--12.

[106] Strachan P. ESP-r: Summary of Validation Studies. Analysis 2000:0–8.

[107] Wei T. A review of sensitivity analysis methods in building energy analysis. Renew Sustain Energy Rev 2013;20:411–9. https://doi.org/10.1016/j.rser.2012.12.014.

[108] Jia H. eplusr n.d. https://hongyuanjia.github.io/eplusr/.

[109] Menberg K, Heo Y, Choudhary R. Sensitivity analysis methods for building energy models: Comparing computational costs and extractable information. Energy Build 2016. https://doi.org/10.1016/j.enbuild.2016.10.005.

[110] Tian W, Wang Q, Song J, Wei S. Calibrating Dynamic Building Energy Models using Regression Model and Bayesian Analysis in Building Retrofit Projects. ESim 2014 2014.

[111] Yang J, Rivard H, Zmeureanu R. Building energy prediction with adaptive artificial neural networks. IBPSA 2005 - Int Build Perform Simul Assoc 2005 2005:1401–8.

[112] Kalogirou SA, Bojic M. Artificial neural networks for the prediction of the energy consumption of a passive solar building. Energy 2000. https://doi.org/10.1016/S0360-5442(99)00086-9.

[113] Aydinalp M, Ugursal VI, Fung AS. Modeling of the space and domestic hot-water heating energy-consumption in the residential sector using neural networks. Appl Energy 2004. https://doi.org/10.1016/j.apenergy.2003.12.006.

[114] Eisenhower B, O'Neill Z, Narayanan S, Fonoberov VA, Mezić I. A methodology for meta-model based optimization in building energy models. Energy Build 2012. https://doi.org/10.1016/j.enbuild.2011.12.001.

[115] Tian W, Song J, Li Z, de Wilde P. Bootstrap techniques for sensitivity analysis and model selection in building thermal performance analysis. Appl Energy 2014. https://doi.org/10.1016/j.apenergy.2014.08.110.

[116] Kim YJN, Aim KU, Park CS, Kim IH. Gaussian emulator for stochastic optimal design of a double glazing system. Proc BS 2013 13th Conf Int Build Perform Simul Assoc 2013:2217–24.

[117] Lunn D, Spiegelhalter D, Thomas A, Best N. The BUGS project: Evolution, critique and future directions. Stat Med 2009;28:3049--3067. https://doi.org/10.1002/sim.

[118] Lunn DJ, Thomas A, Best N, Spiegelhalter D. WinBUGS-a Bayesian modelling framework:

concepts, structure, and extensibility. Stat Comput 2000;10:325–37. https://doi.org/10.1093/ohr/oht039.

[119] Surhone LM, Tennoe MT, Henssonow SF. OpenBUGS. Betascript Publ 2010.

[120] Stan n.d. https://mc-stan.org/ (accessed April 7, 2020).

[121] Stan Development Team. RStan: the R interface to Stan. R News 2019.

[122] Thomas A, O'Hara B, Ligges U, Sturtz S. Making BUGS Open. R News 2006;6:12–7.

[123] Greta introduction n.d.

[124] Martyn P, Nicky B, Kate C, Karen V. CODA: Convergence Diagnosis and Output Analysis for MCMC. R News 2006;6:7–11.

[125] Guideline, ASHRAE. Guideline 14-2015, Measurement of Energy and Demand Savings. Atlanta, Georgia: 2015.

[126] EVO. International performance measurement & verification protocol. Effic Valuat Organ 2007.

[127] U.S. Department of Energy. M&V Guidelines: Measurement and Verification for Performance-Based Contracts Version 4.0 2015.

[128] Gneiting T, Raftery AE. Strictly proper scoring rules, prediction, and estimation. J Am Stat Assoc 2007;102:359–78. https://doi.org/10.1198/016214506000001437.

[129] Sun Y. Closing the building energy performance gap by improving our predictions. Georgia Institute of Technology, 2014.

[130] Zuhaib S, Hajdukiewicz M, Goggins J. Application of a staged automated calibration methodology to a partially-retrofitted university building energy model. J Build Eng 2019;26:100866. https://doi.org/10.1016/j.jobe.2019.100866.

[131] DesignBuilder Optimization n.d.

[132] Parametric Analysis Tool (PAT) n.d. https://nrel.github.io/OpenStudio-user-documentation/reference/parametric_analysis_tool_2/ (accessed June 10, 2021).

[133] TESS Optimization Library n.d. http://www.trnsys.com/tess-libraries/ (accessed June 10, 2021).

[134] BEopt n.d. https://www.nrel.gov/buildings/beopt.html (accessed June 10, 2021).

[135] jEPlus+EA n.d. https://www.jeplus.org/wiki/doku.php?id=docs:jeplus_ea:start (accessed June 10, 2021).

[136] Opt-E-Plus. Opt-E-Plus Software for Commercial Building Optimization. Natl Renew Energy Lab US DOE 2013.

[137] Commercial Building Energy Saver n.d. http://cbes.lbl.gov/ (accessed June 10, 2021).

[138] Chen Y, Hong T, Piette MA. Automatic generation and simulation of urban building energy models based on city datasets for city-scale building retrofit analysis. Appl Energy 2017;205:323–35. https://doi.org/10.1016/j.apenergy.2017.07.128.

[139] City Building Energy Saver (CityBES) n.d.

[140] Sansregret S, Lavigne K, Daoud A, Leclaire L-A. ExCalibBEM Tool Development to Calibrate Building Energy Models. Proc ESim 2014 8th Conf IBPSA-Canada, May 8-9 2014:7A.5.1-7A.5.11.

[141] Palonen M, Hamdy M, Hasan A. MOBO a new software for multi-objective building performance optimization. Proc. 13th Int. Conf. IBPSA, 2013, p. 2567--2574.

[142] Hou D, Hassan IG, Wang L. Review on building energy model calibration by Bayesian inference. Renew Sustain Energy Rev 2021;143:110930. https://doi.org/10.1016/j.rser.2021.110930.

[143] R n.d. https://www.r-project.org/ (accessed June 18, 2021).

[144] Stan n.d. https://mc-stan.org/ (accessed June 18, 2021).

[145] Jia H, Chong A. eplusr: A framework for integrating building energy simulation and data-driven analytics. Energy Build 2021;237:110757. https://doi.org/10.1016/j.enbuild.2021.110757.

[146] Global Tall Building Database of the CTBUH n.d. https://www.skyscrapercenter.com/compare-data (accessed September 1, 2020).

[147] Al Sada IA. Qatar General Electricity and Water Corporation "KAHRAMAA" Presentation. Int. Dist. Cool. Heat. Conf., Doha, Qatar: 2017.

[148] ASHRAE. ASHRAE standard 169-2013: Climatic Data For Building Design Standards. 2013.

[149] ASHRAE. ASHRAE Standard 62.1-2019, Ventilation for Acceptable Indoor Air Quality. 2019.

[150] ASHRAE. ASHRAE Standard 90.1-2019, Energy Standard for Buildings Except Low-Rise Residential Buildings. 2019.

[151] ASHARE. ASHRAE Standard 189.1-2017, Standard for the Design of High-Performance Green Buildings. 2017.

[152] Development GO for R&. Lusail city GSAS 2 Star Rating Guidelines. 2014.

[153] Andric I, Al-Ghamdi SG. Climate change implications for environmental performance of residential building energy use: The case of Qatar. Energy Reports 2019;6:587–92. https://doi.org/10.1016/j.egyr.2019.09.030.

[154] Matala A. Sample Size Requirement for Monte Carlo simulations using Latin Hypercube Sampling. Indep Res Proj Appl Math 2008:1–24.

[155] Sun J, Reddy TA. Calibration of building energy simulation programs using the analytic optimization approach (RP-1051). HVAC R Res 2006;12:177–96. https://doi.org/10.1080/10789669.2006.10391173.

[156] Betancourt M. A Conceptual Introduction to Hamiltonian Monte Carlo. ArXiv Prepr ArXiv170102434 2017.

[157] Lusail City. Lusail City GSAS 2 Star Rating Guidelines. 2016.

[158] Lusail city 2020;53:21–5.

[159] (NASA) NA and SA. Overiew: Weather, Global Warming and Climate Change 2020. https://climate.nasa.gov/resources/global-warming-vs-climate-change/ (accessed February 17, 2020).

[160] National Oceanic and Atmospheric Administration (NOAA). Global Climate Change Indicators 2020. https://www.ncdc.noaa.gov/monitoring-references/faq/indicators.php#warming-climate (accessed February 17, 2020).

[161] Environment and Climate Change Canada. Canadian Environmental Sustainability Indicators: Temperature change in Canada. 2019.

[162] Olive J. David. Multiple Linear Regression. Linear Regres., Springer, Cham; 2017. https://doi.org/https://doi.org/10.1007/978-3-319-55252-1_2.

[163] Scarselli F, Gori M, Tsoi AC, Hagenbuchner M, Monfardini G. The graph neural network model. IEEE Trans Neural Networks 2008;20.

[164] Noble WS. What is a support vector machine? Nat Biotechnol 2006;24:1565--1567.

[165] Friedman JH. Multivariate adaptive regression splines. Ann Stat 1991:1--67.

[166] Bastos LS, O'Hagan A. Diagnostics for Gaussian process emulators. Technometrics 2009;51:425--438.

[167] Asadi S, Bouvier N, Wexler AS, Ristenpart WD. The coronavirus pandemic and aerosols: Does COVID-19 transmit via expiratory particles? Aerosol Sci Technol 2020. https://doi.org/10.1080/02786826.2020.1749229.

[168] Prather KA, Wang CC, Schooley RT. Reducing transmission of SARS-CoV-2. Science (80-) 2020. https://doi.org/10.1126/science.abc6197.

[169] Zhang J. Integrating IAQ control strategies to reduce the risk of asymptomatic SARS CoV-2 infections in classrooms and open plan offices. Sci Technol Built Environ 2020. https://doi.org/10.1080/23744731.2020.1794499.

[170] REMIORZ R. School COVID-19 cases consistent with community transmission, but Quebec could be in trouble, data show - The Globe and Mail 2020.

[171] Number of schools - Covid Écoles Québec 2020.

[172] Du CR, Wang SC, Yu MC, Chiu TF, Wang JY, Chuang PC, et al. Effect of ventilation improvement during a tuberculosis outbreak in underventilated university buildings. Indoor Air 2020. https://doi.org/10.1111/ina.12639.

[173] Sehulster L, Chinn RYW. Guidelines for environmental infection control in health-care facilities. Recommendations of CDC and the Healthcare Infection Control Practices Advisory Committee (HICPAC). MMWR Recomm Rep 2003.

[174] Atkinson J, Chartier Y, Lúcia Pessoa-Silva C, Jensen P, Li Y, Seto W-H, et al. Natural ventilation for infection control in health-care settings. World Heal Organ 2016.

[175] Allen J, Cedeno-Laurent J, Miller S. Harvard-CU Boulder Portable Air Cleaner Calculator for Schools.v1.3 - Google Sheets 2020.

[176] COVID-19: Measures in place as the holidays approach 2020.

[177] Wilton K. 12 Montreal teachers secretly tested classroom ventilation. The results are "problematic" | Montreal Gazette 2020.

[178] Persily A. Indoor Carbon Dioxide Concentrations in Ventilation and Indoor Air Quality Standards. Proc 36th AVIC, Conf Eff Vent High Preformance Build 2015:1–12.

[179] Penman JM. An experimental determination of ventilation rate in occupied rooms using atmospheric carbon dioxide concentration. Build Environ 1980. https://doi.org/10.1016/0360-1323(80)90028-1.

[180] Mumovic D, Palmer J, Davies M, Orme M, Ridley I, Oreszczyn T, et al. Winter indoor air quality, thermal comfort and acoustic performance of newly built secondary schools in England. Build Environ 2009. https://doi.org/10.1016/j.buildenv.2008.06.014.

[181] Batterman S. Review and extension of CO2-based methods to determine ventilation rates with application to school classrooms. Int J Environ Res Public Health 2017. https://doi.org/10.3390/ijerph14020145.

[182] Eykelbosh A. Can CO2 Sensors be Used to Assess COVID-19 Transmission Risk? | National Collaborating Centre for Environmental Health | NCCEH - CCSNE 2021.

[183] Strawderman RL, Gamerman D. Markov Chain Monte Carlo: Stochastic Simulation for Bayesian Inference. J Am Stat Assoc 2000. https://doi.org/10.2307/2669581.

[184] Xu T, Valocchi AJ. A Bayesian approach to improved calibration and prediction of groundwater models with structural error. Water Resour Res 2015. https://doi.org/10.1002/2015WR017912.

[185] ANSI/ASHRAE. Standard 62-2001 Ventilation for acceptable indoor air quality. 2001.

[186] NIOSH. CDC - The National Institute for Occupational Safety and Health (NIOSH) 2020.

[187] Barnhart S, Sheppard L, Beaudet N, Stover B, Balmes J. Tuberculosis in health care settings and the estimated benefits of engineering controls and respiratory protection. J Occup Environ Med 1997. https://doi.org/10.1097/00043764-199709000-00008.

[188] Rudnick SN, Milton DK. Risk of indoor airborne infection transmission estimated from carbon dioxide concentration. Indoor Air 2003;13:237–45. https://doi.org/10.1034/j.1600-0668.2003.00189.x.

[189] Peng Z, Jimenez JL. Title: Exhaled CO 2 as COVID-19 infection risk proxy for different indoor environments and activities. MedRxiv 2020.

[190] Miller SL, Nazaroff WW, Jimenez JL, Boerstra A, Buonanno G, Dancer SJ, et al. Transmission of SARS-CoV-2 by inhalation of respiratory aerosol in the Skagit Valley Chorale superspreading event. Indoor Air 2020. https://doi.org/10.1111/ina.12751.

[191] Jimenez JL. 2020_COVID-19_Aerosol_Transmission_Estimator - Google Sheets 2020.

[192] Katal A, Albettar M, Wang L (Leon). City Reduced Probability of Infection (CityRPI) for Indoor Airborne Transmission of SARS-CoV-2 and Urban Building Energy Impacts. MedRxiv 2021. https://doi.org/10.1101/2021.01.19.21250046.

[193] Wang L (Leon), Katal A, Albettar M. CityRPI for Indoor Airborne Transmission 2020.

[194] Yasuda T, Yonemura S, Tani A. Comparison of the characteristics of small commercial NDIR CO2 sensor models and development of a portable CO2 measurement device. Sensors 2012;12:3641–55. https://doi.org/10.3390/s120303641.

[195] ECCC. Historical Data - Climate - Environment and Climate Change Canada 2020.

[196] ANSI/ASHRAE. ANSI/ASHRAE Standard 62.1-2019, Ventilation for Acceptable Indoor Air Quality. ASHRAE 2019.

[197] Persily A, de Jonge L. Carbon dioxide generation rates for building occupants. Indoor Air 2017. https://doi.org/10.1111/ina.12383.

[198] Mike McGee. Daily CO2. A Pro Oxyg 2016:1.

[199] ANSI/ASHRAE. ASHRAE Guideline 14-2002 Measurement of Energy and Demand Savings. Ashrae 2002.

[200] Buonanno G, Stabile L, Morawska L. Estimation of airborne viral emission: Quanta emission rate of SARS-CoV-2 for infection risk assessment. Environ Int 2020. https://doi.org/10.1016/j.envint.2020.105794.

[201] US Environmental Protection Agency. Exposure Factors Handbook: 2011 Edition. US Environ Prot Agency 2011. https://doi.org/EPA/600/R-090/052F.

[202] Buonanno G, Morawska L, Stabile L. Quantitative assessment of the risk of airborne transmission of SARS-CoV-2 infection: Prospective and retrospective applications. Environ Int 2020. https://doi.org/10.1016/j.envint.2020.106112.

[203] Lin CC, Wang L. Forecasting smoke transport during compartment fires using a data assimilation model. J Fire Sci 2015;33:3–21. https://doi.org/10.1177/0734904114548837.

[204] Lin CC, Wang L (Leon). Real-Time Forecasting of Building Fire Growth and Smoke Transport via Ensemble Kalman Filter. Fire Technol 2017;53:1101–21. https://doi.org/10.1007/s10694-016-0619-x.

[205] Ji J, Tong Q, (Leon) Wang L, Lin CC, Zhang C, Gao Z, et al. Application of the EnKF method for real-time forecasting of smoke movement during tunnel fires. Adv Eng Softw 2018;115:398–412. https://doi.org/10.1016/j.advengsoft.2017.10.007.

[206] Lin CC, Wang L (Leon). Forecasting simulations of indoor environment using data assimilation via an Ensemble Kalman Filter. Build Environ 2013;64:169–76. https://doi.org/10.1016/j.buildenv.2013.03.008.

[207] Sarbu I, Sebarchievici C. General review of ground-source heat pump systems for heating and cooling of buildings. Energy Build 2014;70:441–54. https://doi.org/10.1016/J.ENBUILD.2013.11.068.

[208] Hepbasli A, Kalinci Y. A review of heat pump water heating systems. Renew Sustain Energy Rev 2009;13:1211–29. https://doi.org/10.1016/J.RSER.2008.08.002.

[209] Zhang S, Wang H, Guo T. Experimental investigation of moderately high temperature water source heat pump with non-azeotropic refrigerant mixtures. Appl Energy 2010;87:1554–61. https://doi.org/10.1016/J.APENERGY.2009.11.001.

[210] Beghi A, Cecchinato L, Rampazzo M, Simmini F. Energy efficient control of HVAC

systems with ice cold thermal energy storage. J Process Control 2014;24:773–81. https://doi.org/10.1016/J.JPROCONT.2014.01.008.

[211] Sun Y, Wang S, Xiao F, Gao D. Peak load shifting control using different cold thermal energy storage facilities in commercial buildings: A review. Energy Convers Manag 2013;71:101–14. https://doi.org/10.1016/J.ENCONMAN.2013.03.026.

[212] Ortiz M, Barsun H, He H, Vorobieff P, Mammoli A. Modeling of a solar-assisted HVAC system with thermal storage. Energy Build 2010;42:500–9. https://doi.org/10.1016/J.ENBUILD.2009.10.019.

[213] Shun S, Ahmed NA. Utilizing wind and solar energy as power sources for a hybrid building ventilation device. Renew Energy 2008;33:1392–7. https://doi.org/10.1016/J.RENENE.2007.07.017.

[214] Batista NC, Melício R, Matias JCO, Catalão JPS. Photovoltaic and wind energy systems monitoring and building/home energy management using ZigBee devices within a smart grid. Energy 2013;49:306–15. https://doi.org/10.1016/J.ENERGY.2012.11.002.

[215] Albadi MH, El-Saadany EF. A summary of demand response in electricity markets. Electr Power Syst Res 2008;78:1989–96. https://doi.org/10.1016/J.EPSR.2008.04.002.

[216] Siano P. Demand response and smart grids—A survey. Renew Sustain Energy Rev 2014;30:461–78. https://doi.org/10.1016/J.RSER.2013.10.022.

[217] Chen J, Augenbroe G, Song X. Evaluating the potential of hybrid ventilation for small to medium sized office buildings with different intelligent controls and uncertainties in US climates. Energy Build 2018;158:1648–61. https://doi.org/10.1016/J.ENBUILD.2017.12.004.

[218] Huang KT, Hwang RL. Parametric study on energy and thermal performance of school buildings with natural ventilation, hybrid ventilation and air conditioning. Indoor Built Environ 2016;25:1148–62. https://doi.org/10.1177/1420326X15609773.

[219] Tong Z, Chen Y, Malkawi A, Liu Z, Freeman RB. Energy saving potential of natural ventilation in China: The impact of ambient air pollution. Appl Energy 2016;179:660–8. https://doi.org/10.1016/J.APENERGY.2016.07.019.

[220] Santamouris M, Kolokotsa D. Passive cooling dissipation techniques for buildings and other structures: The state of the art. Energy Build 2013;57:74–94. https://doi.org/10.1016/J.ENBUILD.2012.11.002.

[221] Chenari B, Dias Carrilho J, Gameiro da Silva M. Towards sustainable, energy-efficient and healthy ventilation strategies in buildings: A review. Renew Sustain Energy Rev 2016;59:1426–47. https://doi.org/10.1016/J.RSER.2016.01.074.

[222] Kalman RE. A new approach to linear filtering and prediction problems 1960.

[223] Ali S, Kim DH. Effective and comfortable power control model using Kalman filter for building energy management. Wirel Pers Commun 2013;73:1439–53. https://doi.org/10.1007/s11277-013-1259-9.

[224] Radecki P, Hencey B. Online building thermal parameter estimation via Unscented Kalman Filtering. Proc Am Control Conf 2012:3056–62. https://doi.org/10.1109/acc.2012.6315699.

[225] Sun B, Luh PB, Jia QS, O'Neill Z, Song F. Building energy doctors: An SPC and Kalman Filter-based method for system-level fault detection in HVAC systems. IEEE Trans Autom Sci Eng 2014;11:215–29. https://doi.org/10.1109/TASE.2012.2226155.

[226] Daum F. Extended Kalman Filters. Encycl Syst Control 2015. https://doi.org/10.1007/978-1-4471-5058-9.

[227] Evensen G. Sequential data assimilation with a nonlinear quasi-geostrophic model using Monte Carlo methods to forecast error statistics. J Geophys Res Ocean 1994;99:10143--10162.

[228] Houtekamer PL, Zhang F. Review of the Ensemble Kalman Filter for Atmospheric Data Assimilation. Mon Weather Rev 2016;144:4489–532. https://doi.org/10.1175/MWR-D-15-0440.1.

[229] Gillijns S, Mendoza OB, Chandrasekar J, De Moor BLR, Bernstein DS, Ridley A. What is the ensemble Kalman filter and how well does it work? 2006 Am Control Conf 2006:6 pp. https://doi.org/10.1109/acc.2006.1657419.

[230] Huang J, McBratney AB, Minasny B, Triantafilis J. Monitoring and modelling soil water dynamics using electromagnetic conductivity imaging and the ensemble Kalman filter.

Geoderma 2017;285:76–93. https://doi.org/10.1016/J.GEODERMA.2016.09.027.

[231] Lei X, Tian Y, Zhang Z, Wang L, Xiang X, Wang H. Correction of pumping station parameters in a one-dimensional hydrodynamic model using the Ensemble Kalman filter. J Hydrol 2019;568:108–18. https://doi.org/10.1016/J.JHYDROL.2018.10.062.

[232] Ma W, Jafarpour B, Qin J. Dynamic characterization of geologic CO2 storage aquifers from monitoring data with ensemble Kalman filter. Int J Greenh Gas Control 2019;81:199–215. https://doi.org/10.1016/J.IJGGC.2018.10.009.

[233] Reichle RH, Crow WT, Keppenne CL. An adaptive ensemble Kalman filter for soil moisture data assimilation. Water Resour Res 2008;44:1–13. https://doi.org/10.1029/2007WR006357.

[234] Evensen G. Sequential data assimilation with a nonlinear quasi-geostrophic model using Monte Carlo methods to forecast error statistics. J Geophys Res 1994;99. https://doi.org/10.1029/94jc00572.

[235] Evensen G. The Ensemble Kalman Filter: Theoretical formulation and practical implementation. Ocean Dyn 2003;53:343–67. https://doi.org/10.1007/s10236-003-0036-9.

[236] Evensen G. The Ensemble Kalman Filter for Combined State and Parameter Estimation: Monte Carlo techniques for data assimilation in large systems. IEEE Control Syst 2009;29:83–104. https://doi.org/10.1109/MCS.2009.932223.

[237] Whitaker JS, Hamill TM. Ensemble data assimilation without perturbed observations. Mon Weather Rev 2002;130:1913–24. https://doi.org/10.1175/1520-0493(2002)130<1913:EDAWPO>2.0.CO;2.

[238] Katal A, Wang L, Dols WS, Polidoro BJ. An Investigation of Different Strategies For Solving Coupled Thermal Airflows By Multi-Zone Network Method n.d.:4–9.

[239] Evensen G. Data Assimilation: The Ensemble Kalman Filter. Springer Science & Business Media; 2009.

[240] Houtekamer P., Mitchell HL. A Sequential Ensemble Kalman Filter for Atmospheric Data Assimilation. Am Meteorol Soc 2001;129:123–37.